Liquid crystalline phase transitions in virus and virus/polymer suspensions

A Dissertation

Presented to

The Faculty of the Graduate School of Arts and Sciences

Brandeis University

Department of Physics

Dr. Seth Fraden, Advisor

In Partial Fulfillment

of the Requirements for the Degree

Doctor of Philosophy

by

Zvonimir Dogic

October 2000

This dissertation, directed and approved by Zvonimir Doigc's Committee, has been accepted and approved by the Graduate Faculty of Brandeis University in partial fulfillment of the requirements for the degree of

DOCTOR OF PHILOSOPHY

Dean of Arts and Sciences

Dissertation Committee

Dr. Seth Fraden, Chair

Dr. Robert B. Meyer

Dr. Judith Herzfeld

ABSTRACT

Liquid crystalline phase transitions in virus and virus/polymer suspensions

A dissertation presented to the Faculty of the Graduate School of Arts and Sciences of Brandeis University, Waltham, Massachusetts

by Zvonimir Dogic

Using experimental, theoretical, and simulation methods, we investigate the relationship between the colloidal intermolecular interactions and the resulting phase diagrams. As a model system of rod-like particles we use bacteriophage *fd*, which is a charge stabilized colloid. We are able to engineer complex attractive and repulsive intermolecular interactions by changing the ionic strengths of the suspensions, attaching covalently bound polymers and adding non-adsorbing polymers. Using standard molecular cloning techniques it is also shown that the aspect ratio of the rod-like particle can be manipulated. In the limit of high ionic strength the *fd* virus quantitatively agrees with the Onsager theory for the isotropic-nematic (I-N) phase transition in hard rods. The role of attractive interaction on the nature of the I-N phase transition is investigated. As the strength of the attraction is increased we observe the isotropic-smectic (I-S) phase transitions. Using an optical microscope we follow the kinetics of the I-S phase transition and observe a whole range of novel structures of unexpected complexity. We also investiage the influence hard/spheres or polymer on the nematic-smectic phase transition. We conclude that adding small spheres stabilizes the smectic phase and destabilizes the nematic phase.

Acknowledgments

To Seth Fraden for his support, guidance, and enthusiasm.

To my fellow students Ujitha Dassanayake, Kirstin Purdy, Marie Adams, Joshua Bloustine, Emmanuel Belamie.

To Prof. Bulbul Chakraborty, Prof. Judith Herzfeld and Prof. Robert Meyer for their interest and help.

To my parents, my sister and Krista.

Contents

List of Figures

Chapter 1

Introduction

One of the basic goals of statistical mechanics is to predict the collective phenomena and phase behavior arising from the interaction potential between individual molecules. It was known for a long time that the interactions between two molecules can be separated into a short range repulsive (steric) interactions and other long range interaction due to the van der Waals force [1]. The basic question that follows is that of the relative importance of the short range and long range parts of the intermolecular potential in determining the phase behavior of the molecules. To elucidate this issue the behavior of hard spheres and hard spherocylinders, highly idealized systems which only have the repulsive component of the intermolecular potential, have become very important over the past 50 years. The interaction energy between two hard particles is either zero if they do not overlap, or infinity if they do overlap.

The first step in understanding ordering transitions in hard particles was taken in 1949, when Onsager in his seminal paper considered the phase behavior of hard spherocylinders [2]. He convincingly showed that hard core repulsion between highly anisotropic spherocylinders is sufficient to produce a stable liquid crystalline

nematic phase. The nematic phase is characterized by long range orientational order and short range positional order. At about the same time, Kirkwood speculated that the extremely simple system of hard spheres undergoes a liquid to crystal phase transition. This speculation was the subject of much debate in the 1950's, but subsequent computer simulations have unequivocally shown that the hard spheres undergo a first order liquid to crystal phase transition [3, 4]. The next step came when theory and computer simulations showed that hard spherocylinders also form a stable smectic phase [5, 6]. The smectic phase is characterized by one dimensional long range solid-like order in the direction of the alignment of the rods and short range liquid-like order in other two directions. Today it is widely accepted that the phase ordering transitions of liquid and solid systems is dominated by the shape of the repulsive part of the intermolecular potential between individual particles. A very general consequence of the simple interaction potential of hard particles is that all allowed energy states are equal and therefore all phase transitions in hard particles are entirely entropy driven. An experimental signature of entropy driven transitions is independence of temperature. A summary of the phase transitions in the system of hard particles is given in Fig. 1.

Colloids are the only experimental systems which approximate the behavior of hard particles closely enough that they undergo all the ordering transitions described above. This is due to the fact that at the colloidal length scale it is possible to engineer the interaction potential between two colloids using various chemical or physical modification schemes, while on the molecular scale it is impossible to avoid the ever present long range attractions of van der Waals origin. Today the synthesis of highly monodisperse spherical colloids made of insoluble polymers whose interaction closely approximates hard sphere potential is fairly routine. Experiments on these systems have provided the first experimental confirmation that the assembly

of hard spheres undergoes a liquid to crystal transition [7].

In contrast to spheres, various attempts to chemically synthesize rods have not been so successful. Every chemical synthesis of a hard-rod system invariably results in a wide distribution of rod lengths, which significantly affects the phase behavior of the system. We have circumvented this problem by using rod-like viruses TMV, *fd*, Pf1 and M13 that have a biological rather then a chemical origin. The distinct advantage of these viruses over chemically synthesized rods is that Nature has engineered them to be identical to each other, which results in very high monodispersity. Theory and computer simulation predict that hard rods form isotropic, nematic and smectic phases with increasing concentration [8]. Because of their high monodispersity rod-like viruses are the only experimental hard rod system presently available whose phase behavior agrees with this theoretical prediction [9, 10]. In this thesis we study both theoretically and experimentally some aspects of ordering in rod-like *fd* viruses.

The outline of this thesis is as follows. In Chapter II we present the Onsager theory which forms the conceptual basis for most of this thesis. The theoretical results are compared with the experiments on the bacteriophage *fd* and good quantitative agreement is found for rods in high ionic strengths aqueous suspensions. This justifies using *fd* as a model system which approximated the behavior of hard rods. In Chapter III we introduce the experimental system of *fd* virus. We show that we are able to experimentally manipulate important variables determining the phase behavior. Using standard methods of molecular biology we are able to alter contour length of the virus. The effective diameter of the rod is altered by covalently covering the surface of the virus with poly-(ethylene glycol) (PEG) polymer. These modifications will allow us to test fundamental theories of liquid crystal ordering and demixing in monodisperse and bi-disperse rod-like suspensions. Bacteriophage *fd* forms a cholesteric instead of the nematic phase. In the cholesteric phase the av-

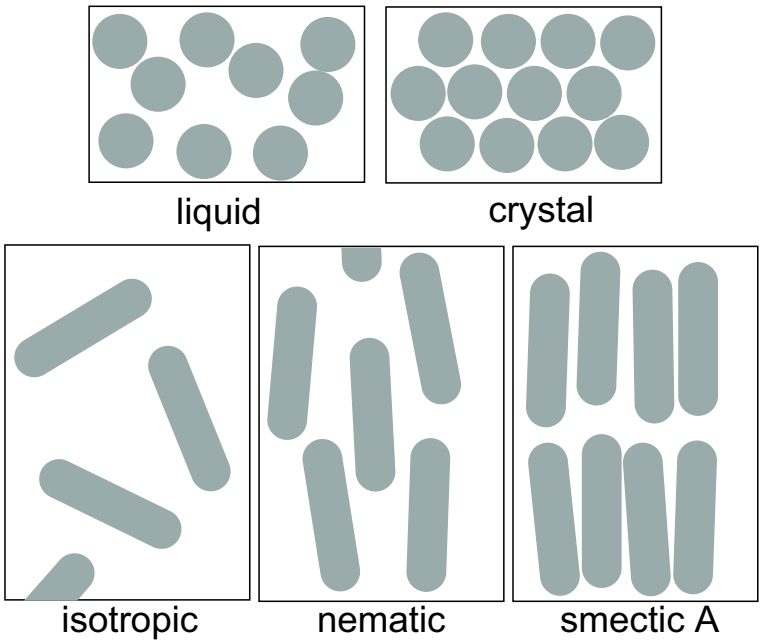

Figure 1.1: An illustration of the stable phases that appear in a system of hard particles. All phase transitions in hard particle fluids are temperature independent and concentration is the only parameter that determines the phase diagram. Hard spheres undergo liquid to crystal phase transition with increasing concentrations, while hard spherocylinders form stable isotropic nematic and smectic phases with increasing concentration. Attractive interactions between spheres are necessary to induce a dilute vapor to dense liquid phase transition. Theoretically these attractions are easily incorporated as a perturbation once the nature of the ground state (hard sphere liquid) is well understood.

erage alignment of the molecules (nematic director) forms a helical superstructure. As discussed in detail in chapter IV the cholesteric phase is a very slight perturbation of the nematic phase and therefore the Onsager theory hold equally well for the isotropic-nematic (I-N) and the isotropic-cholesteric (I-Ch) phase transitions. Although in this thesis we experimentally study the (I-Ch) transition we expect all our results to hold for the (I-N) transitions as well. Therefore we use the I-N and I-Ch terms interchangeably in this thesis. In Chapter IV we investigate the microscopic origin of the cholesteric phase in *fd* virus by measuring the continuum properties of the cholesteric phase.

In Chapter V we turn our attention to the phase behavior of hard rods that interact through both attractive and repulsive interactions. As the strength of the interaction is increased we no longer observe the usual isotropic-nematic phase co-existence. Instead the system exhibits isotropic-smectic phase co-existence. We are able to observe a number of novel kinetic structures during this process of phase separation. Our visual observations are summarized in Chapter VI. In chapter VII we focus our attention on the nematic-smectic phase transition and how this phase transitions is perturbed by the presence of hard spheres or interpenetrating polymers. We investigate this transition theoretically and with the aid of computer simulations.

In this thesis we observe and study both theoretically and numerically a range of novel structures that are formed in a mixture of rods and polymers or rods and spheres. The structure of some of the phases we observe in a rod/sphere mixture are very similar to the structure of amphiphilic (lipid, surfactant, copolymer) systems. However, unlike amphipilic systems where imiscible parts are covalently attached, the rod/sphere and rod/polymer mixtures are free to bulk phase separate at all times. Therefore it is surprising that the rod/sphere mixtures undergo microphase separation under certain conditions. Another surprising aspect, in line with the previous results on ordering in hard particle fluids, is the complexity of the phase

diagram which results from the molecular species interacting with a very simple potential. Experiments on the virus/polystyrene mixture and virus/polymer are an example of an entropy driven microphase separation. All this provides further evidence for the importance of the steric (entropic) interactions in determining the phase behavior.

Chapter 2

Isotropic-nematic phase transition in hard rods and comparison to experiments on *fd* virus

2.1 Introduction

In this chapter we summarize the Onsager theory of the isotropic-nematic (I-N) phase transition of hard rods. The extensions of the Onsager theory to include the effects of charge and flexibility of the rods are presented. Since the Onsager theory is quantitatively valid only for very long rods ($L/D > 100$) we discuss the scaled particle theory which extends the validity of the Onsager theory to smaller aspect ratios. Finally an approximate phase diagram for charged, semi-flexible rods with finite L/D ratios is calculated. This phase diagram is compared to the experimentally available data for the I-N phase transition in the semi-flexible *fd* virus. At ionic strengths higher than 100 mM where ratio of the rod length to diameter L/D_{eff} is large the experiments quantitatively agree with the theory. On the other hand, at low ionic strengths there is a considerable difference between the experiment and the theory. It is speculated that this disagreement is due the counterions disassociated

from the ionic groups on the virus surface, which are not taken into account in the theory.

2.2 Entropy driven ordering and the Onsager theory

At the second virial approximation the most general expression for the free energy of anisotropic hard particle fluid is :

$$\frac{F}{k_bT} = \frac{F_{id}+F_{ex}}{k_bT} = \int_V d\mathbf{\Omega} d\mathbf{r} \rho(\Omega,\mathbf{r}) \ln(\rho(\mathbf{r},\mathbf{\Omega})) - \frac{1}{2}\int_V d\mathbf{r_1} d\mathbf{\Omega_1} \int_V d\mathbf{r_2} d\mathbf{\Omega_2} \rho(\mathbf{r_1},\mathbf{\Omega_1})\rho(\mathbf{r_2},\mathbf{\Omega_2})\Psi(\mathbf{r_1},\mathbf{r_2},\mathbf{\Omega_1},\mathbf{\Omega_2}) \quad (2.1)$$

where $\Psi(\mathbf{r_1},\mathbf{r_2},\mathbf{\Omega_1},\mathbf{\Omega_2})$ is a Meyer-Meyer overlap function whose value equals -1 if there is any overlap between two hard-particles located at positions $\mathbf{r_1}$ and $\mathbf{r_2}$ and angles $\mathbf{\Omega_1}$ and $\mathbf{\Omega_2}$, otherwise it's value is equal to zero. $\rho(\mathbf{r},\mathbf{\Omega})$ is the probability of finding a particle at position $\mathbf{r}$, which points in the direction $\mathbf{\Omega}$. On the one hand, approximating free energy only to the second order in density fails to quantitatively describe the system of hard spheres already at density $\rho \approx 0.05$ [11]. Since the liquid to crystal transition in hard spheres occurs at volume fraction close to 0.5 it is not reasonable to expect that Eq. 2.1 will describe this transition. On the other hand Onsager was the first to recognize that Eq. 2.1 is essentially exact for isotropic rods and the isotropic-nematic phase transition when $L/D \to \infty$ [2]. As will be shown the reason for this is that the I-N phase transition occurs at a volume fraction $\rho \approx 4\frac{D}{L}$. Hence, the larger the aspect ratio, the lower the volume fraction of the I-N transition and therefore expansion of the free energy in density becomes more accurate.

In the Onsager theory the system is assumed to be spatially uniform and

therefore $\rho(\mathbf{r}, \mathbf{\Omega}) = (N/V) f(\mathbf{\Omega})$ where N is the number of rods and V is the volume of the system. Since $f(\Omega)$ indicates the probability that the rod is pointing at a solid angle Ω it should be normalized as follows :

$$\int f(\Omega) d\Omega = 1. \tag{2.2}$$

Once the probability distribution function is known it is easy to calculate the nematic order parameter (S) using the following relation:

$$S = 2\pi \int_0^\pi \left(\frac{3}{2} \cos(\theta) - \frac{1}{2} \right) f(\theta) \sin(\theta) d\theta. \tag{2.3}$$

By minimizing Eq. 2.1 with the respect to the distribution function $f(\Omega)$ we obtain the following integral equation :

$$\log[4\pi f(\theta)] = \lambda - \frac{8\rho}{\pi} \int \sin(\theta) f(\theta) d\theta, \tag{2.4}$$

where $\rho = \frac{\pi}{4} L^2 D \frac{N}{V}$. This integral equation can not be solved analytically but it has been solved with two different numerical procedures which yield almost identical results for the equilibrium distribution function [12, 13]. Although the numerical solution yields the most accurate results it is also possible to proceed by assuming a form of the orientational distribution function :

$$f(\alpha, \cos(\theta)) = \frac{\alpha \cosh(\alpha \cos(\theta))}{4\pi \sinh(\alpha)}. \tag{2.5}$$

Using this ansatz first introduced by Onsager in the second virial approximation to free energy (Eq. 2.1) and evaluating the integrals for the case of hard rods we obtain an expression for the free energy which is a function of dimensionless concentration ρ and orientation parameter α:

$$F(\alpha, \rho) \quad = \quad \rho \log(\rho) + \sigma(\alpha)\rho + \xi(\alpha)\rho^2$$

$$\begin{aligned}\sigma(\alpha) &= \log\left(\frac{\alpha\cosh(\alpha)}{4\pi\sinh(\alpha)}\right) - 1 + \frac{\arctan(e^{\alpha}) - \arctan(e^{-\alpha})}{\sinh(\alpha)} \\ \xi(\alpha) &= \frac{2I_2(\alpha)}{\sinh^2(\alpha)} \end{aligned} \tag{2.6}$$

Although this solution is somewhat different from the numerical solution of Eq. 2.4, the advantage of assuming the probability distribution (Eq. 2.5) is that we obtain an analytical expression for the free energy (Eq.2.6).

It is important to note that in any hard-particle fluid, due to the simplicity of the interaction potential, the energy of any allowed configuration is simply proportional to nkT with n being the number density of particles. Because of this simple fact, the minimum of free energy of a hard particle fluid $F = E - ST = T(\alpha - S)$ (α is a constant) is equivalent to the maximum of entropy. Furthermore, the resulting phase diagram is temperature independent (athermal) because both α and S are independent of temperature. Ordering transitions in hard-particle fluids are still possible because the expression for entropy, or equivalently free energy, splits into two parts. The first integral in Eq. 2.1 is the ideal part of the free energy and always attains a minimum value for the uniform probability distribution $\rho(\mathbf{r}) =$ constant. Therefore this contribution to the free energy always suppresses an ordering transition. The second integral in Eq. 2.1 represents the second virial approximation for the interaction free energy, which under certain circumstances is lower for an ordered state. Therefore the interaction part of free energy drives the system towards ordering. The actual location of the ordering transition is determined from the competition between the ideal and the interaction contribution to the total free energy.

2.3 Onsager theory extended to charged and semi-flexible rods

The Onsager theory outlined in the previous section can be extended to the case where the colloidal rods have a surface charge. The first treatment of the isotropic phase transition of charged rods can be found in the original paper by Onsager [2]. The extension of it to the anisotropic phase can be found in paper by Stoobants et. al. [14]. Besides the hard core repulsion, charged rods have a long range repulsive interaction of the following form :

$$\frac{U_{el}(x)}{kT} = \frac{A' e^{-\kappa(x-D)}}{\sin(\gamma)} \tag{2.7}$$

where x is the closest distance between two charged rods, A' is the proportionality constant obtained by solving the Poisson-Boltzman equation, κ^{-1} is the Debye screening length and γ is the angle between two rods. In the case of charged rods there are contributions to the second virial coefficient from both the hard core excluded volume interaction and the long range electrostatic repulsion interaction. These two contribution can be calculated separately as follows

$$\begin{aligned} \beta(\gamma) &= -2DL^2\sin(\gamma) + 2L^2\sin(\gamma)\int_D^\infty (e^{-\frac{U_{el}(x)}{kT}} - 1)dx \qquad (2.8)\\ &= -2DL^2\sin(\gamma) - 2\kappa^{-1}L^2\sin(\gamma)\left(\ln\left(\frac{A'}{\sin(\gamma)}\right) + C_E + E_1\left(\frac{A'}{\sin(\gamma)}\right)\right). \end{aligned}$$

Integrating function $\beta(\gamma)$ over a uniform orientational distribution function which describes the isotropic phase we obtain the following expression for the second virial coefficient :

$$B_2^{\text{iso}} = \frac{1}{4}\pi L^2 D_{\text{eff}} = \frac{1}{4}\pi D L^2 + \frac{1}{4}\pi\kappa^{-1}L^2(\ln A' + C_E + \ln 2 - \frac{1}{2}) \tag{2.9}$$

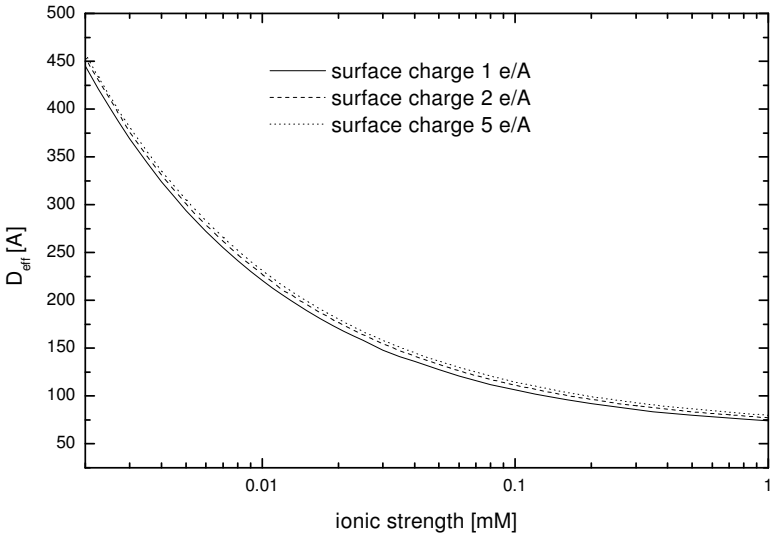

Figure 2.1: The effective diameter for a charged rod calculated from Eq. 2.9 for a range of physical ionic strengths. The physical characteristic take for diameter $D_{\text{bare}} = 66\text{Å}$ is that of the *fd* virus. The value of D_{eff} barely changes as the surface charge is changed from $1e^-/\text{Å}$ to $10e^-/\text{Å}$. Experiments indicate that the surface charge is about $2e^-/\text{Å}$ [15]

Therefore the thermodynamics of charged rods in the isotropic suspension will be equivalent to the thermodynamics of thicker hard rods with the effective diameter (D_{eff}). On the other hand if the cluster function $\beta(\gamma)$ is integrated over an anisotropic distribution function then the relationship given by Eq. 2.9 is no longer exact. The reason for this is that the electrostatic energy is lower for perpendicular rods then for parallel rods. Therefore the charge effectively destabilizes the nematic phase by shifting the I-N transition to higher concentrations and reducing the order parameter of the nematic phase coexisting with the isotropic phase. However, most biopolymers (including *fd* virus) are highly charged in which case it turns out that the electrostatic "twisting" effect is insignificant compared to the excluded volume interactions. Therefore from now on we approximate D_{eff} in the nematic phase by D_{eff} of the isotropic phase. This is reasonable for co-existing phases but we expect this approximation to get progressively worse with increasing concentrations.

The flexibility of the rods is characterized by the persistence length. The

persistence length is the length along the chain after which the direction of the chain becomes uncorrelated. The effect of semi-flexibility on the isotropic-nematic phase transition has been studied by Khokhlov and Semenov [16]. For semi-flexible rods besides orientational and translational entropy it is also necessary to take into account the internal configurations of the semi-flexible chain. This modifies the entropy term in the Eq. 2.1 :

$$\frac{F_(f(\theta),\rho)}{Nk_bT} = \frac{F_{ideal}+F_{ex}}{Nk_bT} = \frac{L}{2P}\int f^{1/2}(\cos(\theta))\nabla f^{1/2}(\cos(\theta))d\Omega + F_{ex}(f(\theta),\rho) \tag{2.10}$$

where ∇ is the Laplacian operator on the surface of the sphere. Eq. 2.10 has been solved in the limit of almost rigid rods (P$\gg$L) and very flexible rods (L$\ll$P) [17, 16]. It is possible to empirically interpolate between these two solutions and obtain numerical approximation for the configurational entropy for rods with arbitrary persistence length as was done by Hentscke, Odijk, and Yang et. al. [18, 19, 20]. In this thesis we use the following approximation for the entropy of a single semi-flexible rod :

$$\sigma(\alpha,\frac{L}{P}) = \ln(\alpha) - 1 + \pi e^{-\alpha} + \frac{L}{6P}(\alpha-1) + \frac{5}{12}\ln\left(\cosh\left(\frac{L}{P}\frac{\alpha-1}{5}\right)\right) \tag{2.11}$$

which was given by the latter authors. The entropy per particle increases with increasing the anisotropy of the orientational distribution function through parameter α.

2.4 Scaled particle theory of semi-flexible rods for Isotropic-Nematic phase transtion

Scaled particle theory for the system of hard rods was developed by Cotter and coworkers [21, 22]. The main advantage of the scaled particle is that it takes into account third and all higher virial coefficients in an approximate way. Therefore this theory should be more adequate at describing the data at higher concentration of rods or equivalently rods with lower L/D ratios. The free energy derived by Cotter is :

$$\frac{F(\delta,\phi,\alpha)}{Nk_bT} = \ln(\phi)+\ln(1-\phi)+\sigma(f(\phi))+\Pi_2(\delta,\alpha)\frac{\phi}{1-\phi}+\frac{1}{2}\Pi_3(\delta,\alpha)\left(\frac{\phi}{1-\phi}\right)^2 \quad (2.12)$$

where ϕ is the volume fraction of rods

$$\phi = \frac{N_{rods}}{V}\left(\frac{\pi}{6}D^3+\frac{\pi}{4}D^2L\right). \quad (2.13)$$

The coefficients Π_2 and Π_3 are given by the following expressions:

$$\Pi_2(\delta,\alpha) = 3+\frac{3(\delta-1)^2}{3\delta-1)}\xi(f(\alpha)), \quad (2.14)$$

$$\Pi_3(\delta,\alpha) = \frac{12\delta(2\delta-1)}{(3\delta-1)^2}+\frac{12\delta(\delta-1)^2}{(3\delta-1)^2}\xi(f(\alpha)) \quad (2.15)$$

and parameter δ is the overall length over diameter ratio of the spherocylinder given by

$$\delta = \frac{L+D}{D}. \quad (2.16)$$

The functions $\xi(\alpha)$ and $\sigma(\alpha)$ are the same translational and orientational entropy terms used in the Onsager theory (Eq. 2.6). We note that the expression for the free energy (Eq. 5.4) reduces to the Onsager second virial approximation for very

long rods ($\delta \to \infty$). On the other hand for spherical particles ($\delta = 1$) it reduces to the Percus-Yevick or scaled particle theory free energy for hard spheres.

2.5 Results

In the previous two sections we briefly summarized the Onsager theory and its extensions to the cases of surface charge, semi-flexibility of the rods, low L/D ratio and high concentration. As was previously done, the most convenient variable to formulate the Onsager theory is the dimensionless concentration

$$\rho = B_2^{iso}\frac{N}{V} = \frac{\pi}{4}L^2 D\frac{N}{V} = \frac{L}{D}\phi \tag{2.17}$$

where ϕ is the volume fraction of the rods and $B_2^{iso} = \pi/4L^2D$ is the second virial coefficient for suspension of hard rods in isotropic solution. By performing the stability analysis of the Onsager equation Kayser and Ravenche found out that the isotropic phase becomes unstable towards orientational fluctuations when $\rho = 4$ [23]. It follows that within the Onsager theory the volume fraction of the hard rods at the I-N transition scales as $\phi = 4\frac{D}{L}$. Therefore the longer the rods are, the volume fraction at the I-N transition decreased and the accuracy of the second virial approximation increases. Numerical calculations of the second and third virial approximations indicate that Onsager theory is quantitatively correct for rods with $L/D > 100$ [24].

However, the second order transition is preempted by a first order phase transition. Numerically minimizing the Onsager free energy with respect to the orientational distribution function and subsequently solving the co-existence equations yields the following concentration of the co-existing isotropic and nematic phases,

$$\rho_{\text{iso}} = 3.289, \quad \rho_{\text{nem}} = 4.192, \quad S_2 = 0.7922, \tag{2.18}$$

as solved by Herzfeld et. al., Lekkerkerker et. al., and Chen [12, 13, 25]. On the other hand the Onsager trial function (Eq. 2.5) yields the following co-existence concentrations :

$$\rho_{iso} = 3.339, \quad \rho_{nem} = 4.487, \quad S_2 = 0.848. \tag{2.19}$$

By comparing exact numerical result with the Onsager approximation we observe a difference in both concentrations of the I-N transition and the nematic order parameter (S_2) of the nematic phase co-existing with the isotropic phase.

The most complete study of the influence of the semi-flexibility on the isotropic-nematic phase transition was presented by Chen [25] who numerically minimized Eq. 2.10 and subsequently calculated the co-existence concentrations. His results and the results obtained by using the Onsager approximation for the orientational distribution function (Eq. 2.5) are shown in Fig. 2.2 for rods with difference degrees of semi-flexibility.

From figure 2.2a we conclude that increasing flexibility destabilized the nematic phase by displacing the I-N transition to higher volume fraction. Increasing the flexibility also drastically reduces the width of the concentration difference between the co-existing isotropic and nematic phases the and the order parameter of the nematic phase as is shown in Fig. 2.2b and Fig. 2.2c respectively. The Onsager approximation (Eq. 2.5) for the ODF qualitatively agrees with the "exact" numerical results. We observe that the difference in $\rho_{\rm iso}$ between the "exact" numerical result and the results obtained with approximate ODF is never larger then 5%. On the other hand, if we compare the nematic order parameter (S_2) at the I-N transition and the co-existence width (W) we observe a large quantitative disagreement (up to 30%) between two different solutions of Eq. 2.10. This demonstrates that comparing I-N co-existence concentrations between a theory and an experiment does not constitute a sensitive test of the theory. For a stringent test of the theory it is also

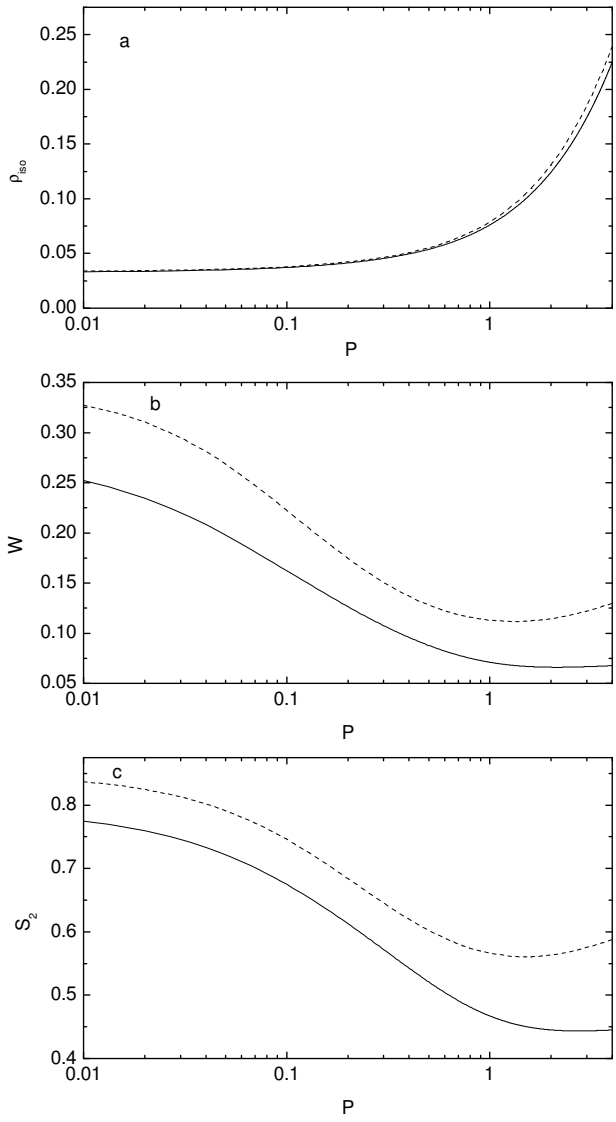

Figure 2.2: Concentration ($\rho_{iso} = (4/\pi)L^2D(N/V)$), number density difference between isotropic and nematic phase ($W = C_n/C_i - 1$) and order parameter (S_2) of the nematic phase co-existing with isotropic phase as a function of the flexibility of the particle $P = L/l_p$. The full line are the exact numerical results within the second virial approximation while, the dashed line are the results obtained by using the Onsager approximation for the orientational distribution function (Eq. 2.5). In all the figures the aspect ratio of the rod is fixed at 100 and the persistence length l_p varies from infinity to 25.

necessary to measure the order parameter (S_2) of the nematic phase. An example of this will be shown in the chapter 5, which deals with the effect of attractions on the I-N transition. In his paper Chen compares his solution with the solution of the Khokhlov and Semenov who also use Onsager approximation to the ODF. The result of Khokhlov and Semenov seemingly agrees much better with "exact" results than what our calculation shows in Fig. 2.2. The reason for this is that Khokhlov and Semenov besides using Onsager approximation for the ODF also approximate the excluded volume $\xi(\alpha)$ by expanding it in powers of α. These two approximations fortuitusly cancel each other and the final result seemingly agrees better with the "exact" numerical solution.

If the flexibility of the rods is increased further a limit is reached where the chain has an overall comformation of the flexible coil which in turn is composed of many persistence length units. If these units themselves satisfy the Onsager criterion ($L > l_p > D$) the problems can be easily solved by rescaling the exclude volume interaction. In this limit it is natural to describe the problem in dimensionless units rescaled by the persistence length :

$$\rho_p = (\pi/4) l_p L D (N/V) = P/D\phi. \tag{2.20}$$

Using the Onsager ODF we obtain the following coexistence concentrations :

$$(\rho_p)_{iso} = 5.409 \quad (\rho_p)_{nem} = 6.197 \quad S_2 = 0.610. \tag{2.21}$$

On the other hand the numerical solution yields the following coexistence concentrations :

$$(\rho_p)_{iso} = 5.124 \quad (\rho_p)_{nem} = 5.509 \quad S_2 = 0.46. \tag{2.22}$$

Here again we note that the values for the coexistence concentrations are in much better agreement with each other than the values for the nematic order parameter.

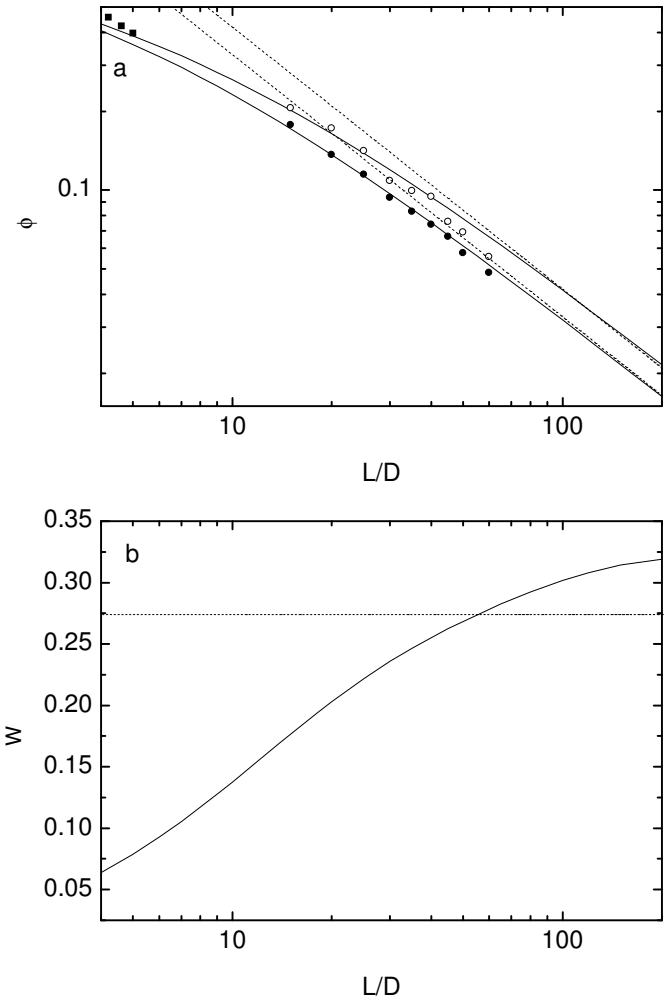

Figure 2.3: Full lines in figure A show the I-N coexistence concentrations as the function of the aspect ratio (L/D) as predicted by the scaled particle theory for rigid rods. The dashed line represents the I-N co-existence as predicted by the theory that only includes second virial coefficient. The circles are the results of the computer simulations [8]. The filled squares at low L/D represents the results from the same work but the coexistence width was too narrow to be measured. The coexistence is plotted in terms of real volume fraction $\phi = \pi D^3/6 + LD^2\pi/4$ while the total aspect ratio including the hemispheres is L/D+1. Figure b shows the predicted width of the co-existence regions $W = C_n/C_i - 1$ as predicted by the scaled particle theory and the second virial coefficient for different L/D ratio.

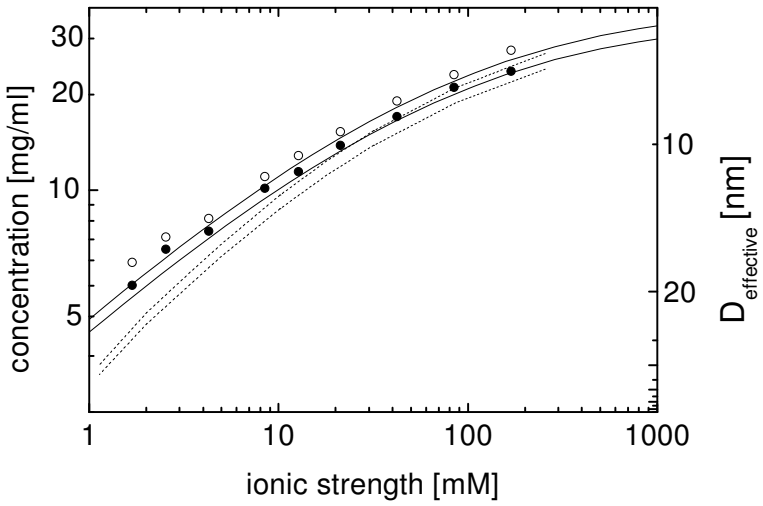

Figure 2.4: The I-N co-existence concentrations measured in an aqueous suspension of *fd* virus by Tang and Fraden [27]. The full line is the numerical solution of Chen for the I-N co-existence which treats excluded volume interactions at the second virial while the orientational distribution function is calculated exactly. The dashed line is the scaled particle solution for the I-N co-existence in which all virial coefficients are included in an approximate way and orientational distribution function has an approximate form given by Eq. 2.5. The scale on the right side indicates the effective diameter of a rod at at I-N transition for a given ionic strength.

The Scaled particle expression (Eq. 5.4) incorporates all the higher virial coefficients in an approximate way. Comparing it's results with the solution obtained through the second virial approximation allows us to test for which range of L/D ratios is the second virial approximation quantitatively valid. The results are shown in Fig. 2.3. At L/D=45 the second virial approximation yields the I-N co-existence concentrations that are 10% different from the scaled particle result. We conclude that for rods with $L/D > 75$ the second virial approximation quantitatively describes the I-N transitions in hard-rods. Currently available computer simulation [8] results agree very well with the scaled particle theory [26]. The scaled particle theory predicts that the width of the coexistence region decreases rapidly with decreasing L/D of the rod.

In figure 2.4 the experimental data points for the isotropic-nematic coexis-

tence concentrations for the semi-flexible virus *fd* are given as measured by Tang and Fraden [27]. The physical characteristics of the *fd* virus are the contour length of 880 nm, bare diameter of 6.6 nm, aspect ration $L/D \approx 130$ and the persistence length $P = L/l_p \approx 0.4$. The colloidal stability of the virus is preserved due to the fact that it has a very high surface charge. The D_{eff} for the dilute isotropic suspension of the *fd* rods is shown in Fig. 2.1 for three different surface charges. Due to the non-linear nature of the Poisson-Boltzman equation changing the surface charge by an order of magnitude has minimal effect on the resulting D_{eff}. The titration experiments indicate that the surface charge of *fd* is about $1e^-/\text{Å}$ [15]. Figure 2.4 shows that increasing ionic strength increases the concentration of the viruses at the I-N transition. On the other hand, increasing ionic strength increases L/D_{eff} which in Onsager theory should decrease the volume fraction of the rods at the I-N transition. The discrepancy can easily be understood if one looks at the condition for instability of the isotropic phase:

$$4/\pi \; L^2 D_{\text{eff}}(N/V) = 4. \tag{2.23}$$

The concentration in figure 2.4 is not proportional to the effective volume fraction but to the number density of the virus. If D_{eff} is decreased with the length of the rod remaining constant, it follows that the number fraction of the virus at the transition has to increase so that condition for the nematic instability (Eq. 2.23) is still satisfied.

The experimental data points are compared to the numerical solution of Chen [25] who approximates the excluded volume interaction by the second virial coefficient and treats the ODF in an "exact" numerical way. When comparing the experiments with the theory we take into account charge by using D_{eff} plotted in Fig. 2.1 instead of the bare diameter. At the first sight the agreement between the theory and the experiment is quite good. However there is reason to believe that this agreement is fortuitous at low ionic strength. For example at 1 mM ionic

strength $D_{\text{eff}} \approx 60$nm which results in the aspect ratio $L/D_{\text{eff}} \approx 15$. Figure 2.3 clearly shows that for these small aspect ratios third and higher virial coefficients can not be ignored. Indeed the results of the scaled particle theory which include these higher coefficients show that the I-N transition is located at significantly lower concentrations than what is found by the experiments and Chen's theory. On the other hand the agreement between the scaled particle theory, the experiments and the theory of Chen is much better at high ionic strengths since L/D_{eff} is larger (at 100mM $L/D_{\text{eff}} \approx 83$) and therefore the excluded volume interactions are more accurately approximated by the second virial coefficient.

We note that the results from the scaled particle theory shown in Fig. 2.4 should also be treated with a degree of scepticism. To compare the scaled particle theory with experiments on charged rods we use the effective diameter of the rod. However the concept of D_{eff} introduced in Eq. 2.9 is only justified for conditions for which the second virial coefficient is quantitatively valid. As was explained earlier the second virial coefficient does not provide a satisfactory treatment of excluded volume interactions of *fd* virus at low ionic strength. There is a recent theoretical attempt to extend the scaled particle theory to charged particles [28, 29]. Unfortunately this theory does not interpolate to Onsager theory for dilute rods as does the scaled particle theory for hard rods. We also note that the twisting factor ignored in our treatment of D_{eff} for *fd* is strongest at low ionic strength [14]. This effect displaces the I-N transition to higher densities. We speculate that the disagreement between the theory and the experiment at low ionic strengths stems from the fact that we ignore the ions dissociated from the charged surface of the virus. Assuming surface charge of $1e^-/\mathring{A}$ a simple calculation yields that at virus concentration of 5 mg/ml the dissociated counterions are present at concentration of 3mM. These dissociated counterions increase the ionic strength which results in displacement of the I-N transitions to higher virus concentration.

2.6 Conclusions

We have started this chapter by summarizing the Onsager theory for the entropy driven I-N transition. To compare the theory to the experimental results on *fd* virus in addition to hard core repulsion we had to account for the surface charge and for the semi-flexibility of the virus. The limits of the second virial approximations are tested by comparing it to the scaled particle theory which account for third and higher virial coefficients. The data on *fd* virus compares very well with the Onsager theory. However the approximations in the Onsager theory, namely $L/D > 50$ fail at low ionic strength. Therefore it is surprising that the theory agrees with the experiment even in this regime where the theory is know to fail. In conclusion the *fd* virus behavior can be quantitatively described as a hard rod with an effective diameter in the regime of high ionic strength. On the other hand there is no comprehensive theory which would take into account all the necessary effects, namely third virial coefficient and surface charge, to described quantitatively the I-N transition in *fd* at low ionic strength. As was previously emphasized a more stringent test of the theory is to measure the order parameter of the nematic phase co-existing with the isotropic phase. Such measurements using small angle x-ray scattering are currently under way in our laboratory [30]

Chapter 3

Bacteriophage *fd* as a versatile model system of rod like colloids

3.1 Introduction

Observation of the nematic phase in aqueous suspensions of rod-like TMV (Tobacco Mosaic Virus) served as an inspiration for Onsager to write his seminal paper on the isotropic-nematic (I-N) phase transition in hard rods (Onsager 1949). Ever since then biopolymers (DNA, TMV, *fd*) have served as important model systems of hard rods and have often been used to test the Onsager theory and its various extensions [31, 32, 33]. In section 3.2 of this paper we briefly outline the advantages of using the semi-flexible rod-like *fd* or closely related M13 virus as a model system of hard rods. We demonstrate that using standard procedures of molecular cloning it is possible to construct genetically modified viruses with widely varying contour length. These viruses are monodisperse enough to form a stable smectic phase. In section 3.3 we outline the synthesis of a *fd*-polymer complex and show that polymers covalently attached to the virus effectively increase the diameter of the rods. By changing the ionic strength it is possible to observe the crossover from the regime where the rods are electrostatically stabilized to where they are sterically stabilized

by repulsion between virus-bound polymers. This synthesis is a convenient way to alter the diameter of the rod and enables us to study bi-disperse rod suspensions with different diameters.

3.2 *fd* virus as a versatile model system of hard rods

TMV and *fd* viruses form, in order of increasing concentration of rods, a stable isotropic, nematic or cholesteric, and smectic phase [9, 10, 34]. These two experimental colloidal systems are the only ones that follow the sequence of liquid crystalline phase transitions that have been predicted by the theory and computer simulations of hard rods [8, 35]. The paucity of systems exhibitng smectic phases is presumably due to polydispersity, which is inherently present in all other polymeric and colloidal experimental systems due to the fact that they are chemically synthesized. In contrast to chemical synthesis, Nature uses DNA technology to produce viruses that are identical to each other, which results in highly monodisperse viruses. This high monodispersity of virus suspensions is the property that makes them an appealing system to experimentally study the phase behavior of hard rods.

However, there are several important disadvantages that viruses have compared to synthethic rod-like polymers. Firstly, although rod-like viruses have very well defined lengths and diameters, studies of how the phase behavior depends on the length to diameter ratio are non-existent for virus suspensions. Secondly, the viruses are charged stabilized and therefore their interactions are not truly hard rod interactions, but in addition to steric repulsion, have a long range soft repulsion. It is important to note that because of the small diameter of the virus the range of this electrostatic repulsion is always comparable to the hard core diameter for the range of ionic strengths for which the stability of the virus against aggregation is not compromised. Also, because of its protein structure it is impossible to de-

crease the surface charge by dissolving it in apolar or weakly polar solvents and preserve the colloidal stability of the virus. It has also been observed that the virus aggregates in an ionic solution of multivalent cations. In this section we show that using standard biological methods it is possible to alter the contour length of the virus while preserving the monodispersity of the virus. In the subsequent section we show that by covalently attaching polymer onto the virus surface we can alter the effective diameter of the virus, and we have achieved stability of the virus even in the presence of multivalent cations. It is our hope that the introduction of these methods will make the viruses a more appealing model system with which to study the phase behavior of rods.

We note that M13 virus with length (L) diameter (D) (L/D≈130) and construct M13-T_n3-15 (L/D≈240) were used in the studies of the concentration dependence of rotational diffusion almost 20 years ago [36]. However, this potentially powerful method was never pursued in subsequent studies. M13 virus is genetically almost identical to *fd* and has the same contour length with coat proteins differing by only a single amino acid; negatively charged aspartate in *fd* (asp_{12}) corresponding to neutral asparagine in M13 (asn_{12}) [37]. This change in a single amino-acid alters the surface charge by about 30 percent and M13 can easily be distinguished from *fd* by gel electrophoresis. All our clones have their origin in M13 virus, which also means that they have lower surface charge than *fd* wild type (*wt*) system.

Since all available data indicates that the length of the virus is linearly proportional to the length of the DNA contained in the virus, the virus length can be extended by simply introducing foreign DNA into M13 wt DNA using restriction endonucleases [38]. However, during large scale preparation we found that the mutant virus would often quickly revert to it's wild type form by deleting the foreign DNA. Another disadvantage of this method is that it is impossible to construct clones that are shorter than M13 wt. Because of these reasons we used a well documented phagemid method to prepare our rod-like viruses with variable contour length [39].

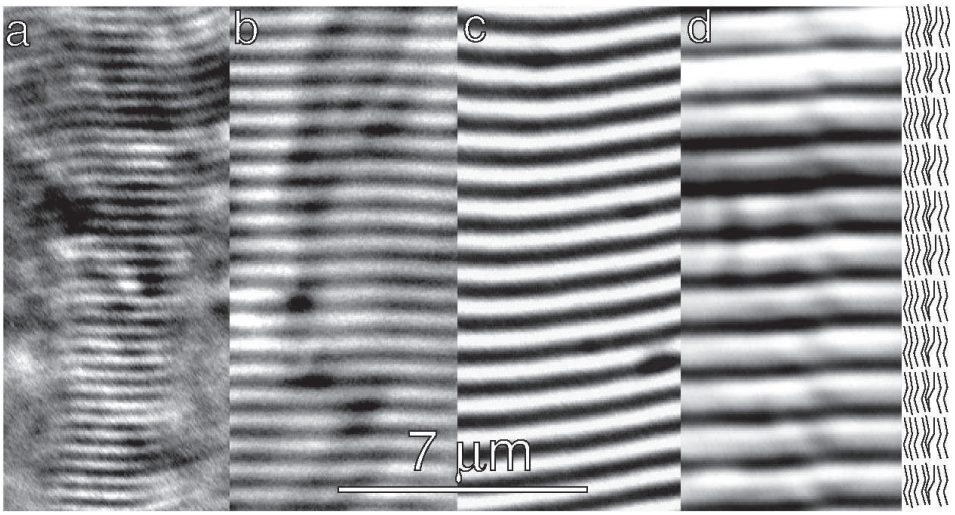

Figure 3.1: Optical micrographs of smectic phases of three different M13 constructs and *fd wt* (c). The periodic pattern is due to smectic layers that are composed of two dimensional liquids of essentially parallel rods, as indicated in the cartoon on the right. From left to right, the contour length of the rod-like viruses forming the smectic phase are 0.39 μm, 0.64 μm, 0.88 μm, and 1.2 μm. The smectic spacing measured from optical micrographs is 0.40 μm, 0.64 μm, 0.9 μm and 1.22 μm from image (a) to (d) respectively.

This method allows us to grow clones that are both longer and shorter than M13 wt. The disadvantage of the phagemid method is that the helper phage M13KO7 (a virus with contour length 1.2 μm) is always present in the final suspension. The volume fraction of the helper phage depends on the bacterial host and can vary from 20% (E. Coli. JM 101) to 5% (E. Coli. XL-1 Blue). Typically, 0.5 - 1 gram of purified virus can be obtained in one to two weeks of work. We found that it is possible to separate the clones from the 1.2 μm long helper phage by adjusting the concentration of the bi-disperse, purified virus suspension such that it is in I-N coexistence. There is a strong fractionation effect at the I-N transition for bidisperse rods, with large rods almost entirely dispersed in nematic phase as is predicted by the theory [13, 40, 41, 42]. Therefore, by keeping only the portion of the suspension in the isotropic phase we can obtain rods with higher monodispersity.

All of the viruses grown using the phagemid method are monodisperse enough

to form stable smectic phases as is illustrated in Fig. 3.1. We note that the measured spacing of the smectic phase (λ) is almost identical to the contour length (L) for all the mutants studied. The qualitative trend that flexibility decreases the smectic layering has been predicted theoretically and observed experimentally [10, 43, 44, 45]. Unfortunately, the theories are not accurate enough to be able to quantitatively predict dependence of smectic spacing on the flexibility of the rod. We expect that the persistence length ($P \sim 2.2\mu$m) of all our clones is the same, because all clones have the same structure and only vary in length. Since the contour length varies, so too does the ratio of contour to persistence length L/P. Thus we expected that the shorter rods ($L = 0.4\mu$m) would be relatively stiffer than the longer ones ($L = 1.4\mu$m) and consequently predicted that the layer spacing would increase for shorter rods. This was not the case as we observed that for all lengths the ratio $\lambda/L \sim 1$.

We also discovered that *fd wt* (Fig 1c) consistently forms a smectic phase at a lower concentration then M13 constructs [29]. This is perhaps explained by the difference in surface charge between M13 and *fd* and the breakdown of the concept of effective diameter at high concentrations. The *fd wt* is more charged than M13 and therefore the highly concentrated aligned rods in nematic phase repel each other more strongly, which results in a higher effective concentration and thus the nematic-smectic phase transition occurs at a lower number density of rods. Note that at low concentrations changing the surface charge by 30% has negligible effect on the effective diameter and the phase behavior of the isotropic - nematic transition (Fig. 1 in [27]).

With the availability of rods with different contour length we are able to experimentally explore a number of important issues pertaining to the phase behavior of hard rods. For pure rods we can address the question of how flexible can a particle be and still form a smectic phase. Another important question is the relative stability of the columnar and smectic phase as a function of rod bidisper-

sity or polydispersity [46, 47, 48, 49, 50]. For mixtures whose lengths are different enough there is also a prediction of microseparated smectic phase [51]. So far there are no experimental studies on these subjects, but with our system we can prepare artificially polydisperse and bidisperse suspensions to explore these issues.

3.3 *fd* virus with covalently attached polymer

Besides preparing viruses with varying contour length we are also able to alter the effective diameter of the virus by coating it with polymer. The amino terminal group of each coat protein of *fd* and M13 virus is exposed to the solution. Through this chemical site we are able to covalently attach water soluble polymer Poly(ethylene glycol) (PEG) to the surface of the virus. End functionalized PEG molecules that readily attach to amino groups were obtained from Shearwater polymers. The chemical reaction was carried out in 100 mM phophate buffer at pH 7.5 for 30 minutes and the virus concentration was kept at 1 mg/ml. For SSA-PEG-5000 the weight concentration of PEG was kept the same as the weight concentration of the virus in the reaction vessel while for SPA-PEG-20000 the concentration was four-fold the virus concentration. The reaction product (*fd*-PEG) was separated from unreacted PEG polymer by repeated centrifugation at 200,000 g. The pellet contained the nematic phase of the *fd*-PEG complex. We diluted a few samples to the concentration of the isotropic-nematic phase co-existence, and after an exceedingly long time (up to few months), we observed macroscopic phase separation. The measured width of the co-existing concentrations did not differ from the measured width in *fd wt*, which is about 10% [27]. This is an indication that the absorbed polymer does not significantly alter the flexibility of the rod-like particles. We infer this from the well established fact that the width of the I-N coexistence is very sensitive to the flexibility of the rod [25]. If we had observed widening of the I-N coexistence it would have been an indication that polymer effectively increases rigidity of the

rod. Because of the extremely long time required for complete phase separation, in order to obtain the points in Figure 2 we diluted the nematic phase until there was no more birefringence observed. We presume that this concentration is equal to the concentration of rods in isotropic phase coexisting with the nematic phase.

To interpret the data in Figure 2 we need the concept of the effective diameter ($D_{\rm eff}$) introduced in previous chapter. Basically it is possible to incorporate the effect of long range repulsion due to surface charge by exchanging the bare diameter with an effective diameter $D_{\rm eff}$, which can be rigorously calculated and is roughly equal to the distance between two rods where the intermolecular potential is equal to thermal energy of 1 k_bT. At high ionic strength $D_{\rm eff}$ approaches the bare diameter, while at low ionic strength $D_{\rm eff}$ is much larger then the bare diameter, and is typically several Debye screening lengths. The condition for the instability of the isotropic phase for charged rods becomes $c\,\pi L^2 D_{\rm eff}/4 = 4$. It follows that the bare rod number density at the I-N phase transition is inversely proportional to $D_{\rm eff}$. This is experimentally observed for *fd wt* over a wide range of ionic strengths as shown with square symbols in Fig. 3.2. The full line, which contains no adjustable parameters, is the numerical solution of the I-N transition for semiflexible rods where $D_{\rm eff}$ is calculated by an extension of the Onsager theory (Chen 1993).

Water at room temperature is a good solvent for PEG polymers, which approximate Gaussian coils. Thus PEG coated surfaces interact with each other through long range repulsion [52, 53]. Therefore in our *fd*-PEG system, in addition to the already present electrostatic repulsion between the charged virus surfaces, we introduce repulsion due to the attached PEG molecules. We expect that for polymers with large molecular weight and/or at high ionic strength the dominant interparticle interaction, and consequently $D_{\rm eff}$ is completely determined by the polymer diameter because the ionic double layer is confined deep within the attached polymer. The opposite is true at low ionic strength and/or low molecular weight polymer. This is exactly the behavior that is shown in Figure 2. For *fd* grafted

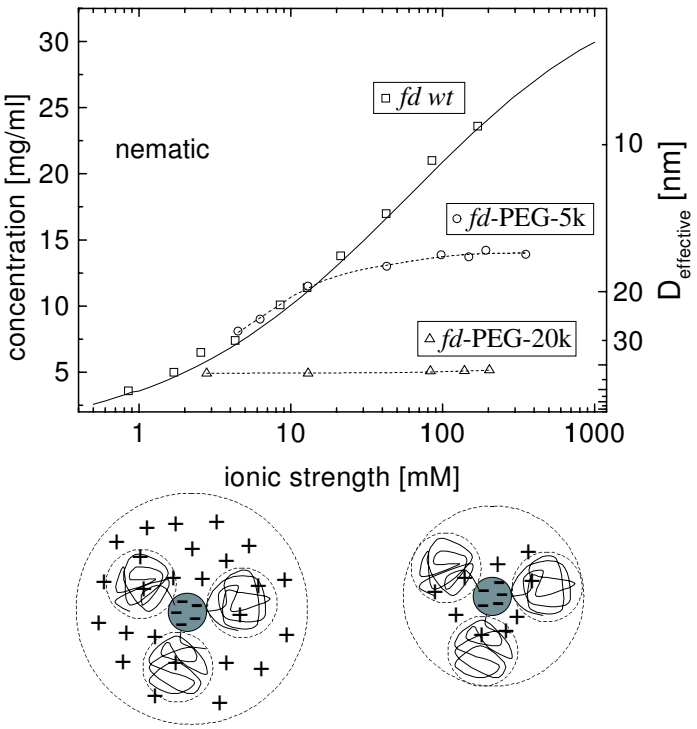

Figure 3.2: Concentration of the virus rods in coexisting isotropic and nematic phases as a function of ionic strength and thickness of the PEG layer covalently attached to the virus. Square points indicate the I-N transition in *fd wt* and were taken from previous work citeTang95. The relationship between the I-N co-existence concentration (c) and electrostatic effective diameter is $c[\mathrm{mg/ml}] = 222/D_{\mathrm{eff}}[\mathrm{nm}]$ and is drawn as a solid line. Circles indicate the I-N transition in *fd* coated with PEG-5,000, while triangles refer to the *fd* virus coated with PEG-20,000. When calculating the concentration of *fd*-PEG we only take into account the *fd* core since the polymer density is not known. The dashed lines are a guide for the eye. At low ionic strength, electrostatic repulsion determines D_{eff}, while the grafted polymer sets D_{eff} at high ionic strength, as indicated in the cartoon of a cross-section of the PEG-virus complex.

with 20 k M.W. PEG (*fd*-PEG-20,000) we observe that for ionic strengths greater than 2 mM the I - N transition is independent of ionic strength. This implies that D_{eff} for the *fd*-PEO-20,000 system is determined entirely by polymer repulsion. The effective diameter of the particle can be extracted from the I-N co-existence concentrations since we have shown that there is a relationship between the effective diameter and concentration of virus: c [mg/ml] $= 222/D_{\text{eff}}$ [nm]. For *fd*-PEG-5,000 the I - N transition changes from being dominated by polymer stabilization at high ionic strength to electrostatic stabilization below 20 mM ionic strength. Because this transition from polymer dominated to electrostatic dominated repulsion occurs at a higher ionic strength for *fd*-PEG-5,000 compared to *fd*-PEO-20,000, the effective diameter of *fd*-PEG-5,000 is smaller than that for *fd*-PEO-20,000. The formula relating the molecular weight (M_w) of PEG to it's radius of gyration (R_g) is $R_g = 0.215 M_w^{0.583}$ Å [52]. From Figure 2 we can calculate that *fd*-PEG-20000 system has $D_{\text{eff}} = 45$ nm, which is approximately equal to $D_{\text{bare}} + 4R_g = 35$ nm. *fd*-PEG-5000 complex has $D_{\text{eff}} = 17$ nm at high ionic strength, while $D_{\text{bare}} + 4R_g = 19$ nm. This suggests the model of the polymer being a sphere of radius R_g attached to the surface of the virus, although we expect that the polymer is deformed by the virus to some extent. In principle, if the exact shape of the repulsive interaction between two polymer covered cylindrical surfaces is known, and if the number of attached polymers per virus is measured, it would be possible to theoretically calculate the phase diagram for rods with attached polymers and compare it to experimental findings. However, we have not yet developed a method to accurately measure the polymer surface coverage.

We can use our system of rods with different diameters to study some basic problems in the physics of colloidal liquid crystals. To prepare a binary mixture of rods with different diameters we simply mix *fd wt* and *fd*-PEO. The ratio of the diameters is equal to the ratio of the concentrations at which these two systems undergo the I-N transition. An additional advantage of this system is that this

ratio can be altered in continuous way by simply adjusting ionic strength. From Fig. 3.2 it is possible to deduce that at 200 mM ionic strength the *fd*-PEO complex has effective diameter about 5 times thicker then *fd* wt. We have observed both isotropic-isotropic and nematic-nematic demixing in binary mixtures of *fd*-PEG-20000 and *fd* wt. Comparison to available theories is currently underway [54, 55]. In summary, a combination of genetic engineering and post-expression chemistry has resulted in the production of gram quantitites of monodisperse rods varying in length from $0.4 - 1.4\mu$m and diameter 10 - 50 nm.

Chapter 4

Cholesteric phase in bacteriophage *fd*

4.1 Introduction

The system with the simplest intermolecular interaction known to exhibit all the essential features of the nematic state is that of a hard rod suspension [2, 35]. Because of its inherent simplicity, much effort has been put into understanding the relationship between the microscopic parameters of hard rods and the resulting liquid crystalline behavior at the macroscopic level. In nature it often happens that a symmetry of the nematic phase can be reduced to form a cholesteric phase, where the nematic director follows a helical path in space. Formation of such a phase at the macroscopic level is usually associated with chirality of molecules at the molecular level. Details of how a simple change of a few atomic positions, required to make a molecule chiral, causes a drastic change in self organization at the macroscopic level remains unknown. However, in the continuum limit, where details of the microscopic interactions are ignored, formation of the cholesteric phase is understood as a competition between two elastic energies. On one hand, the free energy of a chiral nematic is lowered in a twisted state because of the torque a chiral molecule

exerts on it's neighbor. Such a contribution to the free energy is characterized by the "twist" constant K_t. On the other hand, creation of an elastically distorted state characterized by the usual twist elastic constant K_{22} raises the free energy [56]. It follows that the wavelength of the cholesteric pitch is proportional to the ratio of K_t/K_{22}. At present, the challenge lies in calculating the value of the "twist" constant K_t for a given molecule with known microscopic interactions.

Inspired by work of Onsager, Straley made the first attempt to explain the microscopic origin of the cholesteric phase [57, 58]. He considered rods with threads of definite handiness, and for the first time obtained an expression for K_t as a function of the microscopic parameters of a threaded rod. As in the case of Onsager's hard rods, Straley's cholesteric phase is purely entropy driven. The non-zero value of the chiral "twist" constant K_t is associated with the free volume gained as threaded rods approach each other at a well defined angle. This work was later extended to account for flexibility of rods [59, 60].

It is not clear if there are lyotropic liquid crystals where the cholesteric phase is purely entropy driven and therefore most of the predictions of the Straley model remain untested. An alternative proposal for the origin of a non-zero K_t constant involves chiral attractions of van der Waals origin [61]. It is likely that for almost all experimental systems both entropic temperature-independent interactions and attractive temperature-dependent interactions contribute to the cholesteric twist, further complicating the problem. Harris and coworkers noticed that if the threaded rod is allowed to rotate freely around it's long axis, chirality will be effectively averaged away and proposed that short-ranged bi-axial correlations are critical for formation of a cholesteric phase [62, 63]. The implication of their work is that all mean-field theories, like the one of Straley, do not capture the essence of cholesteric phase since they ignore all correlations.

Bacteriophage *fd* is a chiral, monodisperse rod-like colloid that forms a cholesteric phase with a characteristic "fingerprint" texture shown in Fig. 4.1a [64]. *fd* has a

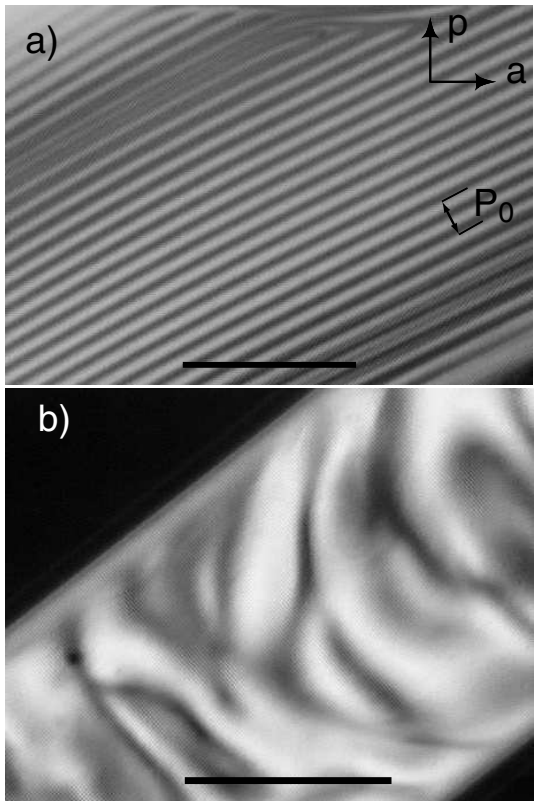

Figure 4.1: (a) Typical texture of a cholesteric phase of a liquid crystalline sample of *fd* observed with polarization microscopy. Dark lines correspond to regions where the rods are perpendicular to the plane of the paper and bright lines correspond to regions where rods are in the plane of paper. The length of the cholesteric pitch (P_0) spans two bright and two dark lines as indicated in the micrograph. The concentration of the *fd* virus is 48 mg/ml and the ionic strength is 8 mM. The positions of the polarizer (p) and analyzer (a) are indicated in the upper right corner. (b) Texture observed with a polarization microscope for a nematic phase formed by filamentous virus Pf1. A lower limit of the pitch of Pf1 is the capillary diameter of 0.3 mm. Although at the molecular level the two viruses have remarkable similarity there is no evidence of a cholesteric phase in Pf1 as indicated by lack of a fingerprint texture. The sample concentration is 38 mg/ml and the ionic strength is 8 mM.

contour length of 880 nm [65], persistance length of 2200 nm [66] and a linear charge density of $2e^{-}/\text{Å}$ at pH 8.1 [15]. However, Pf1 a chiral virus with a structure extremely similar to *fd* [67, 68] does not show any evidence of forming a cholesteric liquid crystal as shown by the absence of a "fingerprint" texture in Fig. 4.1b . This sets the lower limit of the cholesteric pitch of Pf1 virus to the size of the capillary. *The theoretical challenge is to explain why two such similar chiral molecules have extremely different values of the cholesteric pitch.*

The concentrations of the co-existing isotropic and cholesteric phases are quantitatively explained by the Onsager theory establishing *fd* as an ideal model of hard rods [27, 32]. On the other hand, the origin and mechanism of the formation of the cholesteric structure in liquid crystalline *fd* remains a challenge. It is important to note that the Onsager theory predicts equally well the concentration dependence of the isotropic-nematic and isotropic-cholesteric first order phase transition. The reason for this being that the free energy difference between the isotropic and nematic phase is much larger than the free energy difference between the nematic and cholesteric phase. The average twist in the cholesteric phase between two neighboring molecules is generally less then 0.1°. This is negligible when compared to the magnitude of director fluctuations of rod-like molecules in the nematic phase, which are typically around 10 degrees.

In this paper we study in detail the continuum properties of the cholesteric phase formed by *fd* virus. We measure the dependence of equilibrium pitch on concentration and ionic strength and compare it to theory. For two ionic strengths we also measure the value of the twist elastic constant (K_{22}) as a function of concentration. Initial studies of the cholesteric phase of *fd* can be found in the thesis of Oldenbourg [69]

4.2 Experimental Results

Bacteriophage *fd* was grown and purified using standard techniques of molecular biology [39]. A stock solution at a volume fraction of 5% was dialyzed at room temperature against Tris-HCl buffer at pH 8.1 of the desired ionic strength and 3 mM sodium azide (NaN_3) was added to prevent any bacterial growth. This solution was spun in an ultracentrifuge which resulted in very viscous irridescent pellet indicating a smectic or crystalline order. The pellet was resuspended at 4°C overnight in the amount of buffer so that its final concentration was just above the cholesteric-smectic transition [10]. A dilution series was made from the smectic to isotropic phase. The concentration was measured using the extinction coefficient $OD^{1cm}_{269nm} = 3.84$ [32]. Quartz x-ray capillaries of 0.7 mm diameter were cleaned with sulfuric acid and repeatedly rinsed with de-ionized water before being filled with *fd* samples. After 24-48 hours the sample would equilibrate and a typical cholesteric texture was observed. As described previously a *fd* suspension exhibits an increase in the isotropic-cholesteric concentration over a period of few weeks [70]. The origin of this time dependence is not known (although we suspect bacterial growth). We also observed that the cholesteric pitch systematically increases over the same time period. Typically the values of the co-existence concentrations shift by 1% per week for first few months after the sample is prepared [71]. Because of this effect we performed measurements on samples that were at most a few days old.

When viewed under a polarizing microscope the cholesteric phase displays typical dark and bright stripes indicating that molecules are perpendicular and parallel to the plane of polarizers, respectively as is shown in Fig. 4.1. The distance between two bright lines is equivalent to half the value of the pitch P_0. The microscope objective was focused on the mid-plane of the cylindrical capillary and the picture was displayed on a video monitor where the cholesteric pitch was measured using a ruler. Measurements of pitch are very sensitive to defect and boundary conditions and can vary by as much as 20% within the same sample. However,

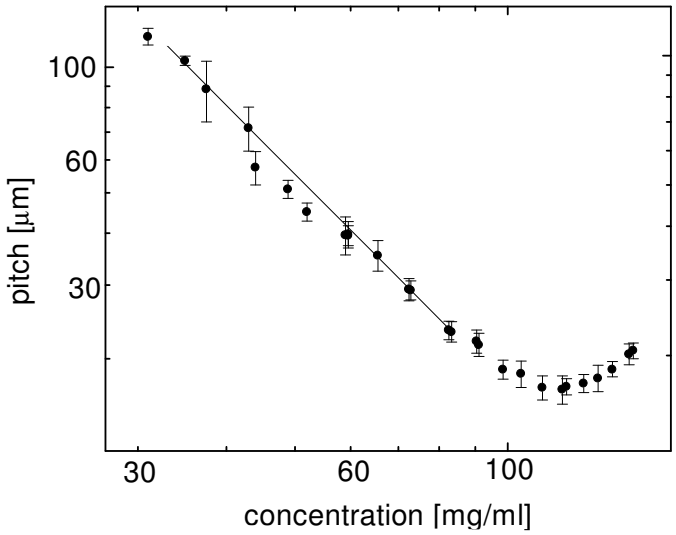

Figure 4.2: Log-Log plot of the cholesteric pitch (P_0) versus concentration (c) of the *fd* virus. The ionic strength was 53 mM. A fit to $P_0 \propto c^{\nu}$ reveals the scaling exponent to be -1.65 ± 0.05. The data spans the entire range of concentrations of the cholesteric phase for this ionic strength and temperature. The sample is isotropic below 30 mg/ml and smectic above 150 mg/ml.

by repeating the measurement 15-25 times along the full length of the sample it is possible to get a reproducible value of the cholesteric pitch.

As the concentration of *fd* is increased we observe a first order isotropic to cholesteric transition [27]; which is followed by a first order cholesteric to smectic phase [10]. We measured the pitch of the cholesteric phase for concentrations ranging from the isotropic to the smectic phase. The typical behavior of cholesteric pitch as a function of concentration is shown in Fig. 4.2. We observe that the pitch decreases with increasing concentration until it saturates at a certain value. As the concentration of the virus increases further and approaches the smectic transition we observe a slight unwinding of the pitch. This unwinding of the cholesteric pitch close to the smectic transition has been observed before in thermotropic cholesteric liquid crystals [72]. It is generally assumed that it is due to pre-smectic fluctuations in the cholesteric. Curiously, when we looked for these pre-smectic fluctuations with light scattering we did not observe any [10], even thought other virus liquid

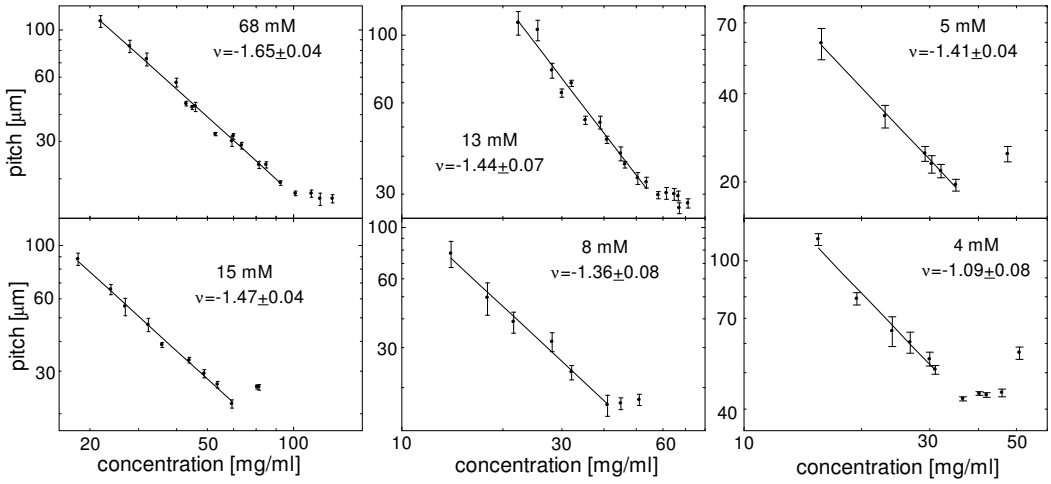

Figure 4.3: Log-Log plots of the cholesteric pitch dependence (P_0) versus *fd* concentration (c) for six different ionic strengths ranging from 68 mM to 4 mM. In each plot data was fitted to an equation of form $P_0 \propto c^{\nu}$. At the highest ionic strength the exponent ν equals -1.65±0.04 and systematically decreases with decreasing ionic strength until it reaches the value of -1.09±0.08 for the lowest ionic strength of 4mM. Each data set spans the entire cholesteric phase from the isotropic boundary at low concentrations to the smectic phase at high concentrations.

crystals (TMV) do show strong pre-smectic fluctuations [73]). At the cholesteric-smectic phase boundary the cholesteric pitch abruptly unwinds. We repeated the measurements for a range of ionic strengths from 4 mM to 63 mM as shown in Fig. 4.3.

By measuring the critical magnetic field necessary to induce the cholesteric to nematic phase transition it is possible to deduce the value of the twist elastic constant [56, 74, 75]. The following formula (in c.g.s. units) relates the critical field to the value of the twist elastic constant K_{22}

$$H_c = \frac{\pi}{2}\left(\frac{K_{22}}{\chi_v}\right)^{\frac{1}{2}} q_0 = \pi^2 \left(\frac{K_{22}}{\chi_v}\right)^{\frac{1}{2}} \frac{1}{P_0} \tag{4.1}$$

The value of the diamagnetic anisotropy $\chi_0 = \chi_{\parallel} - \chi_{\perp}$ per molecule for *fd* is 7×10^{-25} erg/G^2 in c.g.s. units [76]. To convert χ_0 to the diamagnetic anisotropy per unit volume χ_v used in Eq. 4.1 it is necessary to multiply χ_0 with the number of

fd molecules per 1 cm^3 (n) given by $n = cN_A/M_W$ where c is the mass concentration of *fd*, $M_W = 1.64 \times 10^7$ g/M [32] is the molecular weight of *fd*, and N_A is Avogrado's number. We note that the reported value of χ_0 used in this paper [76], is an overestimate (by at most a factor of two) of the actual value [77].

We placed the sample with the long axis of the cylindrical capillary parallel to the magnetic field and simultaneously observed the unwinding of the cholesteric pitch under a microscope. Theoretically we expect that the equilibrium pitch will scale as the fourth power of applied field. Utilizing this sharp dependence on magnetic field we measured the highest value of the field at which the characteristic fingerprint cholesteric texture could still be observed and the lowest field at which we observed no cholesteric texture. Using Eq. 4.1 we can calculate the range within which we expect the true value of twist elastic constant. We have measured the value of the twist elastic constant for various *fd* concentrations at two ionic strengths of 68 mM and 13 mM as is shown in Fig. 4.4.

The dependence of the cholesteric pitch on temperature is shown in Fig. 4.5. For this part of the experiment phosphate buffer was used because of the smaller temperature dependence of pK_a. As the temperature is increased we observe rapid unwinding of the cholesteric pitch. The measurements are reversible and upon a sudden temperature quench the sample winds up within a few minutes as the cholesteric pitch attains its equilibrium value.

4.3 Disscusion and Conclusion

Bacteriophage *fd*, as most other biological colloids, has a charged surface to maintain its stability in solution. Onsager was first to show that in the dilute limit the free energy of a charged rod is approximately equal to a free energy of a neutral rod with an effective diameter larger than its bare diameter [2, 14]. It follows that the volume fraction of the isotropic to nematic phase transition scales with D_{eff}. The

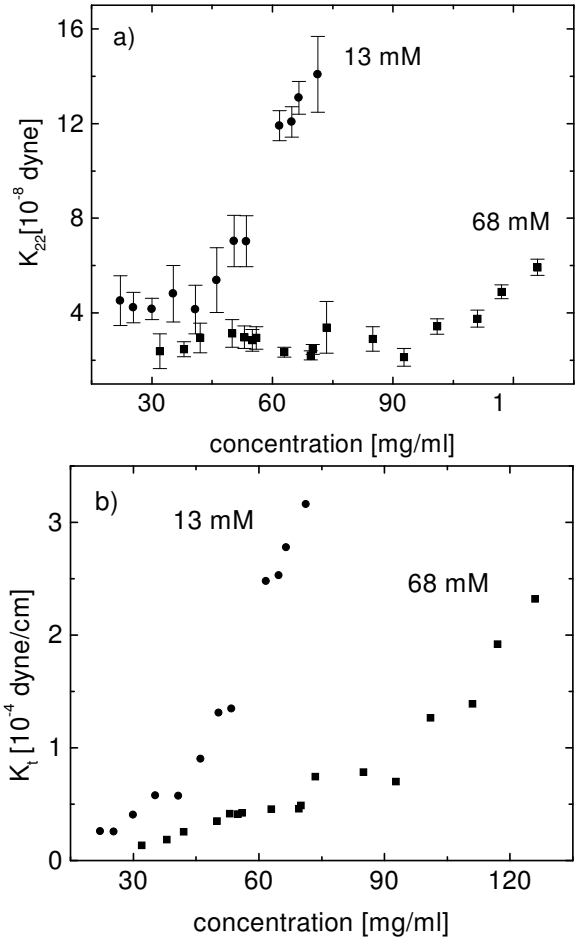

Figure 4.4: a) Concentration dependence of the twist elastic constant (K_{22}) determined by measuring the critical magnetic field required for inducing the cholesteric to nematic transition at two ionic strengths of 13 mM and 68 mM. Error bars indicate a range between lowest magnetic field required to unwind the sample and the highest magnetic field at which there is still evidence of the cholesteric phase. b) Chiral "twist" constant (K_t) calculated from the relation derived from continuum theory $K_t = \pi K_{22}/P_0$ for two ionic strengths of 13 mM to 68 mM. Note that the sample concentrations at higher ionic strength of 68 mM do not span the entire cholesteric range. The reason for this is that the accessible magnetic fields were not strong enough to completely unwind samples with very high concentration.

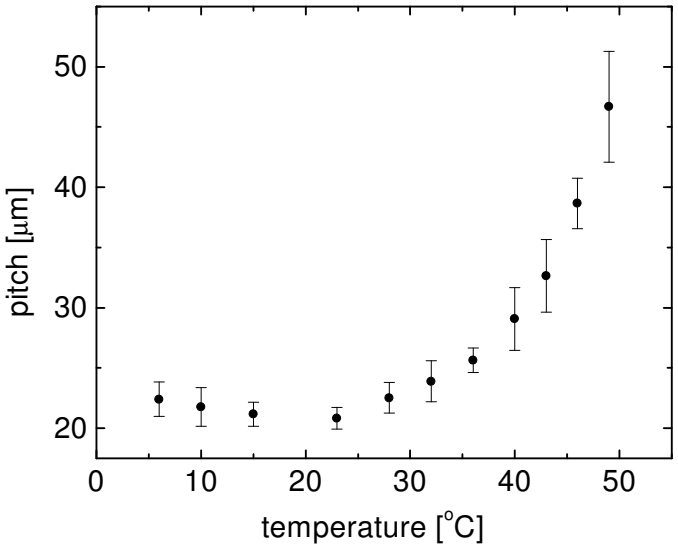

Figure 4.5: Dependence of *fd* cholesteric pitch on temperature. The rapid increase in pitch at high temperatures is not due to denaturing of the virus since the sample regains the original cholesteric structure upon cooling to room temperature. The concentration of the *fd* sample was 32.5 mg/ml and the ionic strength was 8mM. The sample was far from the cholesteric-smectic phase boundary and therefore the pitch unwinding cannot be due to pre-smectic fluctuations.

dependence of D_{eff} on ionic strength for *fd* was calculated previously [27] and the concentration dependence of the co-existing isotropic-cholesteric phases as a function of ionic strength were previously investigated [27].

Motivated by the predictions from various theories [58, 59, 60] we have tried to fit our measurements of the pitch to an exponential form $P_0 \propto c^{-\nu}$ as shown in Fig. 4.3, for ionic strengths from 4 mM to 68 mM. At 68 mM ionic strength we find that the scaling exponent ν has a value of 1.65 ± 0.05. Physically, at high ionic strength the Debye screening length κ^{-1} becomes very small and the effective diameter approaches the hard rod limit [27]. However, even for 68 mM ionic strength, D_{eff} (13nm) is still considerably larger then the bare diameter (6.6 nm). As the ionic strength decreases to 4mM, D_{eff} increases to about 30 nm. Experimentally, we find that the exponent ν systematically decreases with decreasing ionic strength until it reaches the value of 1.09 ± 0.08 for low ionic strengths of 4mM.

Other experimental investigations of lyotropic cholesteric liquid crystals involved the neutral synthetic polymer poly-benzyl-L-glutamate (PBLG) [78, 79], charged DNA [80] and charged cellulose suspensions [81]. In the case of PBLG, the dependence of pitch on concentration scales with exponent $\nu = -1.8$. In the limit of high ionic strength we measure the value of the equivalent exponent for *fd* to be -1.65. It might be expected that as ionic strength is further increased and *fd* increasingly becomes hard rod-like the agreement between PBLG and *fd* data would be even better. Experimental results for both *fd* and PBLG are close to the theoretical prediction for the scaling constant ν due to Odijk and Pelcovits which are -1.66 and -2.0 respectively [59, 60].

For DNA and closely related synthetic double-stranded RNA there are conflicting reports in the literature. Jizuka et. al. [82], in their study of double-stranded RNA, reported the exponent to be -1.1. Senechal et. al. [83] on the other hand, finds that the scaling exponent for an equivalent system to be -0.5. One possible explanation for this discrepancy is the fact that the samples used had different ionic strength. Senechal et. al. did their experiment in distilled water, while Jizuka's experiments were done at an ionic strength of 100mM. This agrees with our observations about the influence of ionic strength on the scaling exponent. For DNA of contour length equal to the persistence length, Van Winkle reported that the cholesteric pitch is independent of the concentration [80]. However, it is also reported that DNA forms a pre-cholesteric phase with large cholesteric pitch and undetermined structure. This is in contrast to the phase behavior of *fd* where there is no sign of any transition between two cholesteric phases of different pitches.

Using a magnetic field induced cholesteric to nematic phase transition we have measured the concentration dependance of the elastic constant K_{22}. Although the data is noisy, the value of K_{22} is almost constant in samples of low concentration. Once the concentration of the virus is close to the smectic phase concentration, the value of K_{22} rapidly increases. It is interesting to note that samples at low ionic

strength have a significantly greater plateau value of K_{22} than the high ionic strength samples, in contradiction to the theory of elastic constants that takes into account the charge of rod-like particles [84]. Dupre [78] measured the value of the twist elastic constant in PBLG and found that there is little variation over the entire concentration range, which agrees with the plateau we observe in *fd* samples. However, in PBLG there is no sudden increase in K_{22} at high concentrations. Measuring values of the twist elastic constant (K_{22}) and the pitch for identical samples enabled us to obtain values of the chiral twist constant K_t using the relation $P_0 = 2\pi K_{22}/K_t$ [63] as shown in Fig. 4.4.

Sato [85] and coworkers have found that the expression for the cholesteric pitch splits into an entropic and enthalpic part. The entropic part, due to hard core repulsive forces, is temperature independent while the enthalpic part, due to attractive forces, scales inversly with temperature. They measured the temperature dependence of the cholesteric pitch for a number of liquid crystalline polymers and found that the pitch scales with inverse temperature. It is important to stress that their analysis is thermodynamic and therefore disregards all complex details of molecular interactions. Surprisingly, we find that the temperature dependence of the cholesteric pitch of *fd* does not agree with this general thermodynamic formalism. A possible source of this discrepancy lies in the assumption used by Sato et. al. that changing temperature has no effect on the internal structure of the polymer. While this is true for most synthetic polymers, it is well known not to be the case for bioploymers. Viruses Pf1 and M13 undergo structural symmetry transitions upon decreasing temperature below 8°C and changing surface charge, respectively [37]. There are also indications that the flexibility of *fd* depends non-monotonically on temperature [71]. Any one of these factors could be the reason for the unusual dependence of pitch on temperature.

Chapter 5

Isotropic-nematic phase transition in rods with attractive interactions

We present an experimental study of the isotropic-nematic phase transitions in a suspension of rods, which besides hard core interactions has additional long range attractive interactions and soft repulsive interactions. The attractive potential is induced by adding polymers, which lead to the well known depletion interaction, while the range of repulsive potential is regulated by the ionic strength of the suspension. The phase diagrams are measured for a variety of intermolecular potentials. The order parameter of the nematic phase co-existing with the isotropic is also measured for a range of polymer concentrations. The experimental results are compared with the existing theoretical predictions for the isotropic-nematic (I-N) transition in rods with attractive interactions and although the theory and experiments agree qualitatively, significant quantitative differences are found.

5.1 Introduction

It has been known for a long time that the interaction betweens two molecules can be separated into short range repulsive (steric) interactions and a long range attractive

interactions. These intermolecular interactions lead to a picture of dense liquids for which the reference system is that of hard spheres with an effective diameter while the attractive interactions are treated as a pertubation to the hard sphere ground state. Such a pertubation theory has it's first origins in the van der Waals equation of state. Due to this reason there has been a substantial effort over the past 50 years to develop an understanding of the behavior of hard spheres.

Parallel to these developments, a statistical mechanical theory of hard anistotropic particles in the context of the isotropic-nematic phase transition was developed by Onsager in 1949. The Onsager theory is based on the realization that while the virial expansion of free energy diverges for hard spheres with increasing concentration, it converges for hard rods with sufficiently large aspect ratio at the isotropic-nematic (I-N) phase transition. In fact, the theory with the second virial approximation quantitatively describes the system with $L/D > 100$ at the I-N transition. The theory of hard rods was extended by Onsager and others to rods which have a soft repulsion due to surface charge[2, 14].

While incorporating attractions into the system of hard spheres is relatively easy, [86, 11] the analogous task for a system of hard rods is much more difficult. The difficulty arises from the the fact that attractive rods are in the lowest energy state when they are parallel to each other. These are exactly the configurations that need to be avoided if the second virial term is to describe the system with sufficient accuracy [87]. Therefore, unlike the system of hard spheres where it is possible to introduce attractions by applying the pertubation scheme about the hard sphere reference state it is not possible for an assembly of rods to be accurately described by the second virial coefficient [88, 89]. For the pertubation theory to work the free energy of the unperturbed liquid of rods needs to take into account third and higher virial coefficients. Lekkerkerker et. al. have used computer simulations and the scaled particle expression for free energy, which approximates higher virial coefficients, to study the influence of attractive interactions on the I-N phase

transition [90, 91].

If attractions are introduced to hard spheres the assembly will decrease it's energy by decreasing the average separation between spheres, which in turn increases the density of the stable liquid phase. Unlike spheres, if attractions are introduced into rod-like particles the system can lower it's energy by either increasing it's density, or increasing it's alignment, or a combination of both responses. Therefore to gain an understanding of the phase behavior it is important to measure both the densities of the coexisting isotropic and nematic phases and the order parameter of the nematic phase.

Experimentally an easy way to induce attraction is to add a non-adsorbing polymer to the colloidal suspensions, which leads to the well known depletion interaction first described by Asakura and Ossawa [92]. The range and the strength of the attraction can be controlled by the size of the polymer and the polymer concentration respectively. One important difference between polymer induced depletion attraction and attraction due the van der Waals origin is that in the polymer/colloid mixture there is polymer partitioning between the two coexisting phases. Due to this partitioning the strength of attraction between two colloids in a coexisting isotropic phase is not the same as between two rods in the nematic phase.

It is important to mention that there have been previous experiments on the I-N transitions in mixture of boehmite rods and polystyrene polymer [93]. However interactions between the boehmite rods are not completely understood and the full measurement of the phase diagram was not possible due to the formation of a number of non-equilibrium states. In this paper we experimentally study the I-N transitions in the presence of attractive interactions. As a reference hard-core system we use the aqueous suspension of the rod-like *fd* virus particles. Previous work has shown that the experimentally determined phase behavior of *fd* virus is consistent with the theoretical predictions for hard rods [27, 32, 10, 34]. As the strength of the attraction is increased we no longer observe the isotropic-nematic

phase transition. Instead a number of novel metastable or stable structures are observed which have been summarized elsewhere [94]. In this chapter we limit our attention only to the range of polymer concentrations or equivalently strength of attractions for which we obtain the isotropic-nematic phase transition. Throughout this part of the phase space we find no evidence for non-equilibrium structures reported in bhoemite/polystyrene mixtures [95].

The outline of this chapter is as follows. In section 5.2 we discuss the interaction potential between two charged rods in an solution of non-absorbing polymers. In the next section the theory that predicts the Isotropic-Nematic coexistence in the presence of the non-adsorbing polymer is outlined. In section 5.4 we give the experimental details and we compare the experimental results and theory in section 5.5. Finally, we present the measurements of the order parameter of the co-existing nematic phase in section 5.6

5.2 Intermolecular potential between two charged rods immersed in polymer solutions

When a colloid is suspended in a polymer solution it creates around it a shell that is excluded to the center of mass of any polymer. If two colloids approach each other there is an overlap of the excluded volume shells which leads to an effective attractive potential also known as the depletion potential. In the depletion picture the polymers are assumed to behave as spheres of radius R_s, which can interpenetrate each other but interact via hard core repulsion with colloids. This approximation introduced by Asakura and Ossawa (AO) [92], is valid as long as the radius of the spherical colloid is much larger then the radius of the penetrable sphere R_s [96, 97, 98]. On the other hand, if the radius of the colloid is equal to or smaller then R_s, the colloid can penetrate the polymer. Consequently in this case the range and the depth of the potential is significantly reduced when compared to

the AO model. In our experiments the diameter of the polymer is up to 5 times the diameter of the rod-like virus and therefore we expect that the depletion potential significantly deviates from the Asakura-Ossawa penetrable sphere model.

Since not much is known about the depletion between rod-like particles we calculate the depletion potential from a simulation. Two perpendicular cylinders are set at a fixed distance apart and an attempt is made to insert a non-self-avoiding the polymer molecule at random positions. If any segment of the polymer overlaps with the colloid the insertion attempt fails and the polymer is not counted. The profile of the depletion potential is then equal to

$$U_{\text{depletion}}(x) = k_b T(N(\infty) - N(x)) \tag{5.1}$$

where N(x) is the number of polymers successfully inserted in the simulation box when the rods are a distance x apart.

The depletion potentials obtained from the simulation are shown in Fig. 5.1. From the exact results, it is known that the depletion potential at small separations between two parallel plates induced by penetrable spheres is equivalent to the depletion potential induced by polymer (without excluded volume interactions), if R_s in the AO model is equivalent to $2R_g/\sqrt{\pi}$. R_g is the radius of gyration of the polymer [99, 98]. If we use this fact, the simulation results for the depletion potential between two plates (indicated by open circles in Fig. 5.1) are in a very good agreement with the potential predicted by the AO theory (indicated by the full line in Fig. 5.1), as long as the separation between the plates is smaller then $3R_g/2$. At larger separations we observe that the potential exerted by the polymer has longer range attraction then the equivalent penetrable sphere, as was previously noted [98]. This is because a polymer is only spherical on average and will adopt elongated conformations. On the other hand, the simulation results of the depletion potential between two spheres immersed in a polymer suspension with $R_g/R_{\text{colloid}} = 3.36$ is significantly weaker and of much shorter range then what is predicted by the pene-

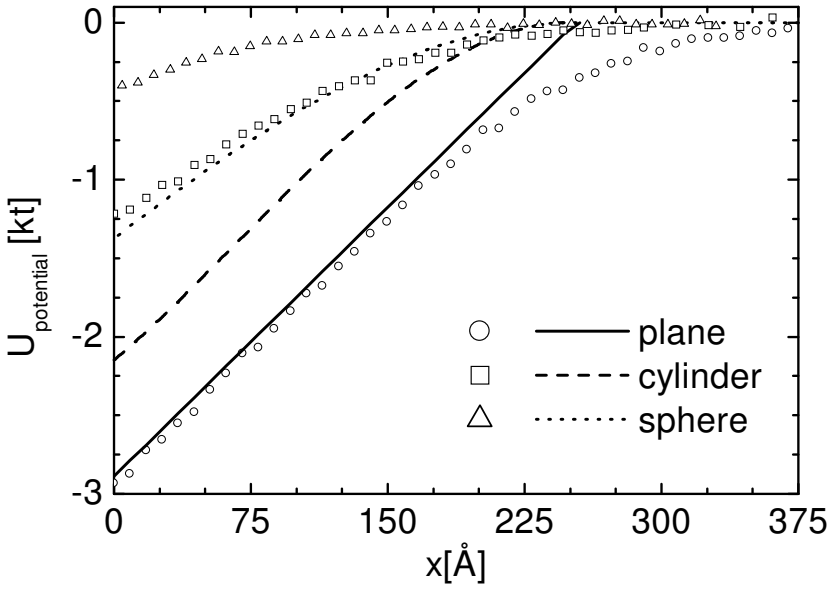

Figure 5.1: Depletion potentials obtained from computer simulation of non-self-avoiding polymer between two walls(open spheres), two perpendicular cylinders (open squares) and two spheres (open triangles). The diameter of the sphere and the cylinder is 66 Å while R_g of the polymer is 111 Å. The lines indicate the depletion potential as predicted by the penetrable sphere (AO) model for the wall (full line), cylinder (dashed line) and sphere (dotted line). The separation x is the closest distance between two colloid surfaces. The concentration of the polymer is equal to the overlap concentration, while the effective radius of the AO penetrable spheres is 125 Å. The AO theory overestimates the potential between spheres and polymers because polymer can deform around these obstacles.

trable AO sphere model. The reason for this is that the small sphere has a higher probability of penetrating a polymer with a large radius of gyration since polymers have very open structures. The cylinders have the profile of an infinite plane in one direction while in the other one they have the profile of a sphere. It follows that a cylinder with the same diameter as a sphere has a lower probability to penetrate the polymer coil. Therefore, as is shown in Fig. 5.1, the depletion interaction between two perpendicular cylinders is stronger than between two spheres of equal diameter. However, even for the case of cylinders, the potential obtained from the AO model still significantly overestimates the strength of the potential obtained from the simulation as is shown in Fig. 5.1. In this paper we assume that the strength of the depletion potential between two cylinders at an angle γ scales as $1/\sin\gamma$ which is proportional to the overlap area. The shape of the depletion potential between parallel rods is found to be identical to the shape of the potential between perpendicular rods, which supports this assumption.

The surface of the rod-like virus *fd* is highly charged and besides the attractive depletion potential there is also the soft repulsive potential due to the double layer repulsion, which has the following form:

$$\frac{U_{el}(x)}{kT} = \frac{Ae^{-\kappa(x-D)}}{\sin\gamma} \tag{5.2}$$

where κ^{-1} is the Debye screening length and γ is the angle between the two rods. The details of calculating constant A can be found elsewhere [100]. The total interaction potential between two perpendicular *fd* viruses at three different ionic strengths relevant to the experiments are shown in Fig. 5.2. Since both the electrostatic repulsion and the depletion attraction scale as $1/\sin\gamma$ the angle between the rods only affects the magnitude of the potential and not the shape of the it.

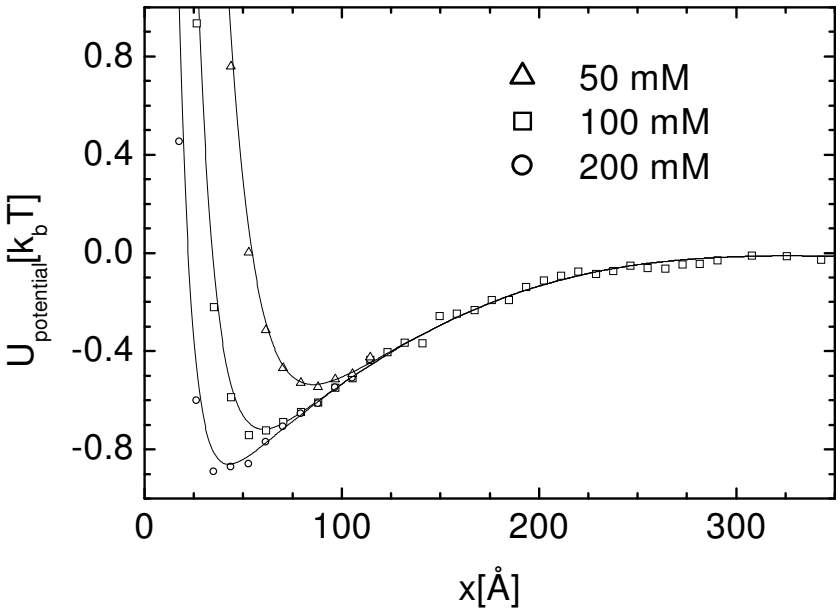

Figure 5.2:]
The total interaction potential between two perpendicular *fd* viruses immersed in a suspension of polymers with $R_g = 111$Å at three different ionic strengths. The surface charge is assumed to be 1 e^-/Å. By decreasing the ionic strength, both the range and the depth of the interaction potential significantly decreases. The concentration of the polymer is equal to the overlap concentration

5.3 Theoretical description of the I-N phase transition in rod/polymer mixtures.

In this section we present the formalism that predicts the phase diagrams for a rod-polymer mixture [90, 100, 101]. We found several misprints in the original paper that are corrected here [90]. It is easily shown that the approximate free energy of the colloid-polymer mixture is given by the following expression [102]:

$$F_{C+P}(\phi) = F_C(\phi) - \Pi_p < V_{free}(\phi) > \tag{5.3}$$

where $F_C(\phi)$ is the free energy of colloid suspension at volume fraction ϕ. The system is assumed to be in equilibrium with a polymer reservoir which is separated from the colloid-polymer mixture by a membrane permeable to polymers only. The osmotic pressure of the polymers in the reservoir is Π_p. V_{free} is the free volume available to a polymer in a solution of pure hard particle colloids. It is assumed that V_{free} in a polymer/colloid mixture is equal to the V_{free} in the pure colloid suspension. In this sense Eq. 5.3 is a thermodynamic perturbation theory.

The expressions for free energy of a pure hard spherocylinder colloidal suspension is given by the scaled particle theory developed by Cotter [22] :

$$\begin{aligned}\frac{F(\delta,\phi,\alpha)}{Nk_bT} = \quad & \ln(\phi) + \ln(1-\phi) + \sigma(f(\alpha), L/P) + \Pi_2(\delta,\alpha)\frac{\phi}{1-\phi} \\ & + \frac{1}{2}\Pi_3(\delta,\alpha)\left(\frac{\phi}{1-\phi}\right)^2 \end{aligned} \tag{5.4}$$

where ϕ is the volume fraction of spherocylinders

$$\phi = \frac{N_{rods}}{V}\left(\frac{\pi}{6}D^3 + \frac{\pi}{4}D^2L\right). \tag{5.5}$$

The coefficients Π_2 and Π_3 are given by the following expressions

$$\Pi_2(\delta,\alpha) = 3 + \frac{3(\delta-1)^2}{(3\delta-1)}\xi(f(\alpha)), \tag{5.6}$$

$$\Pi_3(\delta,\alpha) = \frac{12\delta(2\delta-1)}{(3\delta-1)^2} + \frac{12\delta(\delta-1)^2}{(3\delta-1)^2}\xi(f(\alpha)) \tag{5.7}$$

and parameter δ is the overall length to diameter ratio of the spherocylinder given by :

$$\delta = \frac{L+D}{D}. \tag{5.8}$$

The functions $\sigma(f(\alpha), L/P)$ and $\xi(f(\alpha))$ are the Onsager expressions for the orientational and packing entropy given in Eqs. 2.6 and 2.10 as a function of the orientational distribution function $f(\alpha)$, the contour length (L) and the persistence length (P).

The co-existence concentrations for the I-N transition predicted by the scaled particle theory are in very close agreement with the results from the computer simulations [26]. This indicates that the scaled particles theory provides a good approximation for third and higher virial coefficients. The expression for the free volume is given by:

$$\nu(\phi_c,\gamma,q) = (1-\phi_C)exp\left(-\left(A(\gamma,q)\left(\frac{\phi_C}{1-\phi_C}\right) + B(\gamma,q)\left(\frac{\phi_C}{1-\phi_C}\right)^2 + C\left(\frac{\phi_C}{1-\phi_C}\right)^3\right)\right) \tag{5.9}$$

where

$$\begin{aligned} A(\gamma,q) &= \frac{6\gamma}{3\gamma-1} + \frac{3(\gamma+1)}{3\gamma-1}q^2 + \frac{2}{3\gamma-1}q^3, \\ B(\gamma,q) &= \frac{1}{2}\left(\frac{6\gamma}{3\gamma-1}\right)^2 q^2 + \left(\frac{6}{3\gamma-1} + \frac{6(\gamma-1)^2}{(3\gamma-1)^2}\xi(\alpha)\right)q^3, \\ C(\gamma,q) &= \frac{24\gamma}{3\gamma-1}\left(\frac{2\gamma-1}{(3\gamma-1)^2} + \frac{(\gamma-1)^2}{(3\gamma-1)^2}\xi(\alpha)\right)q^3. \end{aligned} \tag{5.10}$$

The ratio of the polymer diameter to the rod diameter is given by the parameter q. The expression for the pressure and the chemical potentials are :

$$\begin{aligned} \Pi &= \phi^2 \frac{\partial F_c(\phi)}{\partial \phi} + n_p \lambda \left(\nu - \phi \frac{\partial \nu(\phi)}{\partial \phi} \right) \\ \mu &= F_c(\phi) + \phi \frac{\partial F_c(\phi)}{\partial \phi} + n_p \lambda \frac{\partial \nu(\phi)}{\partial \phi} \end{aligned} \tag{5.11}$$

where n_p is the polymer volume fraction and λ is the ration of spherocylinder volume to polymer volume

$$\lambda = \frac{1}{q^3} \left(1 + \frac{3}{2}(\gamma - 1) \right) \tag{5.12}$$

The phase diagram is calculated by first minimizing the free energy with the respect to the parameter α and then solving coexistence equations 5.11.

The theory just outlined is valid for a mixture of hard rods and interpenetrating AO spheres. To compare this theory to our experimental results on charged rods we split the interaction potential into the hard core repulsive part with an effective diameter and the long range attractive part as is shown in figure 5.3. We expect that this approximation works reasonably well only at high ionic strengths where the repulsive part of the interaction potential is very steep and can therefore be approximated by an effective hard diameter. As the effective diameter we chose the value that is obtained from the second virial treatment of charged rods as was discussed in chapter 2 and reference [27]. For the attractive part of the intermolecular potential we chose a penetrable sphere whose effective concentration and size match the depth and range of the potential obtained through the simulation described in section 5.2. This takes into account the fact that the depletion attraction is weakened due to interpenetration of the rods and polymers. As is shown in fig. 5.3 the effective potential used for the calculation of the phase diagram closely approximates the actual interaction potential between two charged rods obtained

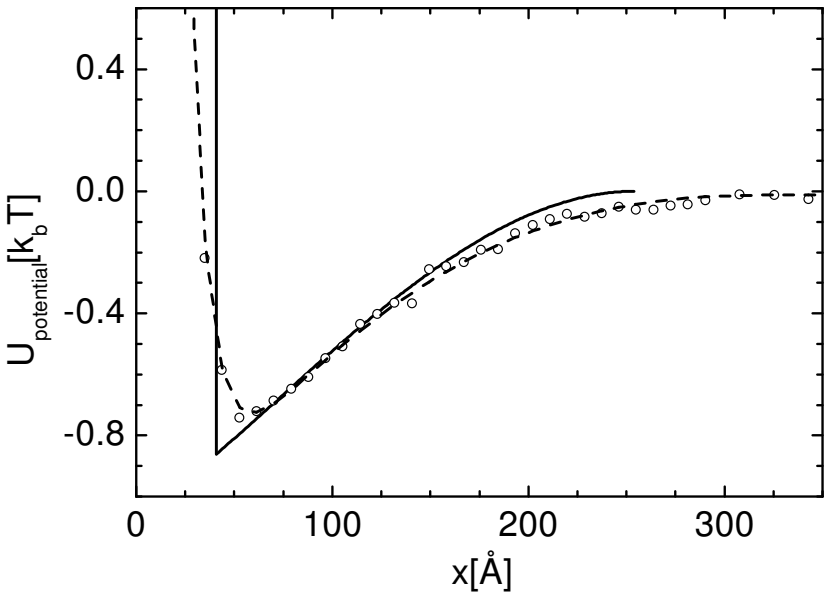

Figure 5.3: [

The effective potential, which is a sum of double layer repulsion at 100mM ionic strength and depletion attraction between two perpendicular rods is shown by the dashed line. The concentration of the polymer that gives this attraction is equal to the overlap concentration $c^\star$. In the calculation this interaction potential is approximated by a hard core repulsion with effective diameter 106Å and penetrable spheres with effective diameter of 107 Å and effective concentration of 0.311 $c^\star$ indicated by the full line.

by the combination of the theory and simulation

5.4 Experimental Methods

Bacteriophage *fd* was grown and purified as described before [32]. The purified virus was extensively dialysed against 20 mM Tris-HCl buffer to which NaCl was added to obtain solutions with total ionic strengths of 50mM, 100mM and 200mM. The pH of the buffer was 8.2 and all the experiments where done at room temperature. As the non-absorbing polymer we used a mixture of 95% Dextran (150,000 and 500,000 M. W. from sigma) and 5% FITC labeled Dextran with the same molecular weight. The reason for using labeled Dextran is that we can easily determine the concentration of the polymer by measuring it's absorbance at 495 nm. It is also important to note that Dextran carries no charge at pH=8.2 and is highly water soluble. The relationship between the radius of gyration R_g and molecular weight MW is $R_g = 0.66MW^{0.43}$ [103, 104]. The reason for the small exponent 0.43 is due to the fact Dextran is not a linear, but a branched polymer.

The virus suspension was mixed with Dextran and the concentrations were adjusted until the sample was in the two phase region. The time required for the macroscopic phase separation varied from overnight to two weeks depending on the width of the coexistence region. Once the phase separation process was complete a small sample was taken from each of the coexisting phases and the concentrations of both the virus and Dextran were obtained by absorption spectroscopy. At higher polymer concentration the sample would no longer phase separate into uniformly co-existing isotropic and nematic phases. Instead, we observed a whole range of slowly evolving metastable phases. For these samples we were only able to measure the concentration of the rods and polymers in the isotropic phase.

The order parameter of the nematic phase was measured by placing the suspension into a quartz x-ray capillary with a diameter 0.7 mm (Charles Supper).

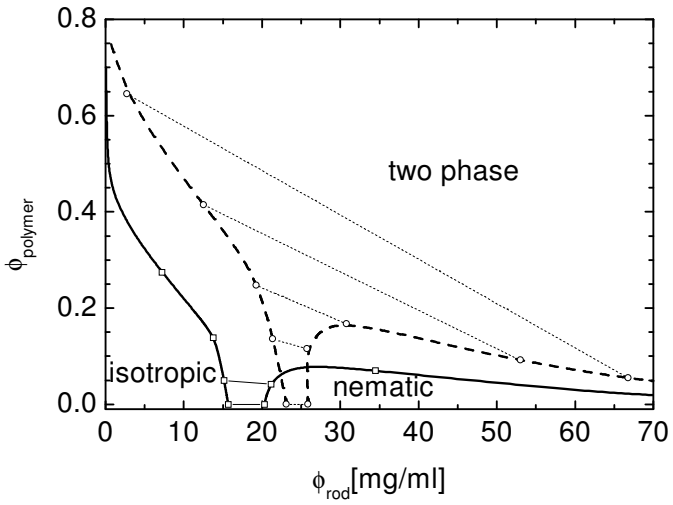

Figure 5.4: The I-N phase diagram predicted by the theory outlined in section 5.3 for rigid and semi-flexible rods. The boundary between the two phase region and the region where a single phase is stable is indicated by the thick dashed line for semi-flexible rods and thick full lines for rigid rods. A few tie lines between the coexisting phases are shown by thin dashed lines for illustratory purposes. For the flexible particle the ratio of the contour length to persistence length is $L/P = 0.4$

Samples were aligned with a 2T magnetic field [105]. The sample were immersed in a water bath and viewed under a polarizing microscope where the width of the capillary was measured. The birefringence of the aligned nematic was measured using a Berek compensator mounted on the Olympus polarizing microscope. The order parameter is obtained using the relationship $S = d\rho n_o$ where ρ is the concentration of the sample d is the thickness of the capillary and n_0 is the birefringence per particle. The n_0 is available from recent experiments where order parameter was determined using X-ray scattering [30].

5.5 Experimental phase diagrams of the isotropic-nematic coexistence and comparison to the theory.

Figure 5.4 shows the shape of the diagram predicted by the scaled particle theory of Lekkerkerker and Stroobants [90]. The theory predicts that addition of the polymer significantly widens the coexistence width and that at higher polymer concentrations there is partitioning of the polymer between the isotropic and nematic phase. The influence of the flexibility of the rod on the phase behavior of the rod/polymer mixture is also shown. Even for hard rods without any polymer present the flexibility of the rod is important in determining the location and the nature of the I-N phase co-existence. As discussed in Chapter 2 and in references [25, 27] there are three main effects of flexibility on the behavior of hard rods. Firstly, the flexibility increases the concentration of the I-N co-existence. Secondly, it decreases the width of the I-N coexistence, and thirdly it reduces the order parameter of the nematic phase co-existing with the isotropic phase. In figure 5.4 the phase diagrams for the two equivalent system of rods with attractions are shown with the only difference being the flexibility of the rod. For the case of the rigid rods the concentration of the polymer needed to induce widening of the concentrations of the coexisting phases is much lower than for that of semi-flexible rods.

Figure 5.2 shows that with decreasing ionic strength both the range and the depth of the attractive potential decreases. In order to be able to calculate the phase diagrams from these interaction potentials they were approximated as effective hard particles as demonstrated in figure 5.3. The resulting phase diagrams corresponding to three different ionic strengths are shown in figure 5.5. As expected from the knowledge of interaction potentials, the polymer concentration needed to induce significant widening of the co-existence concentration increases with decreasing ionic strength.

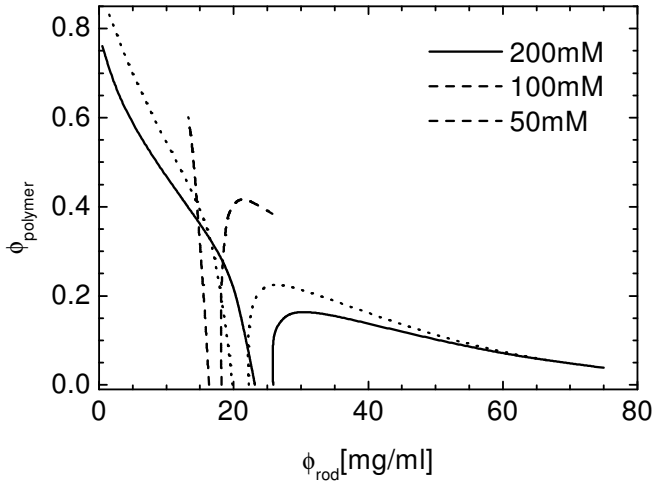

Figure 5.5: The phase diagrams of rod/polymer mixture at three different ionic strengths as predicted by the theory. The contour length over persistence length is $L/P = 0.4$, which corresponds to the flexibility of the *fd* virus.

In figure 5.6a an experimental phase diagram is shown for the full range of accessible polymer concentrations. As discussed in section 5.4 for some polymer concentrations the concentration of the rods in the rod rich phase could not be measured due to the fact that the phase would not macroscopically phase separate. For these samples the process of phase separation was investigated using optical microscopy and our findings are presented elsewhere [94]. From the phase diagram in figure 5.6 we can conclude that the rod/polymer mixtures are highly immiscible for most experimental parameters.

At very high polymer concentration the concentration difference between co-existing isotropic and nematic phase starts decreasing as is shown in figure 5.6 . This depletion re-stabilization was observed before in experimental studies of spherical colloid/polymer mixtures in aqueous suspensions [106]. The presumed reason for this is that at concentrations higher then the overlap concentration ($c^\star$) (the semi dilute regime) the relevant length scale that determines the range of attraction is not the radius of gyration but the correlation length. This correlation length decreases with increasing polymer concentration. Therefore it is expected that at certain poly-

mer concentration the range of attraction becomes smaller than the range of double layer repulsion, which consequently results in the rods interacting through repulsive forces only. In this regime the I-N co-existence concentrations of the rods will be equal to the co-existence concentrations without any polymer present. However, we do not take into account this phenomenon in our theoretical model and therefore the validity of the theory is restricted to the polymer concentrations below $c^{\star}$. In figure 5.6b we show the region of the phase diagram where the sample undergoes the I-N transition.

The experimental phase diagrams for three different repulsive potentials (ionic strength of 50 mM, 100 mM, 200 mM) are shown in figures 5.7, 5.8 and 5.9. All these measurements where done with Dextran polymer of the same diameter and therefore the range of attraction in this experiments does not change. Figure 5.7 shows that at the ionic strength of 50 mM the presence of the polymer has no effect on the coexistence concentrations of the I-N transition. As the ionic strength is increased to 100 mM the addition of the polymer increases the width of the co-existence concentration. At very high polymer concentration we observe restabilization of the I-N. This was also observed in mixtures of *fd* and Dextran (MW 500 000) at 100 mM in figure 5.6. Finally, at the highest ionic strength of 200 mM a relatively low concentration of polymer is needed to induce a complete phase separation between a polymer-rich rod-poor isotropic phase and a rod-rich polymer-poor nematic phase. At this ionic strength no reentrant I-N phase behavior is observed for all accessible polymer concentrations. We also note that in the mixtures of DEX 500 000 and *fd* at 200 mM we do not observe the reentrant I-N phase transition (data not shown). The dependence of the phase behavior on the ionic strength has the same qualitative behavior as predicted by theory in figure 5.5. However, when the theory is quantitatively compared to the experiment there are large differences between the predicted phase boundaries (full lines) and experimentally measured phase boundaries shown (5.7 to 5.9).

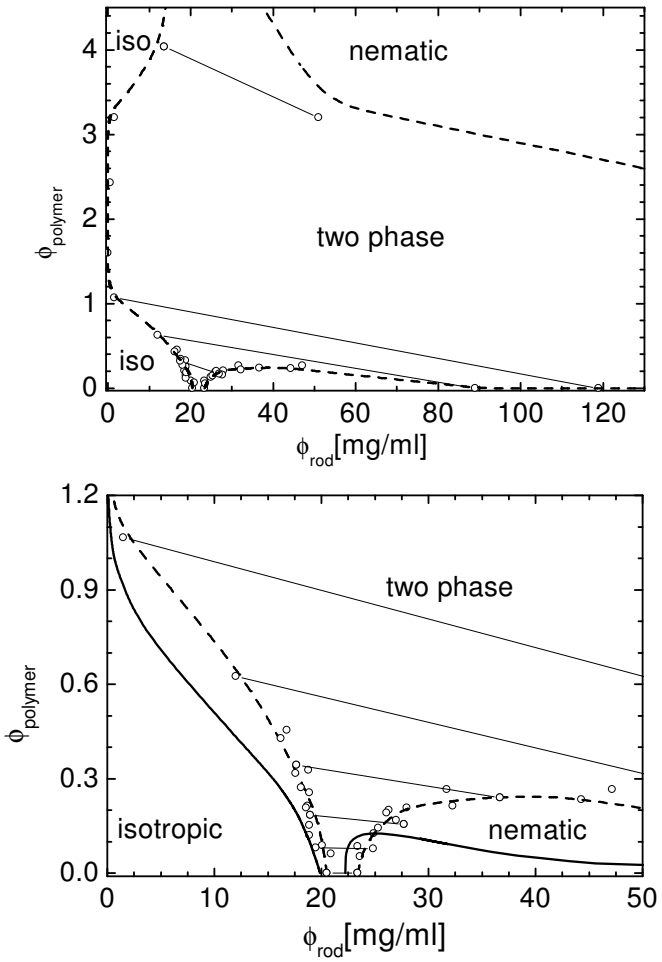

Figure 5.6: a) The complete phase diagram for the mixture of *fd* virus and Dextran (MW500 000, $R_g = 176$Å) at 100mM ionic strength. The measured points are indicated by open circles while the dashed line is a guide to the eye indicating the two phase region. For some samples the tie-lines are indicated by thin full lines. b) The part of the phase diagram where I-N co-existence is observed. The theoretical prediction for the two-phase region is indicated by the thick full line in figure b. The polymer overlap concentration corresponds to $\phi_{\text{polymer}} = 1$

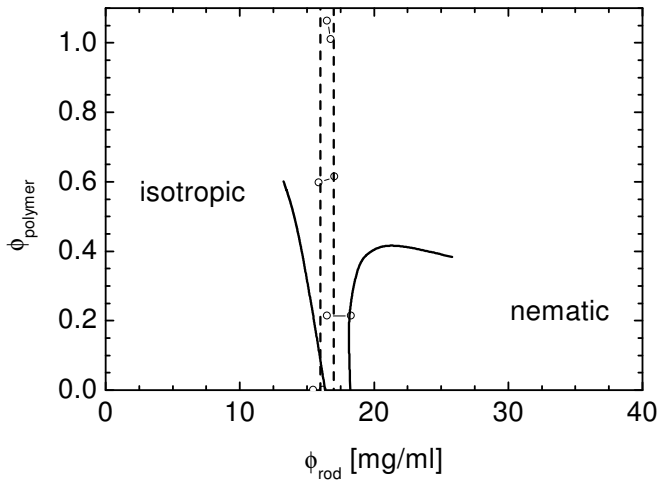

Figure 5.7: The phase diagram of the mixture of *fd* virus and Dextran polymer (MW150 000, $R_g = 111$Å) at 50 mM ionic strength. The coexisting points are indicated by open circles while the dashed line is the guide to the eye separation two phase from one phase region. The theoretical prediction for the phase diagrams is indicated by full black line. The I-N coexistence was measured up to polymer concentration of $4c^\star$ $^*\phi_{\mathrm{polymer}} = 4$ without any changes in coexisting concentrations (data not shown).

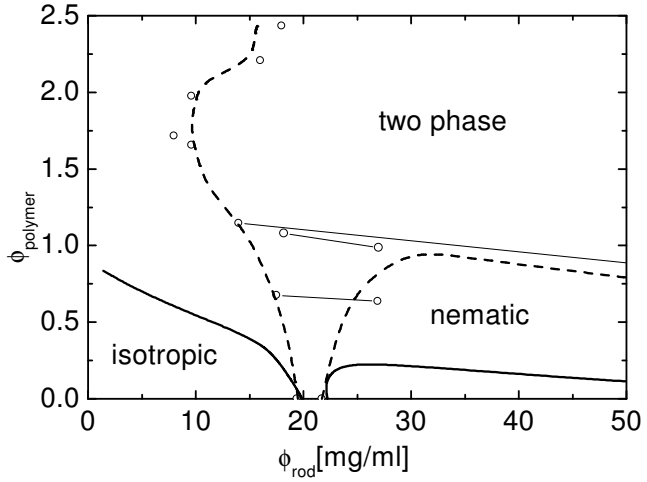

Figure 5.8: The phase diagram of a mixture of *fd* virus and Dextran polymer (MW 150 000, $R_g = 111$Å) at 100 mM ionic strength. The coexisting points are indicated by open circles while the dashed line is the guide to a eye separating the two phase from one phase region. The theoretical prediction for the phase diagrams is indicated by the full black line.

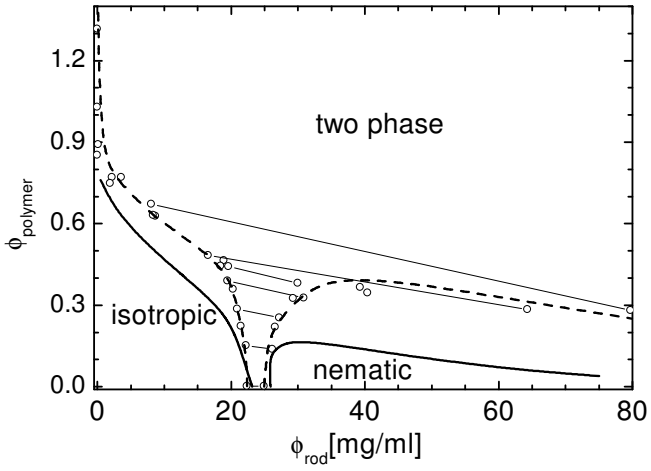

Figure 5.9: The phase diagram of the mixture of *fd* virus and Dextran polymer (MW150 000, $R_g = 111$Å) at 200 mM ionic strength. The coexisting points are indicated by open circles while the dashed line is the guide to the eye separation two phase from one phase region. The theoretical prediction for the phase diagrams is indicated by full black line.

In the original paper by Lekkerkerker and Stroobants, besides I-N transitions there are also predictions for I-I transitions and N-N transitions for certain ranges of parameters. However, for conditions relevant to our experiments the theory only predicts I-N coexistence in agreement with experimental observations.

5.6 Order parameter of the rods with attraction in the nematic phase

As mentioned in the introduction attractive rods can lower their energy by either increasing their parallel alignment or decreasing their average separation. To check if the presence of the polymer increased alignment of the rod-like virus we have measured the order parameter of the nematic phase co-existing with the isotropic phase as described in section 5.4. Figure 5.10 shows the prediction of the scaled particle theory for the order parameter of the nematic phase coexisting with the isotropic phase as a function of polymer concentration. When this order parameter

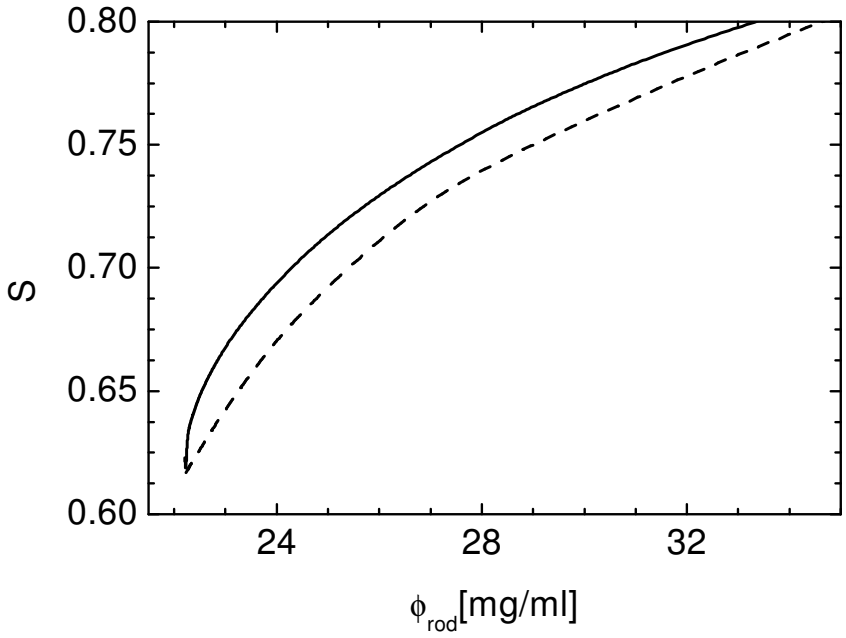

Figure 5.10: Theoretically predicted order parameter of the nematic phase (S) coexisting with the isotropic phase is indicated by the full lines for different polymer concentrations. The dashed line indicates the theoretical prediction for the order parameter of the nematic phase of hard rods without any attraction.

is compared with the order parameter of the nematic phase of hard rods at the same rod concentration but which have no attraction it is obvious that introducing attractions increases the nematic order parameter. Qualitatively the same trend is also observed in experiments on *fd*/Dextran mixtures as is shown in figure 5.11. However, when the experiments are quantitatively compared to the theory we again find large differences, with the experimentally observed effect being much larger then the theoretically predicted one.

5.7 Discussion and Conclusions

In this chapter we have presented experiments on the isotropic-nematic phase transition in a suspension of rod-like particles which have additional attractive interactions. The widening of the coexistence concentrations and partitioning of the poly-

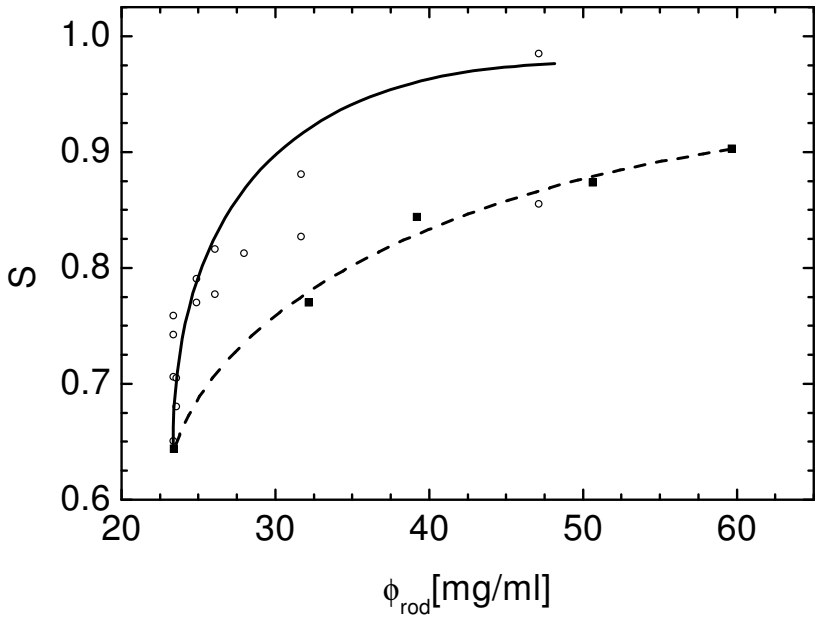

Figure 5.11: The open circles indicate the order parameter (S) of the nematic phase of the *fd* virus coexisting with the isotropic phase at different polymer concentration or equivalently different strengths of attraction. The filled circles correspond to the order parameter of the nematic phase of virus particles without any attraction present. The ionic strength is 100 mM and the polymer used is Dextran (MW 500 000).

mer predicted theoretically are also observed in the experiments on the *fd*-Dextran mixture. Even after taking the following into account; the possibility of the virus and polymer interpenetrating, the charge of the virus, and the semi-flexibility of the virus we found large quantitative differences between the theory and the experiment [107]. The difference is especially pronounced in the nematic phase. We also demonstrate the importance of measuring the order parameter of the nematic phase co-existing with the isotropic phase. At low polymer concentrations the coexisting I-N concentrations do not change appreciably, but the order parameter of the nematic phase does. This indicates that coexistence concentrations for rods with attractive interactions can agree with the Onsager theory of hard rods. Therefore in experimental studies to discern the difference between the hard rods and rods with attraction it is necessary to measure the nematic order parameter.

Chapter 6

Kinetics of the isotropic-smectic transition

6.1 Introduction

In the previous chapter we have discussed in detail the influence of the attractions on the isotropic-nematic phase transition. One of the observation was that with increasing the strength of the attractive potential the concentration of rods between isotropic phase and nematic phase increases. Eventually the concentration of the nematic increases to the point that the state with lowest energy is the smectic state. In this chapter we use optical microscopy to follow the pathways through which a smectic phase is formed.

6.2 Experimental observations

In our experimental studies of mixtures of *fd wt* and polymers we seek polymers which do not interact with the virus. The two polymers we use for this purpose are Poly(ethylene glycol) (PEG) and Dextran. To measure the I-N phase coexistence we mix concentrated *fd* virus and Dextran (M. W. 148,000), dilute the sample with

buffer until two phase co-existence is initiated, and let the sample phase separate at room temperature, which takes about two weeks for the slowest phase separating sample. The R_g of 148,000 Dextran is about 11 nm [104, 103]. In order to measure the concentration of both rods and polymers in the coexisting isotropic and nematic phases we use fluorescently labeled FITC-Dextran. After appropriate dilution the concentrations of both polymer and *fd* are measured on the spectrophotometer. The resulting phase diagram is shown in Fig. 5.6. At low polymer volume fraction the coexisting I-N concentrations change little from the pure virus limit and there is little polymer partitioning between the coexisting phases. At higher polymer volume fractions the phase diagram "opens up" and we measure the coexistence between a polymer-rich rod-poor isotropic phase and a polymer-poor rod-rich nematic phase. The qualitative features in such a phase diagram are very similar to the theoretically predicted phase diagram [90, 91]. In a forthcoming publication we will present detailed experiments of the effects of ionic strength, polymer nature, and molecular weight on the phase diagram.

When the phase diagram "opens up", the concentration of rods in the nematic phase coexisting with the isotropic phase dramatically increases. For the ionic strength of 100 mM *fd* virus forms a stable smectic phase at 160 mg/ml [10] so it is reasonable to expect a stable isotropic-smectic (I-S) phase coexistence to supersede the I-N transition for high enough polymer volume fraction, which is, indeed, the case. Since the size of our virus allows us to visualize individual smectic layers with an optical microscope we can observe the nucleation and growth of the smectic phase out of an isotropic suspension in real time. Observation of typical structures and their temporal evolution are summarized in the remainder of this paper. All the following images were taken with a Nikon optical microscope using DIC optics equipped with a 60x water immersion lens and condenser. Our previous work on mixtures of rods and spheres focused on the nematic - smectic phase transition where we employed *fd* as rods and for spheres utilized either polymers, such as dextran or

PEG, or polystyrene latex with diameters ranging from 40-100 nm, in distinction to the work here, which focuses on the isotropic - smectic transition using smaller polymers of diameters 4-10 nm [108, 109]

A homogeneous sample of composition in the part of the two phase region of Figure 5.6 where the tie-lines connect the isotropic and nematic phases begins phase separation by forming nematic ellipsoidal tactoids as shown in Figure 6.1a. The tactoids are nematic because they are too small to fit the cholesteric pitch. Only when the sample has bulk phase separated does the nematic transform into a cholesteric [34]. The nematic phase appears as a bright droplet elongated along the nematic director with a dark background of isotropic rods. In the picture, the rods are parallel to the plane of the paper and tend to align parallel to the I-N boundary, as illustrated in Figure 6.1g. As the polymer concentration is increased further (Figure **??**, regions 4 - 7), the tie-lines connect the isotropic and smectic phases. However, we still initially observe nematic droplets as shown in Fig. 6.1a, but after a few minutes the droplets begin to change their morphology. Figures 4a to 4k were all taken from the same sample and show the time evolution of an initially smooth tactoid during the first 20-30 minutes of phase separation. In Fig 4b we observe a thin helical sheet wrapped around the nematic tactoid. The width of the sheet along the direction of the tactoid is about 1 μm. We assume that this sheet is a single smectic layer of rods parallel to the direction of the nematic tactoid that has nucleated on the nematic surface. This smectic layer continues to grow and becomes thicker as shown in the side views of the tactoid in Figs 4c and 4d. Figure 4e shows the same helical structure, but this time viewed from above (the alignment of the rods is perpendicular to the paper). We observe that the helical smectic layer can close upon itself to form a single toroidal ring around the nematic tactoid. A typical example of this structure is shown in Fig. 4f where the rods are pointing out of the paper, and in Fig. 4g where rods are parallel to the paper. Two striped tactoids with smectic rings can coalesce (Fig. 4h) to form droplets with a variable

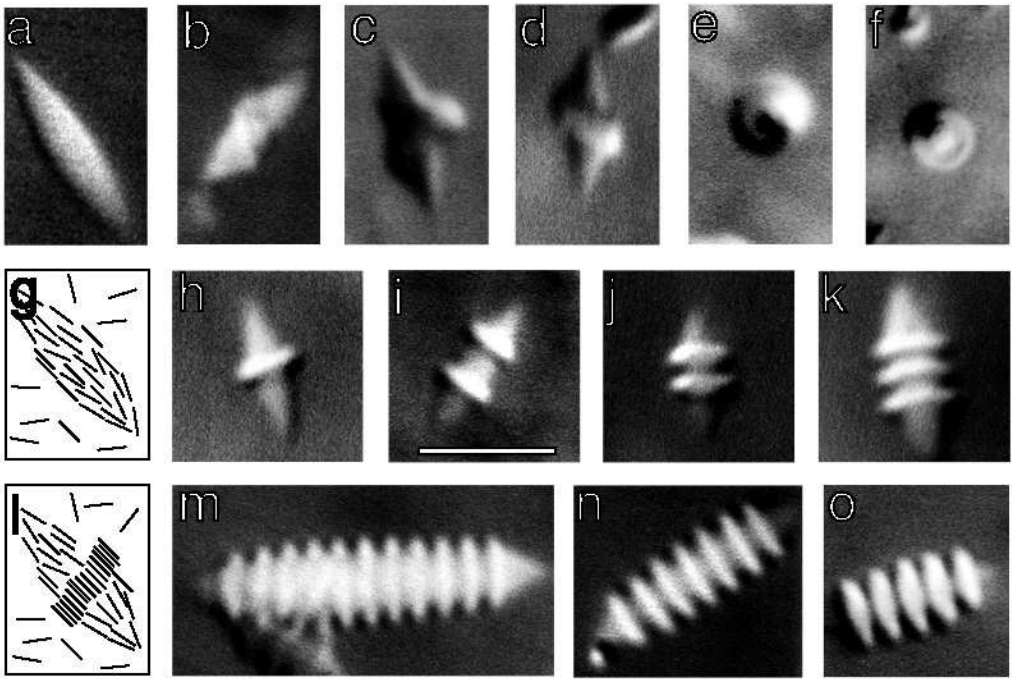

Figure 6.1:]

Initial stages of the phase separation of an initially isotropic suspension *fd* at concentration of 22 mg/ml and Dextran (M. W. 150,000) that shows the formation of striped tactoids upon addition of Dextran. The ionic strength is 110 mM. The concentration of polymer in picture (a) to (f) and (h) to (k) is constant and was added to the pure virus suspension until it became slightly turbid. The concentration of polymer increases in samples (m) to (o). In figure (g) we sketch the conformation of rods in typical tactoid at I-N transition in rods without attraction. The sketch of the nematic tactoid with the smectic ring is shown in figure l. The scale bar is 5 μm long and all images are taken at same magnification.

number of smectic rings as is shown in Fig. 4i, 4j and 4k. Figure 4k to 4m are taken at increasing volume fraction of polymers. From these three figures we observe that with increasing polymer concentration the thickness of the smectic rings increases in comparison to the size of the nematic core. The striped nematic droplets encircled with smectic layers will proceed to coalesce until they sediment to the bottom of the sample and reach a size that is many tens of microns. It should also be noted that not all tactoids have closed ring structures, but some instead have a helical structure that has a beginning and an end. This has important consequences for the further progress of phase separation as is demonstrated in Fig. 6.2.

After the sample has been phase separating for few hours we observe a new kind of structure shown in Fig. 6.2. These are filaments of *fd* that have a cross section of 1 μm, which corresponds to a one particle length. The director is oriented perpendicular to the fiber axis and precesses in a helical fashion as in a cholesteric. This results in the helical structures observed in optical micrographs. The connection between the twisted sheets and the striped tactoids from Fig. 6.1 coexisting in the same sample is clearly shown in Fig. 5c. The twisted strands grow slowly out of the smectic rings and over a period of few days the strands are able to reach lengths of several hundred microns. We should note that the twisted strand is a metastable structure with a pronounced tendency to untwist over a period of days or as one moves along the length of the strand away from its root at the striped I-N droplet. For example Fig. 5b to 5g where all taken from the sample and show very different degrees of twisting. Two strands can also connect with each other as is shown in Fig. 5f. The twisted strands can quite often form a helical superstructure. Figure 5e is focused onto the bottom and Fig. 5g is focused on the top of such a structure. Perhaps such a structure has it's origin in a striped tactoid (Fig 5c) that has for some reason lost its nematic core.

After a few months, as the sample further evolves towards equilibrium, we observe a number of large sheets that are one rod length thick. We believe that

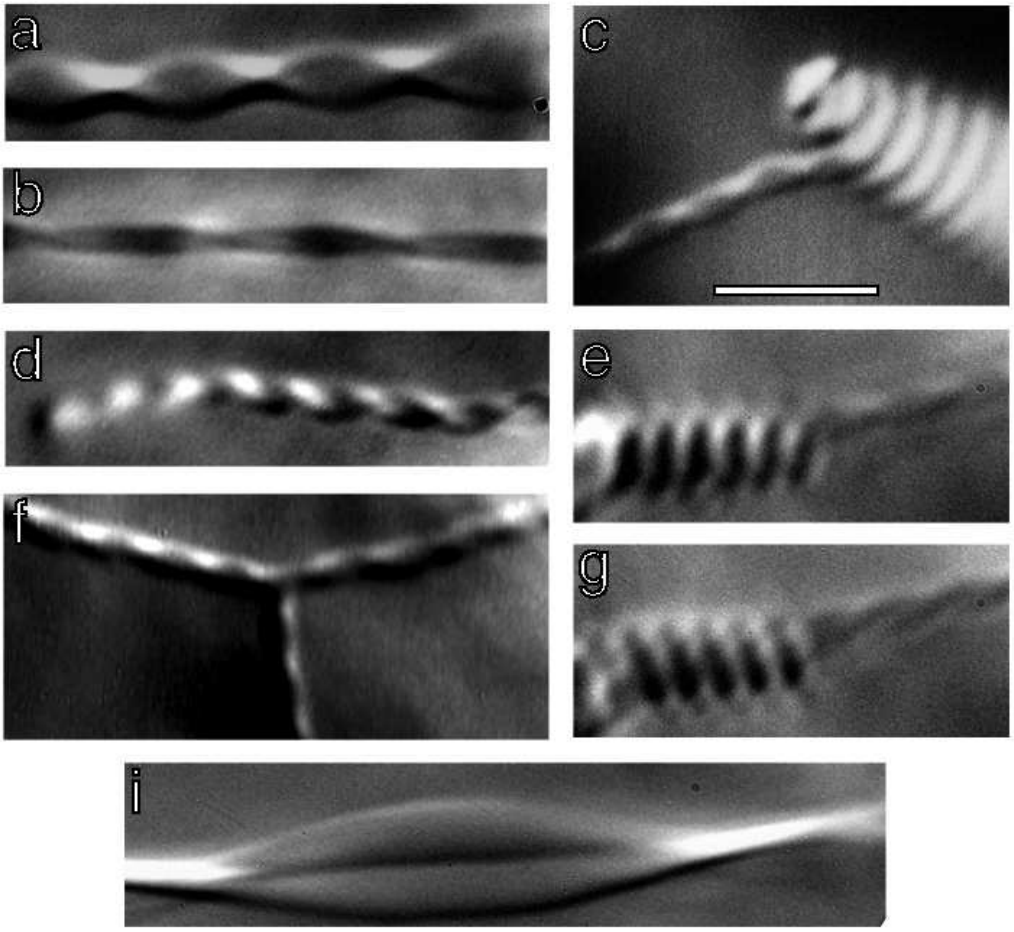

Figure 6.2: The twisted strands in (b) to (g) are with the same conditions as in Figure 4(a). Figure 5(a) is taken at a higher polymer volume fraction, while figure 5(i) is taken at lower virus concentration (5 mg/ml). The scale bar indicates 5 μm.

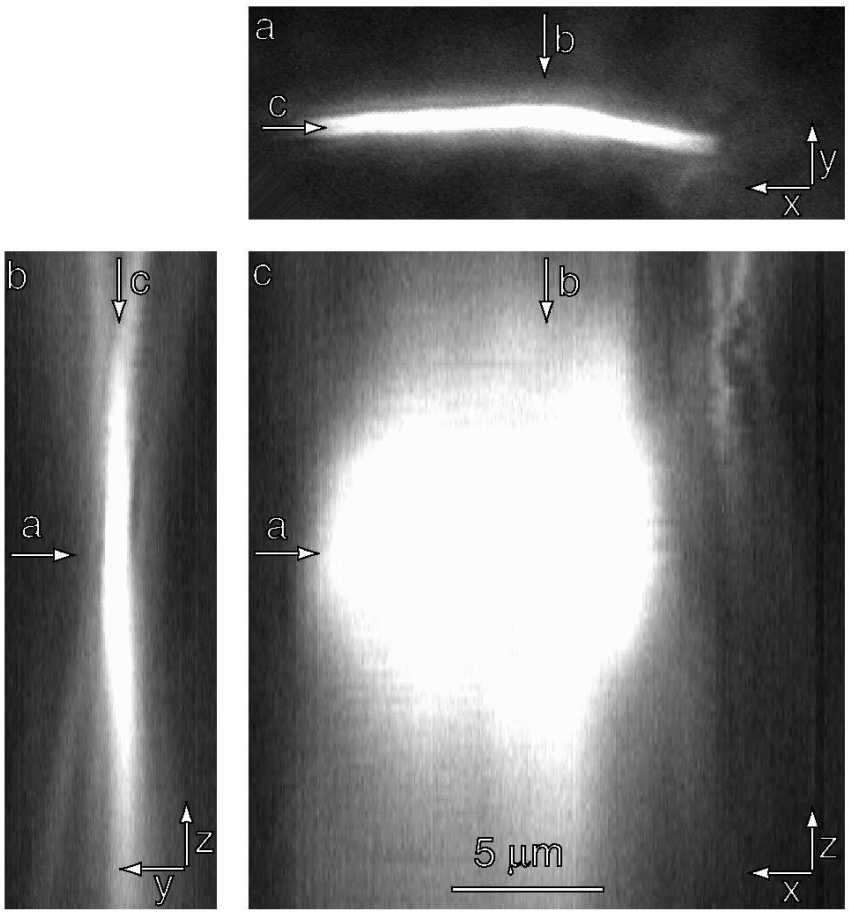

Figure 6.3: A three dimensional reconstruction of a large membrane of a single layer smectic that is observed in a mixture *fd wt* and Dextran 150,000 M.W. after the it has been equilibrating for 2 months. Using the microscope a sequential series of images in the xy plane at different depths z (Fig 6a) were taken and the image was reconstructed in three dimensions. Figure 6b shows the image of the membrane cut along the y direction at the position indicated by arrow (b) in figure 6(a) and 6(c). Equivalently, figure 6c shows the cut of the membrane perpendicular to the virus axis as indicated by arrow (c) in figures 6(a) and 6(b). The scale bar indicates 5 μm.

these are essentially large, single layer smectic membranes. Using the microscope we photograph a sequential series of images in the plane of focus (xy plane, Fig. 6a) evenly spaced at 0.2 μm intervals in the z dimension and from this information we reconstruct the structure of the membrane in three dimensions. Fig. 6c shows the image of the membrane perpendicular to the alignment of the rods from which we deduce that the diameter of the membrane is about 10 μm. The cuts through the xy and yz planes are uniformly one micron thick along the y direction.

In another series of experiments we studied a mixture of *fd* virus and PEG polymer (M. W. 35,000, $R_g = 9.6$ nm) shown in Fig. 6.4. The concentration of rods (10 mg/ml) was lower than in the Dextran/virus mixture described previously, but the ionic strength was again 110 mM. We increased polymer concentration until we observed slight turbidity in our sample indicating the onset of two-phase coexistence. The structures we observed under these conditions with PEG/virus mixtures are very similar to the structures observed in Dextran/virus mixtures illustrated in the previous three figures. As we increased the polymer concentration further, we observed a direct formation of the smectic membrane out of isotropic suspension, instead of their growth from the striped nematic tactoid. An image of such a membrane, where all the rods point out of the surface of the paper is shown in Fig. 7a. The side view (not shown) indicates that the membrane is essentially one rod length thick. The membranes are stable over a period of hours, which is surprisingly long. If the sample is observed for long enough it is possible to observe the process of coalescence of two smectic membranes. Fig. 7e shows such a process in a sequence of frames spaced 1/30 seconds apart. In the first frame the rods in both membranes are aligned in the same direction. Once the membranes are aligned, the process of coalescence is complete in about 0.16 seconds.

As the concentration of the polymer is increased further another pathway to the formation of the smectic phase is observed. We presume that this process initially begins with the formation of the smectic membranes just as the one described in

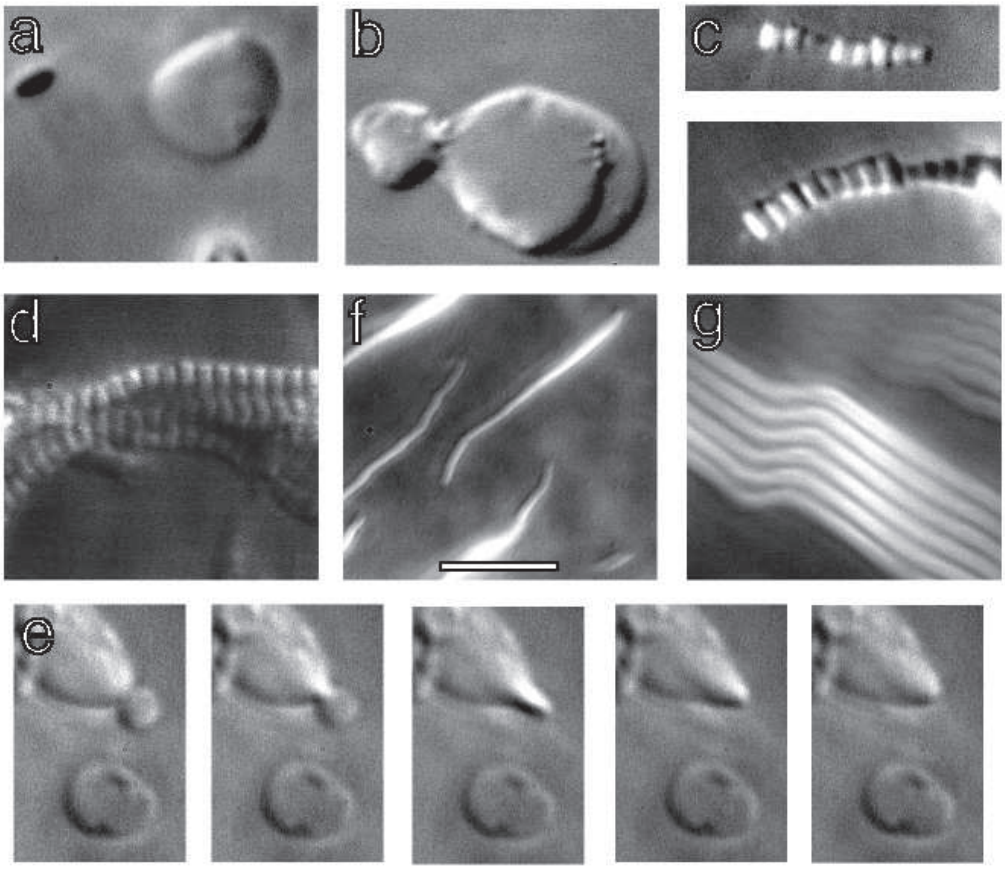

Figure 6.4: Phase behavior of mixture *fd* and PEG (M. W. 35,000). At the lowest concentrations of polymer we observe striped tactoids that are very similar to the ones shown in previous figures. As the concentration is increased, we observe formation of a single membrane one rod-length thick that is shown in figures 7a and 7b. In figure 7e, five successive video frames spaced 1/30 of seconds apart show coalescence of two smectic membranes. At an even higher volume fraction of polymer, we observe filaments shown in figures 7c and 7d that percolate throughout the entire sample. The phase transitions on the surface are shown in figures 7f and 7g. The scale bar indicates 5 μm.

the previous paragraph. However, these membranes never reach the size of the membranes at lower polymer concentration, which coalesce sideways as is shown in Fig. 6.4e. Instead, while the membranes are quite small they stack on top of each other to form long filaments shown in Fig. 6.4c. Within a few seconds after mixing the sample these filaments form a percolating network, which is self supporting and does not sediment over time. As is seen in Figs. 6.4c the thickness of the filament is not uniform, but varies from one layer to the other. The irregular thickness of the filaments does not change even if the sample is left to equilibrate for few days. From this we can conclude that it takes rods a very long time to diffuse from one layer to another. We also observe that as the concentration of the polymer is increased, the thickness of the filament decreases. The formation of the filaments can be understood in terms of depletion attraction. Once a single smectic layer grows to a critical size a lower energy is achieved by stacking two equal diameter membranes on top of each other rather than by letting two membranes coalesce laterally. This is because the strength of the attraction between two surfaces is proportional to the area of the interacting surfaces.

It is well known that depletion attraction between a colloid and a wall is much stronger than the attraction between two colloids [110, 111]. Because of this, in parallel to the bulk phase transitions described previously, there are competing transitions with the surface of the container. Some of the structures we observe on the surfaces due to the depletion attraction are shown in Fig 6.4f and 6.4g. Fig. 6.4f shows a single smectic layer of rods. By focusing through the layer in z direction we conclude that this layer is extremely thin (upper limit of 0.2 μm). Furthermore, these layers can stack on top of each other as is shown in Fig. 6.4g.

Up to now, all the experiments were done with polymers of roughly the same radius of gyration (Dextran 150,000 has $R_g = 11$ nm, PEG 35,000 has $R_g = 9.6$ nm) and at same ionic strength (110 mM). When we decrease the radius of the polymer (PEG 8,000 has $R_g = 4.1$ nm) we still observe two-dimensional membranes which are

composed of parallel rods. However, as is shown in Fig. 6.5, the membranes assume a hexagonal shape, which strongly implies that the rods within the membrane are not a two dimensional fluid, but a two-dimensional crystal. Figures 6.5a to 6.5d where taken at the lowest polymer concentration at which the crystallization was observed. Under these conditions the induction time for critical nuclei formation as indicated by the turbidity of the sample is about 30 minutes. A typical image of a 2D crystal where the rods within the crystal are pointing out of the plane of the paper is shown in Fig. 6.5a, while the side view where the alignment of the rods is in the plane of the paper is shown in Fig 6.5b. The thermal fluctuations within the crystal are easily visible under the microscope and the crystal is readily deformed as is visible in the side view of the crystal. Often, instead of observing a flat membrane, we observe a membrane with screw dislocation located at the nucleation center. The images of such a membrane from the top view and side view are shown in Fig. 6.5c and 6.5d. In Fig 6.5c we can clearly see that the two layers are on top of each other, but if we focus through in the z direction we observe that these two layers belong to the same 2d crystal. This is exactly what we would expect from a crystal that has a screw dislocation.

If we increase the polymer concentration, the induction time decreases and an image of these post-critical nuclei is shown in Fig. 6.5e. A typical crystal that usually grows overnight out of this solution is shown in top view in Fig. 6.5f, while Fig. 6.5g shows the side view of such a crystal. A nucleation center that significantly protrudes out of the 2D crystalline membrane in clearly visible, and sometimes it is even possible to observe two 2D crystal membranes connected through the same nucleation center as shown in Fig 8h. The nucleation centers, which are long, thin needles (Fig. 6.5e appear in the first few minutes after making a sample. It is important to note that such a nucleation center is visible in every 2D crystalline membrane and at all polymer concentrations. Two-dimensional crystals have been observed in rod-like TMV/BSA mixtures [112] and these crystals also have a clearly

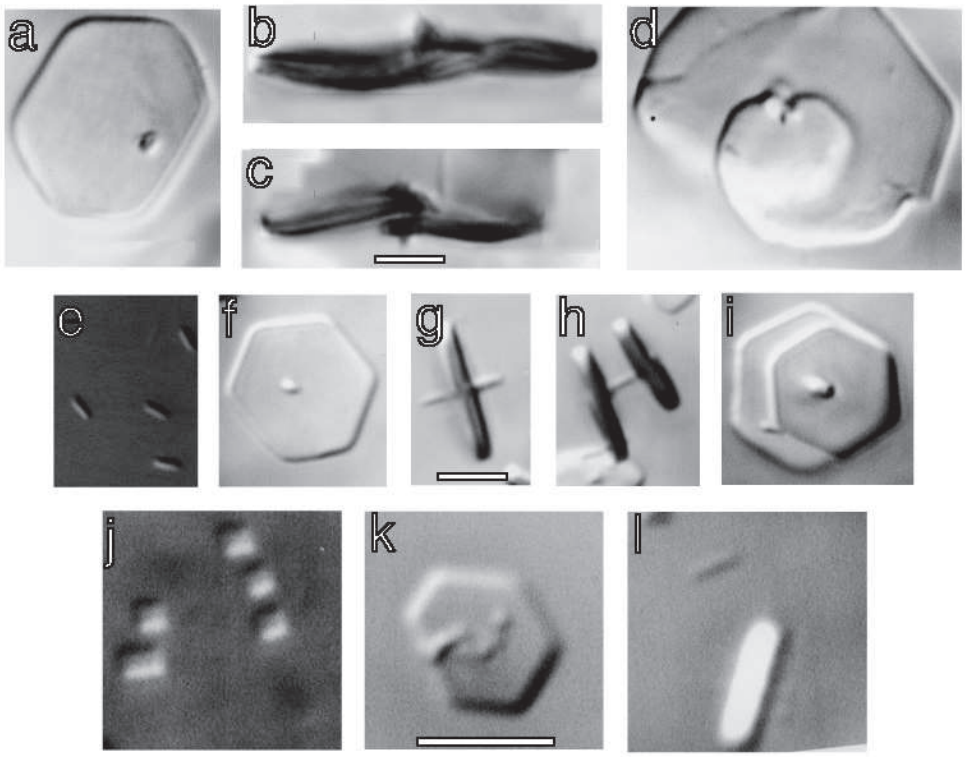

Figure 6.5: Optical micrographs of two dimensional virus crystals observed in a mixture of PEG (M.W. 8,000) and *fd* virus at a constant concentration of 15 mg/ml. The first row of the pictures is at the lowest polymer concentration at which the crystals where observed, the second row is at intermediate polymer concentration, and third row is at highest polymer concentration. The scale bars are 5 μm and images in each row are at the same magnification.

visible single nucleation site protruding. The fact that the structures observed in PEG/fd and TMV/BSA system are extremely similar suggest that the features of 2D crystalline membranes summarized here are generic to any system of rods with short range attraction. Parenthetically we note the resemblance of the virus crystals of Fig. 6.5 to "shish-kebabs", which is the name given to lamellar crystals grown around a central fiber that are observed in polymer crystallization from solution and melt [113]. But whether or not the mechanisms governing shish-kebab and 2D virus crystal formation are related is not clear.

At even higher polymer concentration, the induction time is unmeasureably short and typical nuclei that are formed almost instantaneously are shown in Fig. 6.5j. The resulting crystals display almost no thermal fluctuations, are much smaller than crystals formed at low polymer concentration, their number density is much higher, and typically their edges are much sharper and better defined as is shown in Fig. 6.5k and 6.5l.

The influence of both polymer concentration and polymer range has been extensively studied for three dimensional spherical colloids [114, 115, 100]. The basic parameter that determines the behavior of the system is the ratio of the range of attraction between colloids as compared to the range of the effective hard core repulsion. On the one hand, if the range of attraction is very short the vapor-liquid phase transition will be metastable with regards to the vapor-crystal transition for all conditions. On the other hand, if the range of attraction is sufficiently long ranged under certain conditions the vapor-liquid transition will supersede the vapor-crystal phase transition. Our results on the formation of two dimensional membranes in the polymer/virus mixtures agree with this general rule. In the mixture of large polymer (Dextran M. W. 150,000, $R_g = 11$ nm) and *fd* virus the attraction is long ranged and we observe a two dimensional liquid like membrane. It contrast, in the mixture of small polymer PEG 8,000, $R_g = 4$ nm) where the attraction is short ranged, we observe a two dimensional crystalline membrane.

6.3 Conclusions

We summarized the behavior of virus/polymer mixtures, which behave as hard rods with an attractive potential. Although the interactions between rods in polymer solutions is very simple, we observe a whole range of novel structures of surprising complexity. These experiments and previous studies on rod/sphere mixtures [108] indicate that there is much that remains to be understood about the phase behavior of such mixtures.

Chapter 7

Enhanced stability of the smectic phase due to addition of hard spheres

7.1 Introduction

In hard particle fluids all allowed configurations have the same energy and therefore it is the number of states, or equivalently the entropy of a system that determines the equilibrium phase. Examples of well known phase transitions where the formation of ordered structures are driven solely by an increase in entropy are the liquid to crystal transition in hard spheres [4], the isotropic to nematic [2] and the nematic to smectic transition in hard-rods [5, 6]. Because of their high degree of monodispersity, and because of the dominant role of steric repulsion in the pair-potential, colloidal suspensions of polystyrene latex and rod-like viruses have often been used as experimental model systems for the study of entropy induced ordering in hard-sphere [116, 117, 118] and hard-rod systems, respectively [32, 31].

A natural extension of the above work is to the phase behavior of mixtures, with a number of recent experimental and theoretical studies focusing on the phase

behavior of binary mixtures of hard-spheres [119, 120, 121, 122, 92, 115, 123, 100, 124, 125]. We have recently begun work on less studied systems that closely approximate hard-rod/hard-sphere and hard-rod/polymer mixtures [88, 91, 90, 126, 127, 128, 129]. As a model for hard-rods we used either *fd* or TMV virus, as hard-spheres we used polystyrene latex, and as polymers we used poly(ethylene-oxide) with varying molecular weights [108, 112]. The part of the phase diagram explored consisted of pure rods in either the isotropic, nematic, or smectic phase to which a small volume fraction of spheres or polymers was added. Remarkably, besides the expected uniform mixtures and bulk demixing, we also observed a variety of microphases for a wide range of sphere sizes and concentrations [108]. In microphase separation the system starts separating into liquid-like regions that are rich in either spheres or rods. However, unlike bulk demixing where rod and sphere rich regions grow until reaching macroscopic dimensions, in microphase demixing these liquid-like regions increase only to a critical size after which they order into well defined three dimensional equilibrium structures. One of the micro-separated phases observed, named the lamellar microphase, consists of alternating two-dimensional liquid-like layers of rods and spheres and is the subject of theoretical analysis in this paper.

In this paper we use the second virial approximation first studied by Koda et. al. [130] to examine the influence of molecular parameters such as shape and size, on the phase behavior of rod/sphere mixtures. As the second-virial theory is approximate in nature, we validate the theoretical predictions by comparing them with either computer simulations or experimental results. The remainder of this paper is organized as follows: In section 7.2 we formulate the second virial approximation for the rod/sphere mixture. The general features of the phase diagram are discussed and a physical picture of the factors responsible for the enhanced stability of the layered phase due to the presence of spheres is presented. In Section 7.3 the influence of varying the spherocylinder length on the phase behavior of spherocylinder/sphere mixtures is studied using computer simulations and the results are

compared to theoretical predictions. Section 7.4 examines how changes of the sphere diameter influence the phase behavior of spherocylinder/sphere mixtures. Finally in Section 7.5 we present our conclusions.

7.2 General features of a phase diagram of a spherocylinder-sphere mixture

Although the equilibrium phases of all hard particle fluids are determined by maximizing the entropy, ordering transitions are still possible because the expression for the total entropy, or equivalently free energy, splits into two parts. The ideal contribution to the entropy is of the form $\rho \ln \rho$, where ρ is the density distribution function. This contribution to the entropy attains a maximum for a uniform density distribution and therefore always suppresses transitions from uniform to modulated phases. In contrast, excluded volume entropy sometimes increases with increasing order and therefore drives the system towards a modulated phase. In this paper we use a highly simplified second virial approximation to calculate the excluded volume entropy.

The equilibrium phase in a spherocylinder/sphere mixture is determined by four parameters: length over diameter of a spherocylinder (L/D_{sc}), diameter of spherocylinder over diameter of sphere (D_{sc}/D_{sp}), total volume fraction of spheres and spherocylinders (η) and partial volume fraction of spheres (ρ_{sp}). To help us in interpretation of our results we first define the slope

$$\tau = \lim_{\rho_{sp} \to 0} \frac{\eta(\rho_{sp}) - \eta(0)}{\rho_{sp}} \tag{7.1}$$

where $\eta(\rho_{sp})$ is the total volume fraction of the rod-sphere mixture at the layering transition after the introduction of spheres at partial volume fraction ρ_{sp}. A positive value of τ implies that adding a second component stabilizes the nematic phase

by displacing the smectic transition to higher densities. For the case when both components are spherocylinders of different lengths but with the same diameter, slope τ is positive if the ratio of lengths is less then approximately 7 [51, 48]. In the same manner, negative values of τ imply that the second component stabilizes the smectic phase. There are predictions of a negative value of τ in a bidisperse rod mixture when the ratio of rod lengths is large enough [51], or when added rods have a larger diameter [131]. In this section we focus on the phase behavior of the spherocyinder-sphere mixture for the specific microscopic parameters $L/D_{sc} = 20$ and $D_{sc}/D_{sp} = 1$. We present a physical picture of excluded volume effects that are responsible for the enhanced stability of the lamellar phase. In the next two sections we extend our study on how changes in the molecular parameters L/D_{sc} and D_{sc}/D_{sp} modify the phase behavior and in particular, their influence on the magnitude and sign of the slope τ.

7.2.1 Second virial approximation

The second virial approximation for a mixture of perfectly aligned spherocylinders and spheres of equal diameter was proposed by Koda, Numajiri and Ikeda [130] and is generalized for arbitrary L/D_{sc} and D_{sc}/D_{sp} in the appendix. It was previously shown that the second virial approximation described qualitatively the formation and various features of the smectic phase of hard rods [5, 132, 133, 44]. Here we study how the addition of spheres perturbs the formation of the smectic phase. Since the sphere volume fraction is very low we expect that the second virial approximation is still qualitatively correct for these mixtures. We consider a sinusoidal perturbation from the uniform density for both spherocylinders and spheres. From equations (7.5) and (7.8) in the appendix we obtain the free energy difference between the uniformly mixed and layered state in a spherocylinder/sphere mixture:

$$\delta F = a_1^2 \left(S_{11} - 2\frac{a_1}{a_2} S_{12} + \left(\frac{a_1}{a_2}\right)^2 S_{22} \right) = 0 \tag{7.2}$$

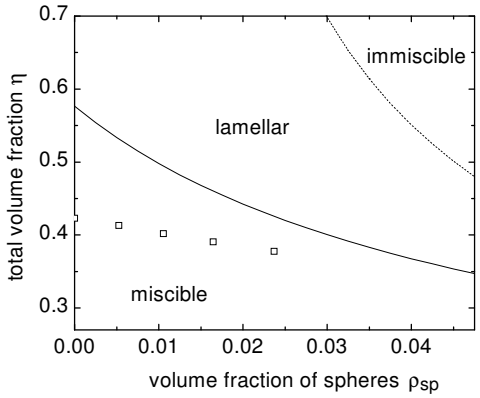

Figure 7.1: Stability boundaries for a mixture of perfectly aligned spherocylinders ($L/D_{sc} = 20$) and spheres with equal diameter ($D_{sc}/D_{sp} = 1$). The full line indicates the theoretical prediction of the volume fraction at which the system becomes unstable towards lamellar fluctuations. The dashed line indicates instability towards demixing into two macroscopically distinct phases. Squares are results of computer simulations at which the layering transition is observed. Theoretically, the periodicity associated with a one-dimensional lamellar instability continuously grows and diverges as the system completely phase separates. Illustrations of the miscible and lamellar phases are shown in Fig. 5a and 5b, respectively.

.

The phase diagram obtained within this approximation for microscopic parameters $L/D_{sc} = 20$ and $D_{sc}/D_{sp} = 1$ is shown in Fig. 7.1. From the phase diagram we see that the first prediction of the model is that spheres, upon addition to a smectic phase, will preferentially occupy space between smectic layers and therefore create a stable micro-separated lamellar phase. The second prediction is that the total volume fraction at which the system undergoes a transition from a uniform miscible state to a layered lamellar state is lowered by increasing the partial volume fraction of spheres. This implies that the slope τ is negative for this particular spherocylinder/sphere mixture and we conclude that in this case *spheres enhance the layering transition.*

We can assign a simple physical origin to every term given in Eq. (7.2) above and Eq.(7.7) of the Appendix. The parts of the spherocylinder-spherocylinder interaction term S_{22} and sphere-sphere term S_{11} that scale as η are due to the ideal

(id) contribution to the free energy, also known as the entropy of mixing and are denoted as S_{22}^{id} and S_{11}^{id}, respectively. The terms having a η^2 dependence in S_{22}, S_{12}, S_{11} are due to the spherocylinder-spherocylinder, spherocylinder-sphere and sphere-sphere excluded volume (ex) interaction, respectively and are denoted as S_{22}^{ex}, S_{12}^{ex} and S_{11}^{ex}. Since the instability is defined as $\delta F(\eta_c, k_c) = 0$, at a critical density η_c and at a critical wavevector k_c all individual contributions to the free energy difference in Eq. (7.2) must add up to zero. In Fig. 7.2 we show the value of all terms with distinct physical origins at the instability density η_c and wavevector k_c as a function of partial volume fraction of spheres. Since from our analysis we cannot determine the absolute amplitude of a_1 we only plot the ratios of all free energy components to the absolute value of the spherocylinder-spherocylinder excluded volume $\mid S_{22}^{ex} \mid$. If we set the partial volume fraction of spheres to zero ($\rho_{sp} = 0$) in Eq.(7.2) we obtain an equation whose solution indicates the nematic-smectic stability limit in a pure suspension of aligned spherocylinders [132]. For these conditions the only two nonzero components of free energy are S_{22}^{ex}, which is negative and therefore drives the transition and S_{22}^{id}, which is positive and therefore suppresses the transition. As we start increasing the partial sphere volume fraction ρ_{sp}, the spherocylinder-sphere free volume term S_{12}^{ex} rapidly assumes large negative values as evidenced by the rapidly decreasing ratio of $S_{12}^{ex} / \mid S_{22}^{id} \mid$. This implies that layering the mixture significantly decreases the excluded volume that is due to the spherocylinder-sphere interaction.

We can use the information gained from the second virial approximation to obtain a clear physical picture of excluded volume effects in spherocylinder/sphere mixtures and explain the enhanced stability of the lamellar phase. Taking any single spherocylinder in a uniform spherocylinder/sphere mixture and replacing it by two spheres will leave the value of excluded volume virtually unchanged. The reason for this lies in the fact that the volume excluded to the spherocylinder due to the presence of a sphere with equal diameter, under the constraint of uniform packing,

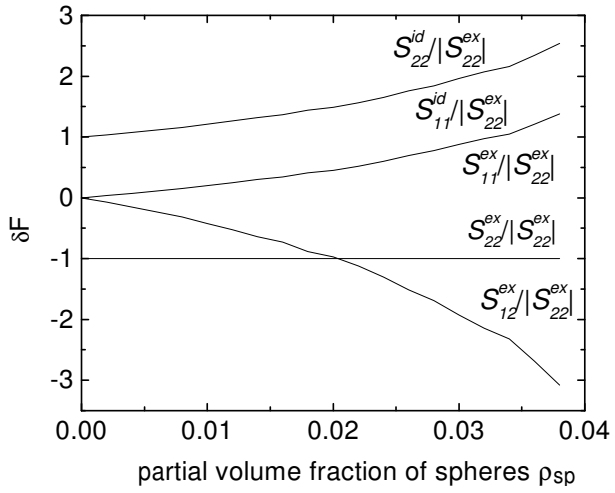

Figure 7.2: Term-by-term dependence of the free energy difference between the miscible and lamellar phases (Eq. 7.2) as a function of the partial volume fraction of spheres for $L/D_{sc} = 20$ and $D_{sc}/D_{sp} = 1$. The S_{11}^{id} and S_{22}^{id} terms are the sphere and spherocylinder ideal contributions to the total free energy difference between the layered and uniform states. S_{11}^{ex}, S_{12}^{ex} and S_{22}^{ex} are excluded volume contributions to the free energy due to sphere-sphere, spherocylinder-sphere and spherocylinder-spherocylinder interactions respectively. Since from our analysis we cannot determine the amplitude in Eq. 7.2 we plot amplitude independent ratios of each of five components of the free energy with different origins to the spherocylinder-spherocylinder excluded volume interactions. The stability condition is that $\delta F = 0$, so for any value of partial volume fraction of spheres ρ_{sp} the sum of the five contributions to δF is zero. δF of the ideal terms are positive, hence they stabilize the uniform, miscible nematic state, while the free volume terms are negative, favoring the lamellar state. The excluded volume sphere-sphere term (S_{11}^{ex})is negligible and the spherocylinder-sphere (S_{12}^{ex}) term dominates the transition.

is a spherocylinder with diameter $2D_{sc}$ and length $(L + 2D_{sc})$ where L and D_{sc} are defined in Fig. 7.3. However, the excluded volume between any two spherocylinders with large L/D_{sc} is only about twice this value as illustrated in Fig. 7.3. Although replacing spherocylinders by spheres in such a manner leaves the excluded volume almost unchanged, it does significantly decrease the total volume fraction of the mixture since the volume of two spheres is much smaller than the volume of a spherocylinder with large L/D_{sc}. Therefore in the spherocylinder/sphere mixture we encounter excluded volume problems similar to those found in a pure spherocylinder solution, but at a lower total volume fraction. As in pure spherocylinders, the system reduces the excluded volume by undergoing a transition to a layered phase. The excluded volume is reduced in the lamellar state because a periodic density distribution forces spheres and spherocylinders into alternate layers thus decreasing the probability of the very unfavorable sphere-spherocylinder contacts as illustrated in Fig. 7.4. This explains the large decrease in the value of the S_{12}^{ex} term at the lamellar transition that we observe in the second virial theory. This term is responsible for the enhanced stability of the lamellar phase in a sphere/spherocylinder mixture. In conclusion, it is the inability to efficiently pack a uniform mixture of spherocylinders and spheres, as reflected in the large spherocylinder/sphere excluded volume term, that destabilizes the nematic phase and enhances the formation of a layered phase.

An alternate way to think about the formation of a layered phase is to focus on the effects of spherocylinder ends [134]. The nematic phase in our simplified model is characterized by random distribution of spherocylinders along their axial and radial direction as illustrated in Fig. 7.5. This end effect is responsible for the formation of the smectic phase, which is characterized by a periodic density distribution. In similar fashion, introducing a sphere into the nematic phase will have the same effect on the surrounding spherocylinders as another spherocylinder end. Therefore adding spheres very effectively increases the density of "spherocylinder ends" and decreases the total volume fraction. To resolve the difficulties in efficient

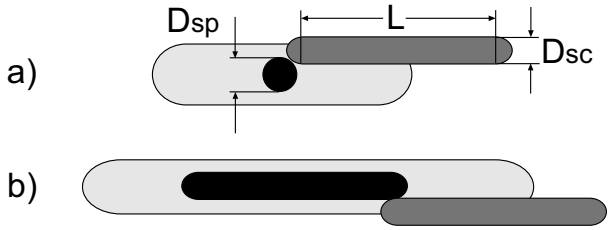

Figure 7.3:]
a) Volume excluded to the center of mass of a spherocylinder (sc) due to the presence of a sphere (sp) is indicated by light shading b) Volume excluded to the center of the mass of a second spherocylinder due to the presence of the first. Replacing a spherocylinder by a sphere decreases the excluded volume by approximately a factor of two, but it decreases the total volume fraction much more since the volume of a spherocylinder with large L/D_{sc} is greater than the volume of a sphere with diameter D_{sc}. The comparatively large excluded volume between a sphere and a spherocylinder is the reason for the enhanced formation of the lamellar phase

packing due to these extra "spherocylinder ends", the mixture layers at a lower total volume fraction.

7.2.2 Monte Carlo Simulation

In the previous section we discussed two predictions of the second virial theory for a spherocylinder/sphere mixture with $L/D_{sc} = 20$ and $D_{sp}/D_{sc} = 1$; the existence of the lamellar phase and the enhanced stability of the lamellar phase when compared to a smectic phase of pure spherocylinders. Our results are in agreement with previous studies of Koda et. al. [130]. However, the second virial approximation is highly approximate and there is reasonable concern about the influence of higher terms on the topology of the phase diagram. To support their conclusions Koda et. al. performed computer simulations, which indicated the existence of a lamellar phase [136, 130]. Still, the question of whether spheres simply fill the voids between layers in an already formed smectic phase, or actually induce layering at lower total volume fraction was not addressed. In this section, using Monte Carlo simulations we address the question of the influence of adding spheres on the phase behavior of

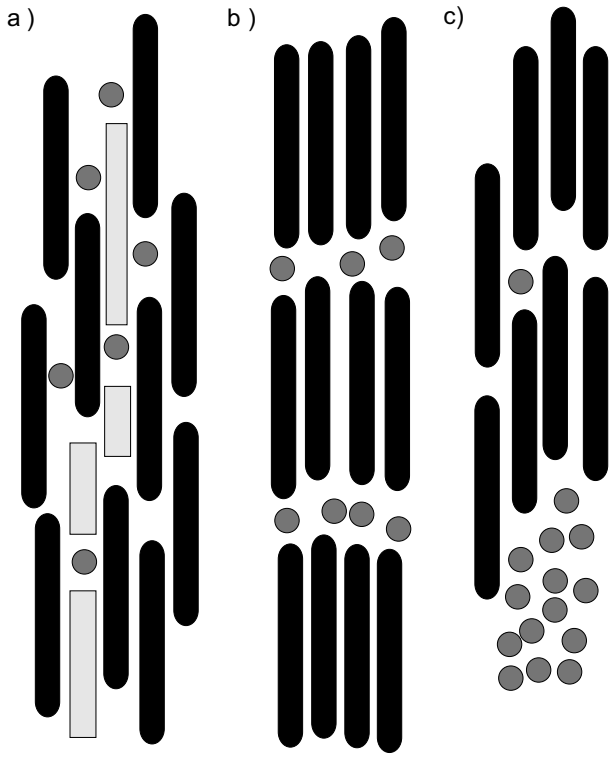

Figure 7.4: a) A schematic illustration of excluded volume effects in a nematic phase in a spherocylinder/sphere mixture. In the nematic or miscible phase each sphere creates a large excluded volume around it, indicated by gray areas, that is inaccessible to spherocylinders. b) When the system undergoes a transition to a layered phase, the large excluded sphere-spherocylinder volume vanishes since the probability distribution severely limits the number of ways that spheres are allowed to approach spherocylinders. (c) Illustration of the immiscible phase where the system bulk phase separates into a rod-rich phase and a sphere-rich phase.

]

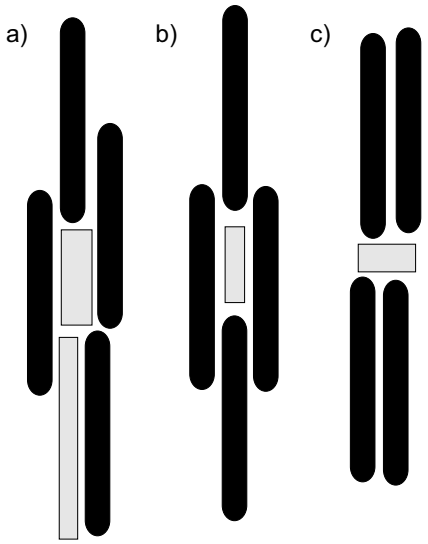

Figure 7.5: a) A schematic example of a typical configuration of spherocylinders in a dense nematic phase. Since the nematic phase is characterized by a uniform density distribution this results in inefficient packing and large excluded volume between spherocylinders both along their radial and axial directions. This large and unfavorable excluded volume is indicated by lightly shadowed areas. b) An illustration of a typical configuration of spherocylinders in a columnar phase where the excluded volume between spherocylinders is lower compared to the nematic phase at the same density, and the ideal part of free energy is higher. In a columnar phase the spherocylinders are forced into registry as one spherocylinder occupies space right above or below another one. Therefore the columnar phase is characterized by two dimensional order in the plane perpendicular to the spherocylinder's long axis and one dimensional disorder parallel to the long axis. c) A representative configuration of spherocylinders in a smectic phase, which is characterized by one-dimensional order along the spherocylinder's long axis and two-dimensional disorder in the perpendicular directions. Both theory and experiment indicate that the columnar phase is always metastable with respect to the smectic phase [132, 135].

spherocylinders by determining the slope τ in Eq. 7.1 in a mixture of spherocylinders and spheres with parameters $L/D_{sc} = 20$ and $D_{sp}/D_{sc} = 1$

A Monte Carlo simulation of a mixture of hard-spheres and perfectly aligned hard-spherocylinders was performed at constant pressure and number of particles [137]. Most simulations contained 392 spherocylinders and a variable number of spheres. To check for finite size effects we also ran simulations with 784 spherocylinders, but saw no significant difference in the results obtained. In one sweep, pressure was increased from a dilute homogeneous mixture up to a well ordered, dense smectic or lamellar phase. At each value of the pressure, the density of spheres and spherocylinders and their corresponding smectic order parameter were measured after the system was allowed to equilibrate. Identical results were obtained when the pressure was slowly decreased from a initially dense phase composed of alternating layers of spherocylinders and spheres to a dilute homogeneous mixture.

Besides lamellar transitions there is a possible demixing transition where spherocylinders and spheres phase separate into macroscopically distinct phases. However, once a layered phase is formed the exchange of spheres between layers drops to a negligible amount, leaving open the possibility that the system would undergo a demixing transition, but is stuck in a lamellar phase, which is only a metastable state. To find out the location of the demixing transition it is necessary to measure the chemical potential of both spherocylinders and spheres in a spherocylinder/sphere mixture [138]. This possibility was not examined in this work, primarily because we are only interested in how low concentrations of spheres perturb the formation of the layered phase. Therefore it is reasonable to expect that at a very low volume fraction of spheres, the lamellar transition is going to be more stable than the demixing transitions as predicted by the second virial theory.

A plot of the smectic order parameter for spherocylinders with $L/D_{sc} = 20$ as a function of increasing total density for different partial volume fractions of spheres is shown in Fig. 7.6. As the system approaches a certain critical density we observe

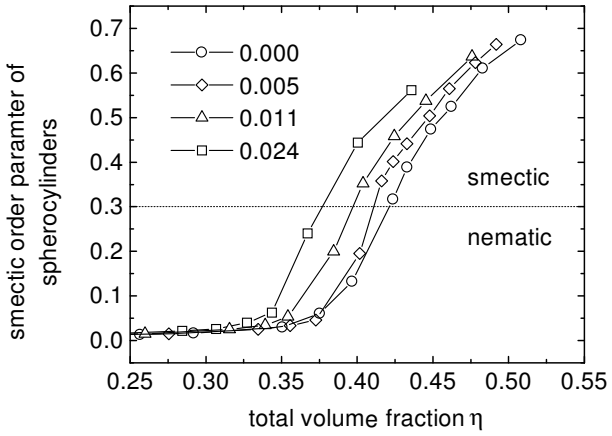

Figure 7.6: Smectic order parameter obtained from Monte Carlo simulations is plotted against the total volume fraction for spherocylinders with $L/D_{sc} = 20$. From right to left, the partial volume fraction of spheres (ρ_{sp}) increases from 0% to 2.4% as indicated by the legend. The phase diagram is reconstructed from this data by defining a phase as layered when the spherocylinder order parameter reaches a value of 0.3.

a rapid non-linear increase in the smectic order parameter that we interpret as a signature of the nematic to smectic phase transition. This critical density shifts to lower values of the total volume fraction as the partial volume fraction of spheres is increased. To reconstruct a phase diagram from the above data we define a phase as layered when its smectic order parameter reaches a value of 0.3 [139]. For a pure spherocylinder suspension this value yields good agreement with previous studies of the volume fraction of the nematic-smectic phase transition [140]. Since we are mostly interested in the qualitative behavior of a spherocylinder/sphere mixture this method should suffice our purposes. Using this phenomenological rule, the phase diagram for a mixture of spherocylinders and spheres ($L/D_{sc} = 20$, $D_{sc}/D_{sp} = 1$) is reconstructed and compared to the second virial theory in Fig. 7.1. An immediate conclusion drawn from Fig. 7.1 is that adding spheres to aligned spherocylinders enhances the stability of the lamellar phase, which is indicated by the negative value of slope τ, in agreement with the prediction of the second virial approximation.

7.3 The effects of spherocylinder length on the phase diagram

Next we proceed to investigate the influence of varying the spherocylinder length on the magnitude of slope τ. The predictions of the second virial theory for the nematic-lamellar instability are shown in Fig. 7.7a. The second virial theory clearly predicts increasing stability of the lamellar phase with increasing length of spherocylinder. To verify this prediction we repeated Monte Carlo simulations for spherocylinders with different L/D_{sc} and used the same rule as before to identify the volume fraction of the nematic-lamellar transition. The simulation results for the location of the nematic to layered transition are shown in Fig. 7.7b. We can conclude that our simulations confirm predictions of the second virial model and that the length of the spherocylinder is an important parameter in forming the lamellar phase, with longer spherocylinders showing an increasing tendency to form a layered phase at a lower volume fraction of added spheres.

Using the physical picture of the excluded volume effects developed in the previous section provides a natural explanation for our simulation results in Fig. 7.7. With increasing spherocylinder length the excluded volume due to the spherocylinder-sphere interaction grows proportionally to the spherocylinder length and consequently the value of the S_{12}^{ex} term increases in magnitude. As we have seen before, the larger the S_{12}^{ex} term, the more likely it is for the system to form a layered phase.

It is interesting to consider the limit of spherocylinders with infinite aspect ratio. In the density regime of the nematic-smectic transition, this model can be mapped onto a system with skewed cylinders with an aspect ratio close to one. The nematic-smectic transition in this model has been studied numerically [91, 43]. If we consider the addition of spheres to this system, then the same affine transformation that maps the infinite spherocylinders onto squat, skewed spherocylinders, will map the spheres onto infinitely thin, parallel disks. As the disks are infinitely thin,

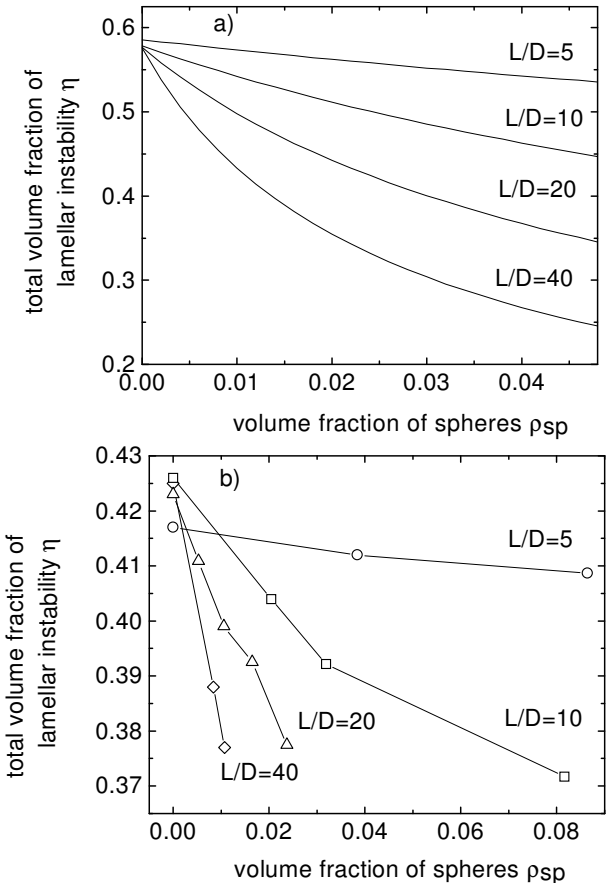

Figure 7.7: a) Prediction from the second virial theory for the total volume fraction η of the lamellar instability as a function of sphere partial volume fraction (ρ_{sp}) for spherocylinders with different L/D_{sc} ratios. The diameter of spherocylinders is kept constant and is equal to the diameter of the spheres. b) Results from Monte Carlo simulations for the lamellar instability of spherocylinders as a function of partial volume fraction of spheres for same conditions as in Fig. 7.7a. The volume fraction at the phase transition was defined as having a smectic order parameter of spherocylinders equal to 0.3

they do not interact with each other but only with the cylinders. Inside the nematic phase, most volume is excluded for these disks. However, in the smectic phase, there is ample space for the disks between the layers. In fact, the stronger the layering, the larger the accessible volume. Hence in this limit, the addition of spheres will strongly stabilize the smectic phase.

7.4 The effects of sphere diameter on the phase diagram

In this section we investigate the influence of sphere diameter on the value of slope τ. Fig. 7.8 shows the prediction of the second virial theory for the dependence of slope τ on the ratio of spherocylinder to sphere diameter (D_{sc}/D_{sp}) for spherocylinders with different L/D_{sc}. In first section we examine the phase behavior of sphere/spherocylinder mixtures when the sphere diameter is smaller than spherocylinder diameter and in the next section we examine the other case when the sphere diameter is larger than the spherocylinder diameter. In our model the presence of the spheres cannot alter the orientational distribution function of spherocylinders, which are always perfectly parallel to each other. It is reasonable to expect that this assumption holds for spheres smaller then the spherocylinder length, but as a sphere becomes larger then the spherocylinder length, long wavelength elastic effects start to dominate the behavior of the system and hard spherocylinders will tend to align parallel to the surface of the sphere [141]. Therefore in Fig. 7.8 we plot the values of slope τ only for those values of D_{sc}/D_{sp} for which our assumptions are at least qualitatively correct. As we increase the sphere size beyond this limit our model describes a highly artificial system of large spheres and parallel spherocylinders. In this regime we observe oscillations in the value of slope τ similar to what is observed in binary mixtures of parallel spherocylinders [51].

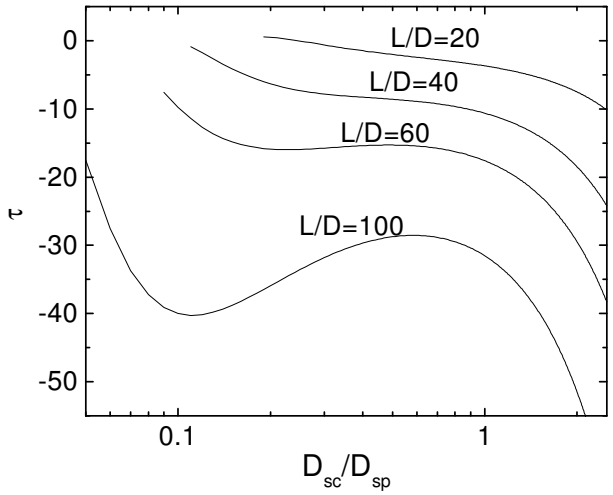

Figure 7.8: Theoretical prediction for the stability criterium of the lamellar phase τ in Eq. 7.1 as a function of spherocylinder (sc) to sphere (sp) diameter ratio for four spherocylinders with different L/D_{sc}. The negative value of slope τ indicates that spheres of that particular size enhance the layering transition. Larger negative values of τ implies the formation of the lamellar phase at a lower total volume fraction.

7.4.1 Sphere diameter smaller than spherocylinder diameter

In the regime where $D_{sc}/D_{sp} > 1$ (for spherocylinders of any L/D_{sc}), decreasing the sphere size increases the stability of the lamellar phase as indicated by the increasing negative value of slope τ seen in the right hand side of Fig. 7.8. This prediction of the theory has a simple explanation in our picture of excluded volume in a sphere/spherocylinder mixture. If we halve the sphere radius D_{sp}, while keeping constant the volume fraction of spheres, we increase the number of spheres eight times. At the same time, the result of reducing the sphere size is to decrease the excluded volume of the spherocylinder-sphere interaction. However, the eightfold increase in the number of spherocylinder-sphere interactions more then compensates for the decrease in excluded volume between the sphere and spherocylinder and consequently the magnitude of S_{12}^{ex} increases with decreasing sphere diameter. This leads to the increased stability of the layered phase with decreasing sphere size.

It becomes difficult to verify this prediction using computer simulations. As the sphere size decreases at constant total volume fraction η, the number of particles in a simulation rapidly reaches the order of thousands requiring simulation times that are prohibitively long. As the ratio of spherocylinder to sphere diameter (D_{sc}/D_{sp}) was varied within the accessible range between 0.5 to 2 we did not observe any changes in the value of slope τ that were larger than our measurement error. Larger and longer simulations are needed for a careful analysis of spherocylinder/sphere mixtures with extreme values of the ratio D_{sc}/D_{sp}.

7.4.2 Sphere diameter larger than spherocylinder diameter

For spherocylinders with small L/D_{sc}, Fig. 7.8 shows that the magnitude of slope τ uniformly decreases with increasing sphere size. Eventually the slope τ changes sign and becomes positive, implying that large spheres stabilize the nematic and not the smectic phase. The phase diagram under conditions where slope τ is positive is shown in Fig. 7.9. The wavevector associated with the layering transition, indicated with a solid line in Fig. 7.9, remains at an almost constant value. Another important point is that the amplitude ratio in Eq. (7.8) is positive. This means that the periodic density modulations of the spherocylinders and spheres are in phase, which implies that spheres no longer go into the gap between two spherocylinder layers, but rather fit into the spherocylinder layer. However, as the partial volume fraction of spheres (ρ_{sp}) is increased further we observe a discontinuous jump in the wavevector to zero value. This implies that there is a discontinuous change from a layering to a demixing transition. As the demixing transition is reached there is also a change in sign of the amplitude ratio, which becomes negative and the spherocylinders and spheres bulk separate. In contrast, the phase diagram for mixtures of small spheres and spherocylinders shown in Fig. 7.1 looks quite different. The amplitude ratio for this case is always negative implying formation of the lamellar phase. Another contrast is that in a mixture of small spheres and spherocylinders the wavevector

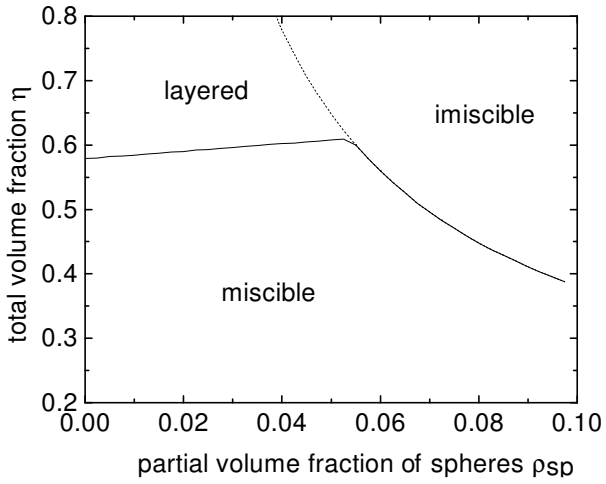

Figure 7.9:]
Stability diagram of a mixture of spherocylinders ($L/D_{sc} = 10$) and large spheres $D_{sc}/D_{sp} = 0.15$. Unlike a mixture of small spheres and spherocylinders (Fig. 7.1), introducing large spheres displaces the layering transition to higher total volume fractions indicating a positive value of slope τ. The structure of the layered phase is also different, with large spheres fitting in the smectic layer rather than into the smectic gap. The smectic periodicity associated with the layering transition does not change significantly until the concentration of spheres is high enough for the system to demix. Then the smectic wavevector discontinuously jumps to zero.

associated with the layering transition decreases in a continuous fashion until it reaches zero value.

We now examine the behavior of individual terms in Eq. (7.2) for a mixture of large spheres and short spherocylinders shown in Fig. 7.9. Most notably, we find that at low volume fractions of spheres where the system undergoes the layering transition, the ratio $S_{12}^{ex}/S_{22}^{ex} << 1$. This implies that upon layering there is almost no reduction of the unfavorable sphere/sperocylinder interaction and that the spherocylinder/spherocylinder interaction alone drives the formation of the layered phase. In contrast, for small spheres this ratio was large and was responsible for enhanced stability of the lamellar phase as was shown in Fig. 7.2. At a higher volume fraction of large spheres where the mixture directly bulk phase separates we find that the ratio $S_{12}^{ex}/S_{22}^{ex} >> 1$. This implies, as expected, that demixing very ef-

fectively reduces the unfavorable sphere/spherocylinder interactions. These results suggest a physical picture of the excluded volume effect. Unlike small spheres, large spheres can not fit into the gap between smectic layers and consequently there is no way to gain free volume by undergoing the layering transition. As an alternative, to gain free volume the system bulk phase separates at the lowest volume fraction of spheres possible.

While for short spherocylinders the magnitude of slope τ uniformly decreases with increasing sphere size, longer spherocylinders exhibit a qualitatively different behavior. For a mixture of spherocylinders with $L/D_{sc} = 100$ and spheres with $D_{sc}/D_{sp} = 0.1$ there is a pronounced increase in the stability of the lamellar phase as shown in Fig. 7.8. By increasing the length of spherocylinders to even larger values, the region of increased stability of the lamellar phase shifts to higher values of the sphere radius. Two conditions emerge, which when satisfied lead to enhanced stability of the lamellar phase. First, it is necessary for a sphere to fit between two smectic layers without disturbing them. This condition is satisfied when $D_{sp}/L \approx 0.1$. The second condition is that $D_{sp}/D_{sc} >> 1$. It was argued before that under these condition large spheres are able to induce smectic correlations amongst neighboring spherocylinders [108], which in turn can enhance the formation of the lamellar phase.

Because of the large size asymmetry it was not feasible to carry out simulations for mixture of spherocylinders and spheres with $L/D_{sc} \approx 100$ and $D_{sc}/D_{sp} \approx 0.1$. However, these conditions are closely approximated by recent experiments on rod-like *fd* ($L = 1\mu$m, $L/D_{sc} \approx 100$) and polystyrene spheres [108]. Therefore, we compare theoretical results of slope τ for spherocylinders with $L/D_{sc} = 100$ shown in Fig. 7.8 to these experimental results [108]. When large spheres $D_{sp} \approx 1\mu$m, ($D_{sc}/D_{sp} \approx 0.01$) are mixed with *fd* at any concentration for which the nematic phase is stable, we observe no formation of the layered phase. Instead, large spheres phase separate into dense aggregates elongated along the nematic director indicat-

ing that the value of slope τ is larger then zero. When the size of the sphere was decreased to $D_{sp} = 0.1\mu$m, ($D_{sc}/D_{sp} \approx 10$) we observed a transition to a layered state at a *fd* concentration of 20 mg/ml. The formation of a smectic phase in a pure *fd* suspension at the same ionic strength occurs at 65 mg/ml. The fact that adding spheres diminishes the rod density by a factor of three indicates a large negative value of slope τ. As the sphere size was further decreased $D_{sp} = 0.022\mu$m, ($D_{sc}/D_{sp} = 0.46$) there was again indication of a lamellar phase, but this time at a much higher concentration of rods of about 50 mg/ml. Thus, although small spheres still stabilize the layering transition, implying a negative value of slope τ, the magnitude of slope τ is much less for $D_{sc}/D_{sp} \approx 0.46$ than for $D_{sc}/D_{sp} \approx 0.1$. These qualitative trends of the non-monotonic behavior of slope τ with sphere size observed in experiments of *fd*-polystyrene mixtures are very similar to the theoretical prediction shown in Fig. 7.8 for spherocylinders with $L/D_{sc} = 100$.

7.5 Conclusions

In this paper we have presented the predictions of the second virial theory for a mixture of parallel hard-spherocylinders and hard-spheres undergoing one dimensional microphase separation. We have been able to verify a number of these predictions using Monte Carlo simulations. We found that spheres induce layering, which implies a negative value of the slope τ, which is the change in total volume fraction of the mixture at the point of nematic-smectic instability with respect to the partial volume fraction of added spheres (Eq. 7.1) . At the same time the magnitude of the slope τ increases with increasing spherocylinder length. In other words, spheres at the same partial volume fraction stabilize layering of longer spherocylinders more than shorter spherocylinders. Besides this, the theory predicts an unusual non-monotonic behavior in slope τ as a function of sphere to spherocylinder diameter. Although the physical origin of this effect is not clear, it is intriguing that similar

qualitative trends are observed in experiments of mixtures of the spherocylinder-like *fd* and polystyrene spheres. However, in real experiments spherocylinders are free to rotate, are flexible, and have charge associated with them. Before quantitative comparisons with experiments are possible it will be necessary to perform simulations and formulate theories that take into account these effects mostly ignored in this highly idealized treatment.

7.6 Appendix

A general expression for the free energy of bidisperse mixture at the second virial level is

$$\beta F(\rho_1, \rho_2) = \sum_{i=1,2} \int_V d(\mathbf{r}) \rho_i(\mathbf{r}) \ln(\rho_i(\mathbf{r})) - \frac{1}{2} \sum_{i=1,2} \sum_{j=1,2} \int_V d\mathbf{r_1} \int_V d\mathbf{r_2} \rho_i(\mathbf{r_1}) \rho_j(\mathbf{r_2}) f_{i,j}(\mathbf{r_1}, \mathbf{r_2}) \tag{7.3}$$

where the function $f_{i,j}$ is the overlap function between two spheres, sphere and spherocylinder or two spherocylinders [130]. It attains the value of -1 if two particles overlap, otherwise it is equal to 0. The terms involving $\rho \ln \rho$ represent the entropy of mixing while the terms involving $f_{i,j}$ represent the free volume entropy. Since we are interested in one dimensional layering we look at the response of the system to following density pertubation

$$\begin{aligned} \delta\rho_1(z) &= a_1 \cos(k_z z) \\ \delta\rho_2(z) &= a_2 \cos(k_z z) \end{aligned} \tag{7.4}$$

The free energy difference between the uniform and perturbed state is

$$\delta F = F(1+\delta\rho_1(z), 1+\delta\rho_2(z)) - F(1,1) = \tilde{\mathbf{a}}\mathbf{S}\mathbf{a} \tag{7.5}$$

where $\tilde{\mathbf{a}} = (a_1, a_2)$ and $\mathbf{S}$ is a two dimensional stability matrix. To find the limit of stability we have to solve the equation $\det(\mathbf{S}) = 0$. For latter convenience we define the following function

$$\begin{aligned} S(\frac{L}{D_{sc}}, \sigma, k) &= \frac{3\sin(k\sigma(2+2\frac{L}{D_{sc}}))}{4k^3} - \\ &\quad \frac{2k\sigma\cos(k\sigma(2+2\frac{L}{D_{sc}})) - \sin(k2\sigma\frac{L}{D_{sc}})}{4k^3} \end{aligned} \tag{7.6}$$

.

The above expression depends only on geometrical factors and is related to the Fourier transform of the spherocylinder which is specified by the excluded volume between a sphere of diameter D_{sp} and a spherocylinder of length L and diameter D_{sc}. Wavevector k is dimensionless because it is rescaled with the spherocylinder diameter (D_{sc}). The parameter σ is defined as ratio of sphere diameter to spherocylinder diameter ($\sigma = D_{sp}/D_{sc}$). In the limit of $L/D_{sc} \to 0$ the above expression reduces to a Fourier transform of a sphere with unit diameter. The stability matrix $\mathbf{S}$ for a mixture of spherocylinders and spheres has the following form

$$\mathbf{S} = \begin{pmatrix} \frac{\eta(1-\rho_{sp})(1+4(1-\rho_{sp})\eta S(0,1,k))}{4} & \\ \frac{2\rho_{sp}(1-\rho_{sp})\eta^2 S(\frac{L}{D_{sc}}, 1+\sigma, k)}{\sigma^6(\frac{2}{3}\frac{L}{D_{sc}}+1)^2} & \end{pmatrix}$$

$$\left.\begin{array}{c} \dfrac{2\rho_{sp}(1-\rho_{sp})\eta^2 S(\dfrac{L}{D_{sc}},1+\sigma,k)}{\sigma^6(\dfrac{2}{3}\dfrac{L}{D_{sc}}+1)^2} \\ \dfrac{\sigma^6(\dfrac{3}{2}\dfrac{L}{D_{sc}}+1)}{4}+\eta\rho_{sp}S(2\dfrac{L}{D_{sc}},2\sigma,k)) \\ \eta\rho_{sp}(\dfrac{\sigma^6(\dfrac{2}{3}\dfrac{L}{D_{sc}}+1)^2}{\sigma^6(\dfrac{2}{3}\dfrac{L}{D_{sc}}+1)^2} \end{array}\right) \tag{7.7}$$

where ρ_{sp} denotes partial volume fraction of spheres and varies between 0 and 1 while η denotes total volume fraction. Note that the terms in matrix elements S_{11} and S_{22} proportional to η are due to configurational entropy while terms proportional to η^2 are due to free volume entropy. As $k \to 0$ the condition $\det(\mathbf{S}) = 0$ reduces to the usual thermodynamic condition for the stability of the system against bulk phase separation.

To reconstruct the stability diagram from the determinant we slowly increase the total volume fraction η. At a certain value of total volume fraction (η_c) the determinant of $\mathbf{S}$ will equal zero for a specific wavevector (k_c). If the wavevector k_c obtained has a finite value it implies that system is undergoing a layering transition. On the other hand, the condition $\det(\mathbf{S}) = 0$ when $k_c = 0$ implies complete demixing. Once we obtain values of η_c and k_c we can find out the ratio of amplitudes from the following formula

$$\frac{a_1}{a_2} = -\frac{S_{12}(\eta_c, k_c)}{S_{11}(\eta_c, k_c)}. \tag{7.8}$$

A positive value of the amplitude ratio implies that the spheres and spherocylinders are in the same layer (the periodic modulations are in phase), while a negative value implies that the spheres and spherocylinders intercalate (the periodic modulations are out of phase).

Bibliography

[1] J. Israelechvili. *Intermolecular and Surafce Forces*. Academic Press, London, 2nd edition, 1991.

[2] L. Onsager. The effects of shape on the interaction of colloidal particles. *Ann. NY Acad. Sci.*, 51:627, 1949.

[3] J. K. Percus. *The many body problem, proceedings*. Interscience Publisher, New York, 1957.

[4] B. J. Alder and T. E. Wainwright. Phase transitions for a hard sphere system. *J. Chem. Phys.*, 27:1207, 1957.

[5] M. Hosino, H Nakano, and H. Kimura. Nematic-Smectic transitions in an aligned rod system. *J. Phys. Soc. Jpn.*, 46:1709, 1979.

[6] D. Frenkel, H.N.W Lekkerkerker, and A. Stroobants. Thermodynamic stability of smectic phase in a system of hard rods. *Nature*, 332:822, 1988.

[7] P. N. Pusey and W. van Megen. Phase behavior of concentrated suspensions of nearly hard colloidal spheres. *Nature*, 320:340, 1986.

[8] P. G. Bolhuis and D. Frenkel. Tracing the phase boundaries of hard spherocylinders. *J. Chem. Phys.*, 106:668–687, 1997.

[9] X. Wen, R. B. Meyer, and D. L. D. Caspar. Observation of smectic-A ordering in a solution of rigid-rod-like particles. *Phys. Rev. Lett.*, 63:2760, 1989.

[10] Z. Dogic and S. Fraden. The smectic phase in a colloidal suspension of semi-flexible virus particle. *Phys. Rev. Lett.*, 78:2417, 1997.

[11] J. P. Hansen and I. R. McDonald. *Theory of Simple Liquids*. Academic Press, London:, second edition, 1986.

[12] J. Herzfeld, A. E. Berger, and J. W. Wingate. A highly convergant algorithm for computing the orientation distribution functions of rodlike particles. *Macromolecules*, 17:1718–1723, 1984.

[13] H. N. W. Lekkerkerker, P. Coulon, V. der Haegen, and R. Deblieck. On the isotropic-nematic liquid crystal phase separation in a solution of rodlike particles of different lengths. *J. Chem. Phys.*, 80:3427–3433, 1984.

[14] A. Stroobants, H. N. W. Lekkerkerker, and T. Odijk. Effect of electrostatic interaction on the liquid crystal phase transition in solutions of rodlike polyelectrolytes. *Macromolecules*, 19:2232, 1986.

[15] K. Zimmermann, J. Hagedorn, C. C. Heuck, M. Hinrichsen, and J. Ludwig. The ionic properties of the filamentous bacteriophages pf1 and fd. *J. Biol. Chem.*, 261:1653, 1986.

[16] A. R. Khokhlov and A. N. Semenov. Liquid-crystalline ordering in the solution of partially flexible macromolecules. *Physica*, 112a:605, 1982.

[17] A. R. Khokhlov and A. N. Semenov. Liquid-crystalline ordering in the solution of long persistent chains. *Physica*, 108a:546, 1981.

[18] R. Hentschke. Eqation of state for persisteny-flexible liquid crystal polymers. comparison wiht poly(γ-benzyl-l-glutamate) in dimethylformamide. *Macromolecules*, 23:1192–1196, 1990.

[19] T. Odijk. Theory of lyotropic polymer liquid crystals. *Macromolecules*, 19:2313, 1986.

[20] D. P. DuPre and S. Yang. Liquid crystaline properties of solutions of persistent polymer chains. *J. Chem. Phys.*, 94:7466–7477, 1991.

[21] M. A. Cotter and D. C. Wacker. Van der waals theory of nematogenic solutions. i. derivation of the general equations. *Phys. Rev. A*, 18:2669, 1978.

[22] M. A. Cotter. Hard particle theories of nematics. In G. R. Luckhurst and G. W. Gray, editors, *The Molecular Physics of Liquid Crystals*, pages 169–189. Academic Press, London, 1979.

[23] R. F. Kayser, Jr. and H. J. Raveche. Bifurcation in onsager's model of the isotropic-nematic transition. *Phys. Rev. A*, 17:2067, 1978.

[24] D. Frenkel. Structure of hard-core models for liquid crystals. *J. Phys. Chem.*, 92:3280, 1988.

[25] Z. Y. Chen. Nematic ordering in semiflexible polymer chains. *Macromolecules*, 26:3419, 1993.

[26] E. M. Kramer and J. Herzfeld. Distribution function for reversibly self-assembling spherocylinders. *Phys. Rev. E*, 58:5934–5947, 1998.

[27] J. Tang and S. Fraden. Isotropic-cholesteric phase transition in colloidal suspensions of filamentous bacteriophage fd. *Liquid Crystals*, 19:459–467, 1995.

[28] E. M. Kramer and J. Herzfeld. Avoidance model for soft particles. I. charged spheres and rods beyond the dilute limit. *J. Chem. Phys.*, 110:8825–8834, 1999.

[29] E. M. Kramer and J. Herzfeld. Avoidance model for soft particles. II. positional ordering of charged rods. *J. Chem. Phys.*, 61:6872–6878, 2000.

[30] K. R. Purdy, Z. Dogic, S. Fraden, A. Ruhm, L. Lurio, and S. G. J. Mochrie. Measuring the nematic order of colloidal fd virus by x-ray diffraction and optical birefringence. *Phys. Rev. E*, 67:031708, 2003.

[31] R. B. Meyer. Ordered phases in colloidal suspensions of Tobacco Mosaic Virus. In A. Onuki and K. Kawasaki, editors, *Dynamics and Patterns in Complex Fluids*, page 62. Springer-Verlag, 1990.

[32] S. Fraden. Phase transitions in colloidal suspensions of virus particles. In M. Baus, L. F. Rull, and J. P. Ryckaert, editors, *Observation, Prediction, and Simulation of Phase Transitions in Complex Fluids*, pages 113–164. Kluwer Academic Publishers, 1995.

[33] F. Livolant. Supramolecular organization of double-stranded DNA molecules in the columnar hexagonal liquid crystalline phase. *J. Mol. Biol.*, 218:165, 1991.

[34] Z. Dogic and S. Fraden. Cholesteric phase in virus suspensions. *Langmuir*, 16:7820–7824, 2000.

[35] G. J. Vroege and H. N. W. Lekkerkerker. Phase transitions in lyotropic colloidal and polymer liquid crystals. *Repts. on Prog. Phys.*, 8:1241, 1992.

[36] J. F. Maguire, J. P. McTague, and F. Rondalez. Rotational diffusion of sterically interaction rodlike macromoleculse. *Phys. Rev. Lett.*, 45(23):1891–1894, 1980.

[37] S. Bhattacharjee, M. J. Glucksman, and L. Makowski. Structural polymorphism correlated to surface charge in filamentous bacteriophages. *Biophys. J.*, 61:725, 1992.

[38] R. Herrmann, K. Neugebauer, E. Pirkl, H. Zentgraf, and H. Schaller. Conversion of bacteriophage fd into an efficient single-stranded DNA vector system. *Molec. gen. Genet.*, 177:231–242, 1980.

[39] T. Maniatis, J. Sambrook, and E. F. Fritsch. *Molecular Cloning.* Cold Spring Harbor University Press, 1989.

[40] T. Sato and A. Teramoto. Statistical mechanical theory for liquid-crystaline polymer solutions. *Acta. Polymer.*, 45:399–412, 1994.

[41] A. Abe and P. J. Flory. Statistical thermodynamics of mixtures of rodlike particles. 2. ternanry systems. *Macromolecules*, 11:1122, 1978.

[42] P. J. Flory and A. Abe. Statistical thermodynamics of mixtures of rodlike particles. 1. therory of polydisperse systems. *Macromolecules*, 11:1119, 1978.

[43] J. M. Polson. First-order nematic-smectic phase transtion for hard spherocylinders in the limit of infinite aspect ratio. *Phys. Rev. E*, 56:R6260, 1997.

[44] P. van der Schoot. The nematic-smectic transition in suspensions of slightly flexible hard rods. *J. Phys. II France*, 6:1557, 1996.

[45] A. V. Tkachenko. Nematic-smectic transition of semiflexible chains. *Phys. Rev. Lett.*, 77:4218–4221, 1996.

[46] M. A. Bates and D. Frankel. Influnce of polydispersity on the phase behavior of colloidal liquid crystals: A monte carlo simulation study. *J. Chem. Phys.*, 109:6193–6199, 1998.

[47] A. M. Bohle, R. Holyst, and T. Vilgis. Polydispersity and ordered phases in solutions of rodlike macromolecules. *Phys. Rev. Lett.*, 76:1396–1399, 1996.

[48] A. Stroobants. Columnar versus smectic order in binary mixtures of hard parallel spherocylinders. *Phys. Rev. Lett.*, 69:2388, 1992.

[49] R. van Roij. *Simple Theories of Complex Fluids*. Universiteit Utrecht, 1996.

[50] S. Cui and Z. Y. Cheng. Columnar and smectic order in binary mixtures of aligned hard cylinders. *Phys. Rev. E.*, 50:3747, 1994.

[51] T. Koda and H. Kimura. Phase diagram of the nematic-smectic A transition of the binary mixture of parallel hard cylinders of different lengths. *J. Phys. Soc. Jpn.*, 63:984, 1994.

[52] K. Devanand and J. C. Selser. Asymptotic behavior and long-range interactions in aqueous solutions of poly(ethylene oxide). *Macromolecules*, 24:5943, 1991.

[53] T. L. Kuhl, D. E. Leckband, D. D. Lasic, and J. N. Isrealachvili. Modulation of interaction forces between bilayers exposing short-chained ethylene oxide headgroups. *Biophys. J.*, 66:1479, 1994.

[54] R. van Roij, B. Mulder, and M. Dijkstra. Phase behavior of binary mixture of thick and thin hard rods. *Physics A*, 261:374–390, 1998.

[55] R. P. Sear and B. M. Mulder. Phase behavior of a symmetric binary mixture of hard rods. *J. Chem. Phys.*, 105:7727–7734, 1996.

[56] P. G. de Gennes and J. Prost. *The Physics of Liquid Crystals*. Oxford Science, second edition, 1993.

[57] J. P. Straley. Frank elastic constants of the hard-rod liquid crystals. *Phys. Rev. A*, 8:2181, 1973.

[58] J. P. Straley. Theory of piezoelectricity in nematic liquid crystals, and of the cholesteric ordering. *Phys. Rev. A*, 14:1835–1841, 1976.

[59] T. Odijk. Pitch of a polymer cholesteric. *J. Phys. Chem.*, 91:6060–6062, 1987.

[60] R. A. Pelcovits. Cholesteric pitch of rigid and semiflexible chiral liquid crystals. *Liq.Cryst.*, 21:361, 1996.

[61] S. A. Issaenko, A. B. Harris, and T. C. Lubensky. Quantum theory of chiral interactions in cholesteric liquid crystals. *Phys. Rev. E.*, 60:578, 1999.

[62] A. B. Harris R. D. Kamien and T. C. Lubensky. Microscopic origin of cholesteric pitch. *Phys. Rev. Lett.*, 78:1476, 1997.

[63] A. B. Harris, R. D. Kamien, and T. C. Lubensky. Molecular chirality and chiral parameters. *Rev. Mod. Phys.*, 71:1745, 1999.

[64] J. Lapointe and D. A. Marvin. Filamentous bacterial viruses. VIII. liquid crystals of fd. *Mol. Cryst. Liquid Cryst.*, 19:269, 1973.

[65] L. A. Day, C. J. Marzec, S. A. Reisberg, and A. Casadevall. DNA packing in filamentous bacteriophages. *Ann. Rev. Biophys. Chem.*, 17:509, 1988.

[66] L. Song, U. Kim, J. Wilcoxon, and J. M. Schurr. Dynamic light scattering from weakly bending rods: Estimation of the dynamic bending rigidity of the m13 virus. *Biopolymers*, 31:547, 1991.

[67] D. L. D. Caspar and L. Makowski. The symmetries of filamentous phage particles. *J. Mol. Biol.*, 145:611, 1981.

[68] D. A. Marvin. Filamentous phage structure, infection and assembly. *Curr. Opin. Struct. Biol.*, 8:150, 1998.

[69] R. Oldenbourg. *Elastiche and quasielastiche Lichtstreuung an magnetisch ausgerichteten polyelektrolytischen Stäbchen.* PhD thesis, Universitat Konstänz, 1981.

[70] J. Tang and S. Fraden. Magnetic field induced isotropic-nematic phase transition in a colloidal suspension. *Phys. Rev. Lett.*, 71:3509, 1993.

[71] J. Tang and S. Fraden. Temperature dependence of the flexibility of fd: Behavior of the isotropic - cholesteric phase boundary and magnetic birefringence. *Biopolymers*, 39:13, 1996.

[72] R. S. Pindak, C. C. Huang, and J. T. Ho. Divergance of cholesteric pitch near a smectic-a transition. *Phys. Rev. Lett*, 32(2):43, 1974.

[73] J. H. Wang, F. Lonberg, X. Ao, and R. B. Meyer. Light scattering studies of a nematic to smectic-a phase transition in rigid rod polymer solutions. In A. Teramoto, M. Kobayashi, and T. Norisuje, editors, *Ordering in Macromolecular Systems*. Springer-Verlag, 1994.

[74] R. B. Meyer. Distortion of a cholesteric structure by a magnetic field. *Appl. Phys. Lett.*, 14:208, 1969.

[75] R. B. Meyer. Effects of electric and magnetic fields on the structure of cholesteric liquid crystal. *Appl. Phys. Lett.*, 12:281, 1968.

[76] J. Torbet and G. Maret. High-field magnetic birefringence study of the structure of rodlike phages pf1 and fd in solution. *Biopolymers*, 20:2657, 1981.

[77] In ref. [76] χ_0 was determined by measureing the Cotton - Mouton constant, which is proportional to $\Delta n_{\rm sat}\chi_0$. In turn, $\Delta n_{\rm sat}$, the birefringence of a perfectly aligned sample, was determined by measuring the birefringence (Δn) of a nematic sample of *fd*. But the measured birefringence of a nematic is given by $\Delta n = S\Delta n_{\rm sat}$, with S the nematic order parameter. For *fd*, the order parameter at the isotropic - nematic (I-N) transition is estimated to be $S_{\rm I\text{-}N} = 0.5$, while $S = 1$ only for a perfectly aligned nematic. In ref. [76] Δn was equated with $\Delta n_{\rm sat}$ and was measured for a sample above the I - N transition ($S > 0.5$), but far from the concentration where $S \sim 1$. Thus $\Delta n_{\rm sat}$ given in ref. [76] is an underestimate of the true value by at most a factor of two, and consequently the reported χ_0 is an overestimate by the same amount.

[78] D. B. DuPre and R. W. Duke. Temperature, concentration, and molecular weight dependence of the twist elastic constant of cholesteric poly-gamma-benzyl-L-glutamate. *J. Chem. Phys.*, 63:143, 1975.

[79] I. Uematsu and Y. Uematsu. Polypeptide liquid crystals. *Adv. Poly. Sci.*, 59:37, 1984.

[80] D. H. Van Winkle, M. W. Davidson, W. X. Chen, and R. L. Rill. Cholesteric helical pitch of near persistence length (DNA). *Macromolecules*, 23:4140–4148, 1990.

[81] X. M. Dong and J. T. Yang. Effect of counterions on ordered phase formation in suspensions of charged rodlike cellulose crystallites. *Langmuir*, 13:2404–2409, 1997.

[82] E. Jizuka and J. T. Yang. Formation of the liquid crystals of polyribonucleotide complexes. In J.F. Johnson, editor, *Liquid Crystals and Ordered Fluids*. Plenum Press, 1978.

[83] E. Senechal, G. Maret, and K. Dransfeld. Long-range order of nucleic acids in aqueous solutions. *Int. J. Biol. Macromol.*, 2:256, 1980.

[84] G. J. Vroege and T. Odijk. Elastic moduli of a nematic liquid-crystalline solution of polyelectrolytes. *J. Chem. Phys.*, 87:4223, 1987.

[85] T. Sato et.al. Polyisocyanates and the interplay of experiment and theory in the formation of lyotropic cholesteric states. *Macromolecules*, 26:4551, 1993.

[86] A. P. Gast and C. K. Hall W. B. Russel. Polymer-induced phase separations in nonaqueous colloidal suspensions. *J. Colloid Interface Sci.*, 96:251–167, 1983.

[87] P. van der Schoot and T. Odijk. Statistical theory and structure factor of semidilute solution of rodlike macromolecules interacting by van der waals forces. *J. Chem. Phys.*, 97:515–524, 1992.

[88] P. B. Warren. Depletion effect in a model lyotropic liquid crystal theory. *J. Phys. I (France)*, 4:237, 1994.

[89] R. P. Sear. Phase behavior of athermal mixtures of rigid-rod and flexible polymers. *J. Phys. II (France)*, 7(877-886), 1997.

[90] H. N. W. Lekkerkerker and A. Stroobants. Phase behaviour of rod-like colloid + flexible polymer mixtures. *Nuovo Cimento D*, 16:949, 1994.

[91] P. G. Bolhuis, A. Stroobants, D. Frenkel, and H. N. W. Lekkerkerker. Numerical study of the phase behavior of rodlike colloids with attractive interactions. *J. Chem Phys*, 107:1551, 1997.

[92] S. Asakura and F. Oosawa. Interactions between particles suspended in solutions of macromolecules. *J. Polym. Sci.*, 33:183, 1958.

[93] J. Buitenhuis, P. A. Buining L. N. Donselaar, A. Stroobants, and H. N.W. Lekkerkerker. Phase separation of mixtures of colloidal boehmite rods and flexible polymers. *J. Colloid Interface Sci.*, 175(46-56), 1995.

[94] Z. Dogic and S. Fraden. Development of model colloidal liquid crystals and the kinetics of the isotropic-nematic transition. *Phil. Trans. R. Soc. Lond. A.*, 359:997–1014, 2001.

[95] M. P. B. van Bruggen and H. N. W. Lekkerkerker. Tunable attractions directing nonequilibrium states in dispersions of hard rods. *Macromolecules*, 33:5532–5535, 2000.

[96] A. P. Chatterjee and K. S. Schweizer. Correlation effects in dilute particle-polymer mixtures. *J. Chem. Phys.*, 109:10477–10488, 1998.

[97] A. Hanke, E. Eisenriegler, and S. Dietrich. Polymer depletion effects near mesoscopic particles. *Phys. Rev. E.*, 59:6853–6878, 1999.

[98] R. Tuinier, G. A. Vliegenthart, and H. N. W. Lekkerkerker. Depletion interaction between spheres immersed in a solution of ideal polymer chains. *J. Chem. Phys.*, 113:10768–10775, 2000.

[99] S. Asakura and F. Oosawa. On interaction between two bodies immersed in a solution of macromolecules. *J. Chem. Phys.*, 22(1255), 1954.

[100] H. N. W. Lekkerkerker. Disorder-to-order phase tranitions in concentrated colloidal dispersions. In S. H. Chen, et.al., editor, *Structure and Dynamics of Strongly Interacting Colloids and Supramolecular Aggregates in Solution*, page 97. Kluwer Academic Publishers, 1992.

[101] E. J. Meijer and D. Frenkel. Computer simulation of polymer-induced clustering of colloids. *Phys. Rev. Lett.*, 67:1110–1113, 1991.

[102] H. N. W. Lekkerkerker, W. C.-K. Poon, P. N. Pusey, A. Stroobants, and P. B. Warren. Phase behavior of colloid + polymer mixutre. *Europhys. Lett.*, 20:559, 1992.

[103] F. R. Senti, N. N. Hellman, N. H. Ludwig, G. E. Babcock, R. Tobin, C. A. Glass, and B. L. Lamberts. Viscosity, sedimentation and light-scattering properties of fractions of an acid-hydrolyzed dextran. *J. Poly. Sci.*, 17:527, 1955.

[104] E. Nordmeier. Static and dynamic light-scattering solution behavior of pullulan and dextran in comparison. *J. Phys. Chem.*, 97:5770, 5785.

[105] R. Oldenbourg and W. C. Phillips. Small permanent magnet for fields up to 2.6 t. *Rev. Sci. Instrum.*, 2362-2365(57), 57.

[106] A. P. Gast, C. K. Hall, and W. B. Russel. Phase separations induced in aqueous colloidal suspensions by dissolved polymer. *Farday. Discuss. Chem. Soc.*, 76:189–201, 1983.

[107] R. P. Sear. Cohesion and aggregation of flexible hard rods with an attractive interaction. *Phys. Rev. E*, 55:5820–5824, 1997.

[108] M. Adams, Z. Dogic, S. L. Keller, and S. Fraden. Entropically driven microphase transitions in mixtures of colloidal rods and spheres. *Nature*, 393:349, 1998.

[109] Z. Dogic, D. Frenkel, and S. Fraden. Enhanced stability of the layered phases in parallel spherocylinders due to addition of hard spheres. *Phys. Rev. E*, 62:3925–3934, 2000.

[110] A. D. Dinsmore, P. B. Warren, W. C. K. Poon, and A. G. Yodh. Fluid-solid transitions on walls in binary hard-sphere mixtures. *Europhys. Lett.*, 40:337–342, 197.

[111] R. P. Seaar. Depletion driven adsorption of colloidal rods onto a hard wall. *Phys. Rev. E*, 57:1983–1989, 1998.

[112] M. Adams and S. Fraden. Phase behavior of mixtures of rods (tobacco mosaic virus) and spheres (polyethylene oxide, bovine serum albumin). *Biophys. J.*, 74:669, 1998.

[113] A. J. Pennings, R. Lageveen, and R. S. DeVries. Hydrodynamically induced crystallization of polymers from solution. *Colloid Polymer Sci.*, 255:532–542, 1977.

[114] M. H. J. Hagen and D. Frenkel. Determination of phase diagram for the hard-core attractive yukawa system. *J. Chem. Phys.*, 101:4093–4097, 1994.

[115] A. P. Gast, W. B. Russel, and C. K. Hall. An experimental and theoretical study of phase transitions in the polystyrene latex and hydroxyethylcellulose system. *J. Colloid Interface Sci.*, 109:161, 1986.

[116] P. A. Forsyth, Jr., S. Marcelja, D. J. Mitchell, and B. W. Ninham. Ordering in colloidal systems. *Adv. in Coll. and Int. Sci.*, 9:37, 1978.

[117] R. Piazza, T. Bellini, and V. Degiorgio. Equilibrium sedimentation of screened charged colloids: A test of the hard-sphere equation of state. *Phys. Rev. Lett.*, 71(25):4267, 1993.

[118] M. A. Rutgers, J. H. Dunsmuir, J. Z. Xue, W. B. Russel, and P. M. Chaikin. Measurment of the hard sphere equation of state using screened charged polystyrene colloids. *Phys. Rev. B.*, 53:5043, 1996.

[119] T. Biben and J. P. Hansen. Phase separation of asymmetric binary hard-sphere fluids. *Phys. Rev. Lett.*, 66:2215, 1991.

[120] A. D. Dinsmore, A. G. Yodh, and D. J. Pine. Phase diagrams of nearly hard-sphere binary colloids. *Phys. Rev. E*, 52:4045, 1995.

[121] A. Imhof and J. K. G. Dhont. Experimental phase diagram of binary colloidal hard sphere mixtures with a large size ratio. *Phys. Rev. Lett.*, 75:1662, 1995.

[122] M. D. Eldrige, P. A. Madden, and D. Frenkel. Entropy-driven formation of a superlattice in a hard-sphere binary mixture. *Nature*, 365:35, 1993.

[123] E. J. Meijer and D. Frenkel. Colloids dispersed in polymer solutions. A computer simulation study. *J. Chem. Phys.*, 100:6873, 1994.

[124] M. Dijkstra and R. van Roij. Entropy driven demixing in binary hard core mixtures: From hard spherocylinders towards hard spheres. *Phys. Rev. E*, 56:5594, 1998.

[125] Y. Mao, M. E. Cates, and H. N. W. Lekkerkerker. Depletion force in colloidal systems. *Physica A*, 222:10, 1995.

[126] M. P. B. Bruggen. *Liquid crystal formation and diffusion in dispersions of colloidal rods.* PhD thesis, Universiteit Utrecht, 1998.

[127] H. N. W. Lekkerkerker, P. Buining, J. Buitnhuis, G. J. Vroege, and A. Stroobants. Liquid crystal phase transitions in dispersions of rodlike colloidal particles. In M. Baus, L. F. Rull, and J. P. Ryckaert, editors, *Observation, Prediction and Simulation of Phase Transitions in Complex Fluids*, pages 53–112. Kluwer Academic Publishers, 1995.

[128] P. G. Bolhuis and D. Frenkel. Numerical study of the phase diagram of a mixture of spherical and rodlike colloids. *J. Chem. Phys.*, 101:9869, 1994.

[129] G. A. Vliegenthart, A. van Blaaderen, and H. N. W. Lekkerkerker. Phase trasnstions, aggregation and crystallization in mixed suspensions of colloidal spheres and rods. *Faraday Discuss.*, 112:173, 1999.

[130] T. Koda, M. Numajiri, and S. Ikeda. Smectic-A phase of bidisperse system of parallel rods and hard spheres. *J. Phys. Soc. Jpn.*, 65:3551, 1996.

[131] R. van Roij and B. Mulder. Demixing versus ordering in hard rod mixture. *Phys. Rev. E*, 54:6430, 1996.

[132] B. Mulder. Density-function approach to smectic order in an aligned hard-rod fluid. *Phys. Rev. A*, 35:3095, 1987.

[133] R. van Roij, P. Bolhuis, B. Mulder, and D. Frenkel. Transverse interlayer order in lyotropic smectic liquid crystals. *Phys. Rev. E*, 52:R1277, 1995.

[134] X. Wen and R. B. Meyer. Model for smectic-A ordering of parallel hard rods. *Phys. Rev. Lett.*, 59:1325, 1987.

[135] J. A. C. Veerman and D. Frenkel. Relative stability of columnar and crystalline phases in a system of parallel hard rods. *Phys. Rev. A*, 43:4334, 1991.

[136] T. Koda and S. Ikeda. Effect of addition of hard spheres to the smectic-A phase of parallel hard spherocylinders. *Mol. Cryst. Liq. Cryst.*, 318:101, 1998.

[137] D. Frenkel and B. Smith. *Understanding Molecular Simulation.* Academic Press, 1996.

[138] T. Koda and S. Ikeda. Estimation of the chemical potential of the system of hard molecules. in press.

[139] The smectic order parameter is defined as $\mid \sum_j e^{ik_z r_j} \mid^2 /N^2$ evaluated at k_z for which the expression attains its maximum value, where r_j is the center of mass of the spherocylinder or sphere and k_z is the wave vector along the spherocylinder's long axis.

[140] A. Stroobants, H. N. W. Lekkerkerker, and D. Frenkel. Evidence of one-, two-, and three-dimensional order in a system of hard parallel spherocylinders. *Phys. Rev. A*, 36:2929, 1987.

[141] A. Poniewierski and R. Holyst. Nematic alignment at a solid substrate: The model of hard spherocylinders near a hard wall. *Phys. Rev. A*, 38:3721, 1988.